
This is an electronic reprint of the original article.
This reprint may differ from the original in pagination and typographic detail.

Abed, Ayman; Korkiala-Tanttu, Leena

Stability analysis for road-cutting : Review, recommendations and examples

Published: 01/01/2018

Document Version

Publisher's PDF, also known as Version of record

Please cite the original version:

Abed, A., & Korkiala-Tanttu, L. (2018). *Stability analysis for road-cutting : Review, recommendations and examples*. (Liikenneviraston tutkimuksia ja selvityksiä; Vol. 2018, No. 49). Liikennevirasto. https://julkaisut.liikennevirasto.fi/pdf8/lts_2018-49_stability_analysis_web.pdf

This material is protected by copyright and other intellectual property rights, and duplication or sale of all or part of any of the repository collections is not permitted, except that material may be duplicated by you for your research use or educational purposes in electronic or print form. You must obtain permission for any other use. Electronic or print copies may not be offered, whether for sale or otherwise to anyone who is not an authorised user.

Ayman A. Abed
Leena Korkiala-Tanttu

Stability analysis for road-cutting

Review, recommendations and examples



Ayman A. Abed, Leena Korkiala-Tanttu

Stability analysis for road-cutting

Review, recommendations and examples

Research reports of the Finnish Transport Agency
49/2018

Finnish Transport Agency
Helsinki 2018

Cover picture: Panu Tolla

Online publication pdf (www.liikennevirasto.fi)

ISSN-L 1798-6656

ISSN 1798-6664

ISBN 978-952-317-608-9

Finnish Transport Agency
P.O.Box 33
FIN-00521 HELSINKI, Finland
Tel. +358 (0)295 34 3000

Ayman A. Abed and Leena Korkiala-Tanttu: Stability analysis for road-cutting – Review, recommendations and examples. Finnish Transport Agency, Engineering and Environment. Helsinki 2018. Research reports of the Finnish Transport Agency 49/2018. 59 pages and 2 appendices. ISSN-L 1798-6656, ISSN 1798-6664, ISBN 978-952-317-608-9.

Abstract

The construction works of the railway connection Seinäjoki-Oulu in Pohjanmaa revealed several stability problems and failures in the road cuttings of underpasses particularly in soft clays. During design stage, cutting slopes have been checked against stability using the slices method (LEM) and they have then fulfilled the stability requirements. This report reviews the fundamental principles of limit equilibrium and choice of shear strength parameters as employed in the slices method for the evaluation of road-cutting stability. The provided data and design studies show that, generally speaking, the designer has followed the common practical rules in checking the stability of the designed soil cutting slopes. This study aims at identifying the possible reasons (uncertainties) behind the overestimated safety and to conclude with design recommendations to reduce the possibilities of future failures.

After recapitulation on Mohr-Coulomb failure criterion and the effect of the followed stress path on the soil strength at failure, the report discusses the choice of the shear strength parameters in undrained and drained conditions. This is followed by an overview on the method of slices, its different versions and how to incorporate groundwater flow in the analysis. Based on the findings of the review, two case histories (in Tuuliharju and Zateelliiti locations) that suffered failure in reality are re-evaluated for stability. The evaluation shows that the in appropriate design is related to the inaccurate choice of shear strength parameters and also to the inadequate modelling of pore water pressure during short and long-terms.

The report concludes with recommendations to be followed during the design phase. The recommendations cover the choice of suitable strength parameters for undrained and drained conditions. They also give guidance on the determination of the length of undrained phase, groundwater flow calculations and suitable tests for shear strength estimation.

One of the most important recommendations in case of cutting is that the employed shear strength parameters should be estimated using the direct simple shear test or alternatively based on the reduced values of the in-situ vane shear test. The shear parameters derived from the triaxial compression test tend to be non-conservative whereas those from the triaxial extension test are conservative. The simple shear test (or reduced vane shear) gives average shear strength that is appropriate in the cutting situation.

On top of that, the reasonable estimation of soil permeability and the transient changes in pore water pressure during and after cutting shows to be extremely important, especially for drained analysis. For example, the calculations show that in the case of clay with low permeability ($K < 1.0 \times 10^{-9} \text{m/s}$), the commonly adopted dewatering system in practice is not efficient and the water level stays almost at its initial conditions after two months of pumping. Example calculations for cutting in three different soil-layering profiles are documented. These examples are sought to be representative of practical cases and illustrate how to implement the recommendations given in this report to improve the safety evaluation of the cutting during design phase.

Ayman A. Abed ja Leena Korkiala-Tanttu: Teiden leikkausluiskien stabiliteettianalyysi – Tutkimustarkastelu, suositukset ja esimerkit. Liikennevirasto, tekniikka- ja ympäristöosasto. Helsinki 2018. Liikenneviraston tutkimuksia ja selvityksiä 49/2018. 59 sivua ja 2 liitettä. ISSN-L 1798-6656, ISSN 1798-6664, ISBN 978-952-317-608-9.

Avainsanat: tiet, luiskat, vakavuus, pohjavesi

Tiivistelmä

Pohjanmaan radalla pehmeään saveen tai silttiin kaivetut teiden alikulujen leikkausluiskat ovat osoittautuneet epästabiileiksi ja sortumiakin on tapahtunut. Kuitenkin näiden kohteiden suunnittelu on tehty käyttäen nykyisen ohjeistuksen mukaisia parametrien määrittämistä ja liukupintalaskentamenetelmiä. Tämä tutkimuksen tavoitteena on tunnistaa liukupintalaskelmiin, geometriaan sekä maaparametreihin liittyviä epätarkkuuksia, epävarmuuksia ja mahdollisia syitä varmuuden yliarviointiin. Työssä on tavoitteena myös esittää suosituksia laskentojen tekemiseen, maaparametrien määrittämiseen sekä luiskien rakentamiseen.

Tässä raportissa kerrataan Mohr-Coulombin murtoehto ja arvioidaan jännityspolun vaikutusta murtotilassa mobilisoituvaa lujuuteen. Työssä käsitellään leikkauslujuusparametrien määrittämistä suljetussa ja avoimessa tilassa. Lisäksi tarkastellaan lamellimenetelmien eri versioita ja sitä, miten pohjavedenvirtaus ja siihen liittyvä huokosvedenpainevaihtelut voidaan ottaa laskelmissa huomioon. Raportissa tarkastellaan tarkemmin kahta kohdetta, joissa havaittiin sortumia rakennusaikana. Nämä kohteet ovat Tuuliharjun ja Zateiitin alikulut. Havaintojen mukaan kohteissa oli epätarkkuutta maaparametrien määrittämisessä ja huokosvedenpainetta ei oltu onnistuttu mallintamaan oikein lyhyt- ja pitkäaikaistarkasteluissa.

Raportin johtopäätökset on esitetty loppuosan suunnitteluvaiheen suosituksina. Nämä suositukset kattavat maaparametrien valinnan suljetussa ja avoimessa tilassa, käytetyistä testausmenetelmistä, arvion siitä, milloin suljetun tilan laskelmista pitäisi siirtyä avoimen tilan laskentaan sekä pohjavedenvirtauslaskelmien tekemiseksi. Yksi tärkeimpiä suosituksia koskee leikkauslujuuden määrittämistä leikkaustapauksessa suoraan leikkauskoetta käyttäen tai vaihtoehtoisesti redusoitua siipikairauslujuutta. Kolmiakselikokeen puristuskokeesta määritetyt parametrit yliarvioivat leikkauslujuutta, kun taas vetokokeen lujuusarvot aliarvioivat sitä. Suoran leikkauskokeen (tai redusoitu siipikairauksen) tulokset antavat keskiarvotuloksen, joka on lähempänä todellista rakenteessa toteutuvaa murtolujuutta.

Erittäin tärkeää on myös määrittää mahdollisimman realistisesti avoimen tilan tarkasteluihin kuuluen maan vedenläpäisevyys ja huokosvedenpaineen vaihtelut, jotka tapahtuvat kaivuun aikana ja pian sen jälkeen. Esimerkiksi laskelmien mukaan imupainepumppaus huonosti läpäisevien savien ($k < 1 \times 10^{-9}$ m/s) kerroksissa ei ole riittävä laskemaan pohjavedenpintaa suunnitelmien mukaan. Laskelmien mukaan käytetty kahden kuukauden pumppaus ei ehtinyt juurikaan alentaa pohjavedenpintaa. Työssä esitetään myös kolmen eri pohjamaaprofiilin esimerkkilaskelmat. Esimerkkien pohjamaaprofiilit ovat valittu siten, että edustavat käytännön kohteita ja tuovat esiin työssä esitettyjä suosituksia.

Ayman A. Abed och Leena Korkiala-Tanttu: Stabilitetsanalys av vägarnas skärningslänter – Undersökning, rekommendationer och. Trafikverket, teknik och miljö. Helsingfors 2018. Trafikverkets undersökningar och utredningar 49/2018. 59 sidor och 2 bilagor. ISSN-L 1798-6656, ISSN 1798-6664, ISBN 978-952-317-608-9.

Sammanfattning

Vägtunnlars skärningslänter som grävts i mjuk lera eller silt längs Österbottenbanan har visat sig vara instabila och det har skett skred. Planeringen av dessa objekt har emellertid genomförts med fastställande av parametrar och metoderna för beräkning av glidytor enligt de nuvarande anvisningarna. Syftet med denna undersökning är att identifiera inexaktheter och osäkerheter som hänför sig till beräkningen av glidytor, geometrin och jordparametrarna samt eventuella orsaker till överskattning av säkerheten. Arbetet strävar även efter att ge rekommendationer för beräkningar, fastställande av jordparametrarna och byggnation av slänterna.

Rapporten upprepar Mohr-Coulombs brottkriterium och uppskattar effekten av spänningscirkeln på den hållfasthet som mobiliseras i skjuvzonen. Arbetet handlar om fastställande av parametrarna för skjuvstyrka i stängda och öppna utrymmen. Vidare granskar arbetet de olika versionerna av lamellmetoderna samt hur grundvattenströmningen och tryckvariationerna hos porvatten kan beaktas i beräkningarna. Rapporten granskar två objekt där man upptäckte skred under byggnadstiden i mer detalj. Dessa objekt är vägtunnlarna under Tuuliharju och Zateelliitti. Enligt observationerna fanns det oexaktheter i fastställandet av jordparametrarna och porvattentrycket hade inte kunnat modelleras på rätt sätt vid kort- och långtidsgranskningarna.

Rapportens slutsatser har presenterats som rekommendationer för det senare planeringsskedet. Rekommendationerna omfattar val av jordparametrarna i slutna och öppna utrymmen, de testmetoder som använts, en uppskattning om när beräkningar för slutna utrymmen ska bytas mot beräkningar för öppna utrymmen samt beräkningar av grundvattenströmningar. En av de viktigaste rekommendationerna handlar om fastställande av skjuvstyrka genom direkta skjuvprov eller reducerad hållfasthet för vingsondering. Parametrar som fastställts med tryckprovning vid treaxialförsök överskattar skjuvstyrkan, medan värdena från dragprov underskattar den. Resultaten från ett direkt skjuvprov (eller från reducerad hållfasthet för vingsondering) ger ett genomsnittresultat som är närmare den faktiska brotthållfastheten i strukturen.

Det är mycket viktigt att vid granskningar av öppna utrymmen även så realistiskt som möjligt fastställa vattengenomträngligheten i jordmånen och variationerna i porvattentrycket under och snart efter grävningarna. Enligt beräkningarna är t.ex. insugningstrycket i jordlager av lera med dålig vattengenomtränglighet ($k < 1 \times 10^{-9}$ m/s) inte tillräcklig för att sänka grundvattenytan enligt planerna. Enligt beräkningarna hann pumpningen under två månader inte just sänka grundvattennivån. Arbetet innehåller även exempelberäkningar för tre olika profiler av undre jordmån. Jordmånsprofilerna har valts som exempel på faktiska objekt och de rekommendationer som framställts i arbetet.

Foreword

Several grade-separated crossings on the Ostrobothnia rail line have exhibited issues with the stability of cut slopes of underpass roads in areas with a lean clay or clayey silt soil. The objective of this survey was to examine the principles used in stability calculations of similar sites and offer recommendations on the methodology for seepage flow and slip surface calculations.

The survey was primarily conducted by Ayman A. Abed, postdoctoral researcher at Aalto University, with the assistance of Professor Leena Korkiala-Tanttu. On the part of the Finnish Transport Agency, Panu Tolla and Veli-Matti Uotinen participated in steering the survey. Teuvo Holappa from WSP Finland Oy also participated in the survey steering group. The survey utilises geometric and soil survey data from the Tuuliharju and Zateelliitti underpasses. The soil parameters used are based on site investigations and laboratory tests conducted by Olga Goncharko at Aalto University.

Helsinki, September 2018

Finnish Transport Agency
Engineering and Environment

List of content

1	INTRODUCTION AND PROBLEM IDENTIFICATION	9
2	STRESS PATH AND FAILURE CRITERION	10
2.1	Failure criterion	10
2.2	Failure and stress paths in slopes	11
2.3	Stress path during soil cutting.....	12
2.4	Stress state along the slip surface	13
3	CONSIDERATION OF DRAINED AND UNDRAINED BEHAVIOUR.....	15
4	ESTIMATION OF SOIL SHEAR STRENGTH PARAMETERS.....	18
4.1	Sources of uncertainties in estimating undrained shear strength in case of soft soil.....	18
4.2	SHANSEP method (Stress History and Normalized Soil Engineering Properties)	23
5	THE LIMIT EQUILIBRIUM METHOD (LEM) FOR SLOPE STABILITY	24
5.1	Definition of safety factor and LEM fundamentals.....	24
5.2	About slip surface assumption	26
5.3	Shear strength in the unsaturated zone	26
5.4	Strength and weaknesses of LEM analysis	27
6	THE FINITE ELEMENT METHOD (FEM) IN SLOPE STABILITY CALCULATIONS	28
6.1	About FEM	28
6.2	Strength reduction method	28
6.3	Recommendations for the use of FEM in slope stability analysis	29
7	PORE WATER PRESSURE ESTIMATION.....	30
7.1	Estimation of soil permeability.....	30
7.2	In-situ pore water pressure measurements.....	32
8	PRACTICAL APPLICATIONS.....	34
8.1	Tuuliharju location as a master case	34
8.1.1	Soil profile and soil cutting geometry	34
8.1.2	Relevance of undrained behaviour.....	36
8.1.3	Drained and Undrained strength parameters	37
8.1.4	Design undrained shear strength.....	37
8.1.5	Design drained strength parameters.....	40
8.1.6	Undrained analysis results	41
8.1.7	Drained analysis results.....	41
8.2	Safety evaluation at Zatelliitti site.....	42
8.2.1	Soil profile	42
8.2.2	First approximation analysis.....	44
8.2.3	Analysis of excavation stage 1.....	45
8.2.4	Analysis of excavation stage 2.....	48
8.2.5	Analysis of excavation stage 3.....	49
8.2.6	Sensitivity to the groundwater table position.	51
8.2.7	Notes on Zatelliitti site calculations	51

9	DESIGN GUIDANCE.....	53
9.1	Recommendations for LEM calculations (including: parameters identification, water flow conditions, layering, permeability, drained/undrained calculations).....	53
9.2	Recommendations for site investigation	55
9.3	Recommendations for construction (feasibility of lowering water table and staged construction)	55
9.4	Recommendations for erosion protection of superficial slope failure.	55
10	NOTATION.....	56
	REFERENCES.....	58
	APPENDICES	
Appendix 1	Results of numerical study about the effect of permeability and discharge rate on lowering the groundwater table at Tuuliharju site	
Appendix 2	Examples 1–3	

1 Introduction and problem identification

A research project started at Aalto University to eventually provide recommendations to enhance the practical use of the Limit Equilibrium Method (LEM) for road cutting stability analysis. The motivation behind this project is the increasing number of failed “soil cutting” slopes, particularly in the sites prevailed by soft clayey silts. The failures took place during the construction of new roads that intersect with an existing railway. During design stage, most of these slopes have been checked against stability using the slices method (LEM). The provided data and design studies show that, generally speaking, the designer has followed the common practical rules in checking the stability of the designed soil cutting slopes. This study aims at identifying the possible reasons (uncertainties) behind the overestimated safety and to conclude with design recommendations to reduce the possibilities of future failures.

This report reviews and discusses the fundamental concepts related to slope stability calculations including parameters estimation and the basics of Limit Equilibrium method. The light is shed on the dominant stress path in the case of cutting slope and the suitable determination of strength parameters for both drained and undrained analyses. The following section contains recapitulation about stress paths and soil shear strength, which would form the basis for the further discussion in this work.

2 Stress path and failure criterion

Stress path reflects how the stresses are changing during the loading history. In literature, there are many options to represent the stress path, in this report however, the concentration will be on the stress path in the plane $p' - q$. The stress invariants p' and q are the effective isotropic pressure and deviatoric pressure, respectively. For practical reasons, the most important issues will be also discussed and reflected in the plane $\tau - \sigma'_n$ where τ and σ'_n are the shear and normal effective stress on the failure plane, respectively.

2.1 Failure criterion

It is common to define failure in soil mechanics in accordance with Mohr-Coulomb failure criterion where the shear strength at failure (ultimate shear strength) τ_f is given as:

$$\tau_f = c' + \sigma'_n \tan\varphi' = c' + (\sigma_n - p_w) \tan\varphi' \quad (1)$$

The effective cohesion, normal stress on failure plane and effective friction angle are denoted as c' , σ'_n and φ' , respectively. The total normal stress and pore water pressure are represented by σ_n and p_w . The generalized Mohr-Coulomb failure criterion f can be written in terms of stress invariants p' , q and θ as:

$$f = p' \sin\varphi' + q \left(\frac{\cos\theta}{\sqrt{3}} - \frac{\sin\theta \sin\varphi'}{3} \right) - c' \cos\varphi' \quad (2)$$

where θ is Lode's angle. In terms of principal stresses, the invariants are given as follows:

$$p' = \frac{\sigma'_1 + \sigma'_2 + \sigma'_3}{3};$$

$$q = \sqrt{\frac{1}{2} [(\sigma'_1 - \sigma'_2)^2 + (\sigma'_2 - \sigma'_3)^2 + (\sigma'_3 - \sigma'_1)^2]}; \quad (3)$$

$$\theta = \frac{1}{3} \arcsin \left[\frac{2}{9} \frac{(\sigma'_1 + p')(\sigma'_2 + p')(\sigma'_3 + p')}{q^3} \right]$$

According to Equation (2), failure occurs when the stress state results in $f = 0$. A three dimensional representation of Mohr-Coulomb failure surface with geometrical representation of the meaning of stress invariants is depicted in Figure 1. The Lode's angle determines the angular position of the stress state with respect to the failure surface (for example: triaxial compression, plane-strain, triaxial extension or in between). It is clear from Figure 1 that the soil has higher strength in compression compared to extension. This feature has important consequences on the determination of the suitable soil strength parameters and will be discussed in details in the remainder of this report.

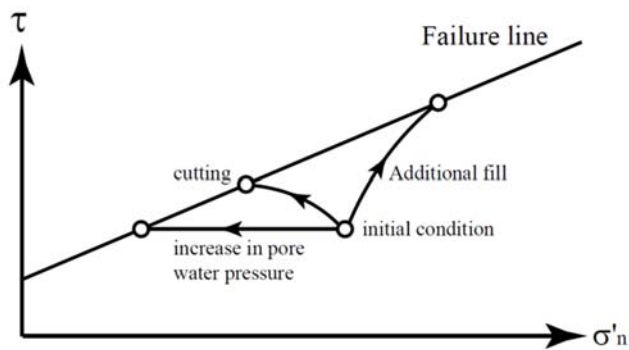


Figure 3. Dominant average stress path during slope failure after (Lambe, 1997).

By investigating the corresponding dominant average stress path as it shown in Figure 3, it is clear that the slope would exhibit higher resistance in case of loading-dominant stress path if compared to the cutting case (unloading by total stress reduction). Among them, the worst-case scenario is the increase of pore water pressure, which produces the lowest shear resistance of the system and as a consequence the lowest factor of safety. This indicates the importance of choosing the correct shear strength parameters (and consequently the correct testing procedure) which should represent the situation as much accurate as possible. In soil cutting projects, the unloading path due to total stress reduction, being associated in most cases by a later increase in pore water pressure, represents the most interesting case and is the focus of this study.

2.3 Stress path during soil cutting

Figure 4 illustrates the evolution of the stress path in drained conditions at a point near the toe of the designed cutting slope, where ground water level is deep down. Assuming that the final depth of cutting is 5.0m and the coefficient of lateral earth pressure at rest is $K_0 = 0.5$, the initial stresses before cutting and with a horizontal ground level are:

$$\sigma'_1 = \gamma \times z = 16.0 \times 5.2 = 83.2 \text{ kPa}; \quad \sigma'_3 = K_0 \times \sigma'_1 = 0.5 \times 83.2 = 41.6 \text{ kPa}$$

With the help of Equation (3), the corresponding stress invariants are:

$$p' = \frac{83.2 + 2.0 \times 41.6}{3.0} = 55.47 \text{ kPa};$$

$$q = \sqrt{\frac{1}{2} [(83.2 - 41.6)^2 + (41.6 - 41.6)^2 + (41.6 - 83.2)^2]} = 41.6 \text{ kPa}$$

This gives the first point of the stress path in in $p' - q$ plane with coordinates (55.47, 41.6). In the previous calculations, the soil is assumed to have a bulk unit weight of $\gamma = 16.0 \text{ kN/m}^3$ and the studied point is at a depth $z = 5.2 \text{ m}$ (0.2m below the final cutting depth).

The gradual reduction in total stresses due to excavation in front of the slope causes a reduction in effective stresses. Consequently, the ultimate soil shear strength is approached following the unloading path. For a point at the designed slope toe, the progress in excavation process causes rotation in principal stresses taking the stress state, ultimately, from an initial plane strain compression state towards the less safe plane strain extension state, see Figure 4 for clarification with numerical values.

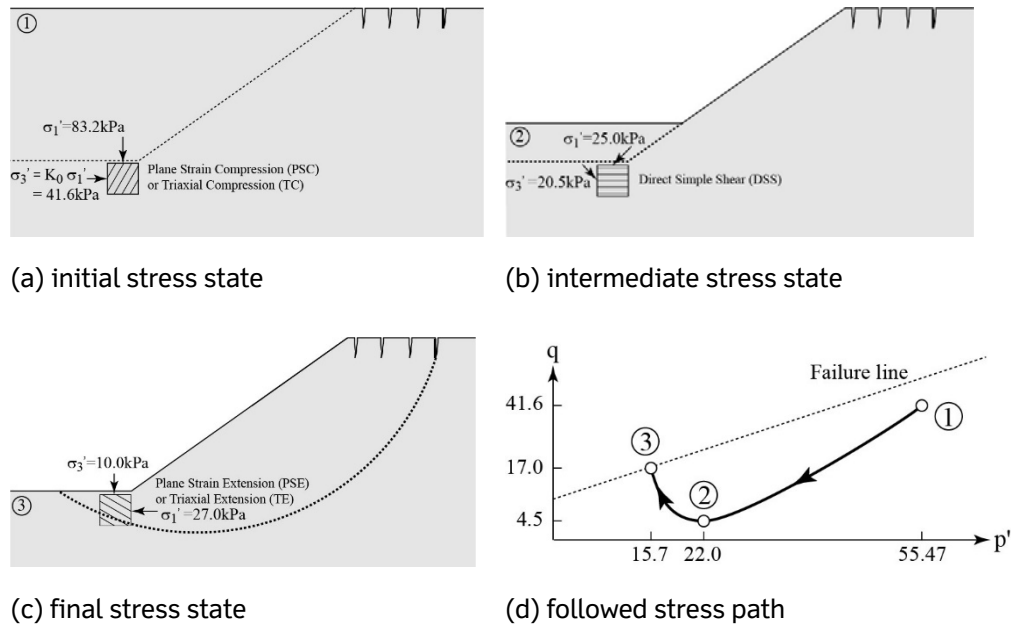


Figure 4. Principal stress rotation and stress path during cutting process at the toe of the slope.

In fact, in practical applications the failures triggered by effective stress reduction prevails. As mentioned before, this reduction in effective stresses could happen due to reduction in the applied total stresses (cutting, excavation etc.), due to increase in pore water pressure or a combination of all these factors. Practical experiences (Kankare, 1969; Lambe, 1997) show that most of the failures happen due to the increase in pore water pressure though. This opens up the discussion on how to determine the role of pore water pressure, how to calculate it and how to take it into account in the calculations (drained and undrained behaviour).

2.4 Stress state along the slip surface

Following similar logic to that in the previous section, the prevailing final stress state at certain locations along a slip surface is depicted in Figure 5. The upper part is dominated by plane strain compression stress state, the mid part is well represented by direct simple shear and at the lower part of the slope near the toe, plane strain extension stress state prevails. The major principal stress direction at failure along the slip surface is also shown in Figure 5. It seems by comparison that for loading problems, the plane strain compression part of the slope would be the most stressed one and as such higher shear strength can be expected. In contrary, in cutting situation the confining pressure at the slope toe is reduced, rendering the soil in the plane strain extension dominated state with lower shear strength. The increase in pore water pressure reduces the effective stress everywhere in the affected region.

The previous discussion has direct consequences on the choice of strength parameters for stability analysis which would be very much problem-type dependent. However, according to Ladd and Foott (Ladd and Foott, 1974) one might use an average shear strength parameters from triaxial compression test (TC) and triaxial extension test (TE) or alternatively, use the shear strength parameters coming from direct simple shear test (DSS) as an average value directly.

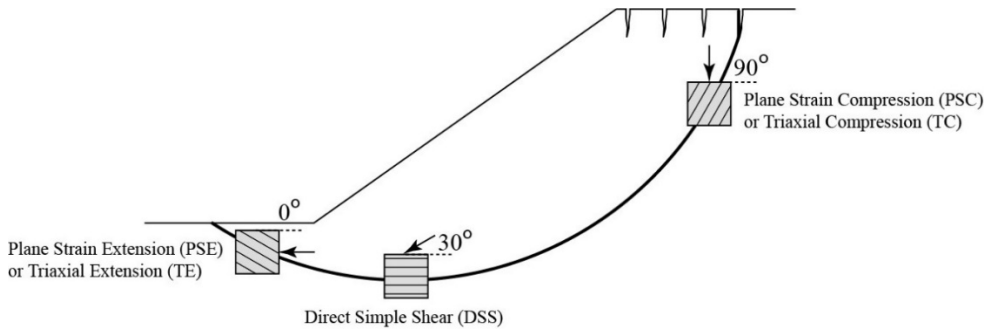


Figure 5. Stress state and direction of major principal stress along slip surface at failure.

Among in-situ geotechnical experiments, the vane shear test provides the best undrained shear resistance values that fit well the simple direct shear results, see Figure 10 (a). As such, the vane shear test results represent an acceptable alternative in absence of DSS data.

In general, it seems that the errors coming from determining the suitable shear strength (and accordingly shear properties) are much more affecting the reliability of the calculations compared to the method used to determine the mobilized stresses in the soil body (method used for analysis).

3 Consideration of drained and undrained behaviour

In drained conditions, changes in external loading do not generate changes in pore water pressure. That is due to high soil permeability or in some case due to the slow rate of loading. In contrary, under undrained conditions, the soil low permeability or the fast rate of loading does not allow the water to flow into or out of the soil and consequently excess pore water pressure builds up. For practical purposes, the clay can be considered undrained immediately after loading (unloading). To distinguish which type of behaviour should one concentrate on, the following criteria can be employed (Duncan et al., 2014; Vermeer and Meier, 1998) by estimating the dimensionless time factor, T :

$$T = \frac{C_v t}{D^2} = \frac{k E_{oed} t}{\gamma_w D^2} \quad (4)$$

where C_v is the coefficient of consolidation, t is construction time and D is the length of drainage path. The symbols k , E_{oed} and γ_w denote permeability, constrained compression modulus and water unit weight, respectively.

If $T > 3.0$ (or 0.4 according to (Vermeer and Meier, 1998)) then it is reasonable to treat the material as a drained material only. If $T < 0.01$ then the material can be treated as undrained only. However, if $0.01 < T < 3.0$ (0.4) then both types of behaviour should be considered (Duncan et al., 2014). If no information is available about T then the materials with permeability $k > 10^{-6}$ m/s is considered as drained for normal rate of loading whereas for $k < 10^{-9}$ m/s the material is undrained.

It is worth noting that the above criteria are developed for loading problems such as embankment construction on soft clays. However, for unloading problems such as road-cutting, the soil removal causes soil swelling which, under undrained conditions, generates negative excess pore water pressure (suction). This negative excess pore pressure temporarily increases the undrained shear strength. In this case, the following consolidation is the phase of negative excess pore water pressure dissipation. Given that the undrained shear strength used in the analysis is measured at initial conditions before cutting, the calculated safety factor will be conservative during consolidation process. To take that into account, the authors propose that the time t_{90} needed for 90% of consolidation to take place ($T = 0.848$) is used as a limit between the undrained and drained conditions, where:

$$t_{90} = 0.848 \frac{D^2}{C_v} \quad (5)$$

If t_{90} is longer than the planned time then undrained conditions control the design. As an example, for a clay coming from Liminka area with $k \approx 10^{-9}$ m/s and consolidation coefficient $C_v \approx 30.0$ cm²/hr, by assuming an average length for the drainage path $D = 5.0$ m, one ends up with $t_{90} \approx 10.0$ months. That is a longer time than the planned cutting time (usually 2-3 weeks). As such, the undrained behaviour of clay controls the early stage design of the cutting but should be followed by a drain analysis for the long working conditions of the cutting slope.

There is a transitional period between t_{90} and the end of consolidation t_{99} ($T = 3.0$) where drained conditions is considered to be controlling the design. The transition from undrained to drained conditions is a complicated process. If there is any doubt about the material behaviour during this period of time, it is advised to check stability for both conditions or employ more advanced methods (e.g. finite element method). The evolution of excess pore water pressure and safety factor after cutting is clarified in Figure 6(a) and (b), respectively.

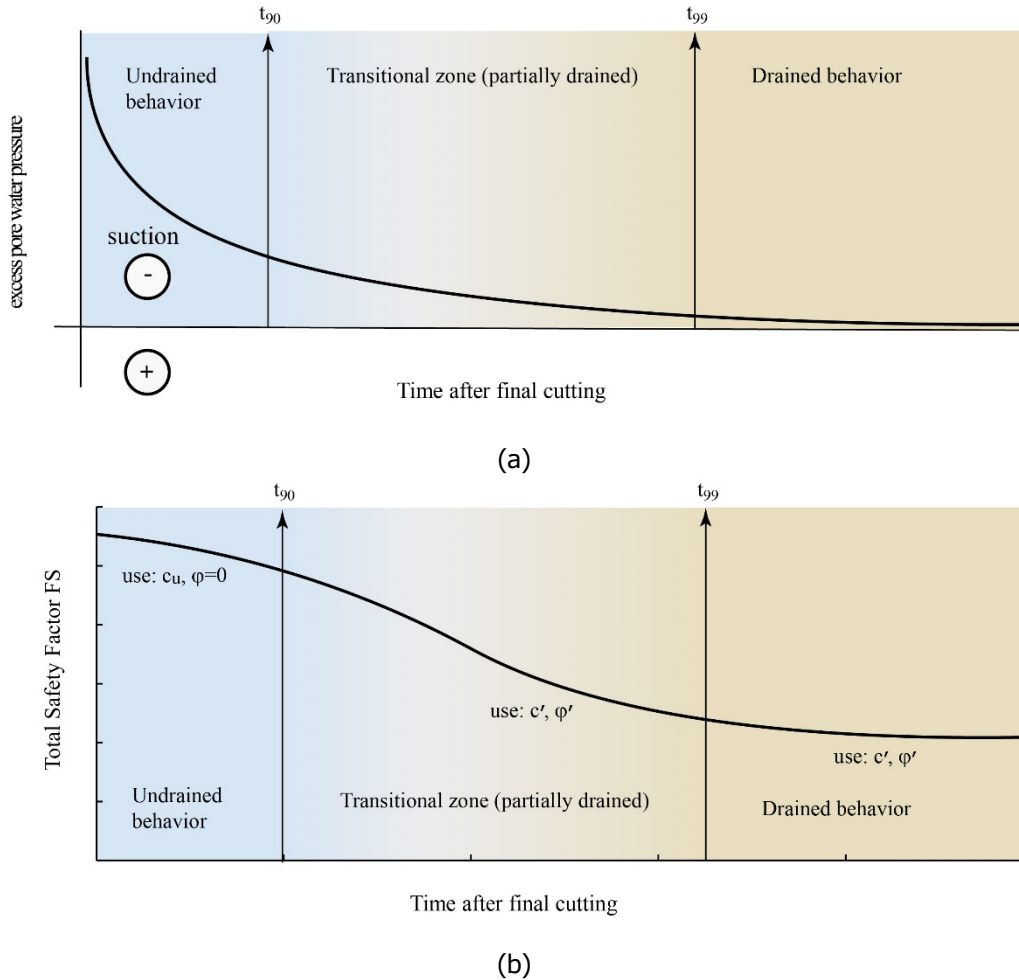


Figure 6. Undrained and drained conditions after final cutting: a) evolution of negative pore water pressure with time; b) evolution of factor of safety.

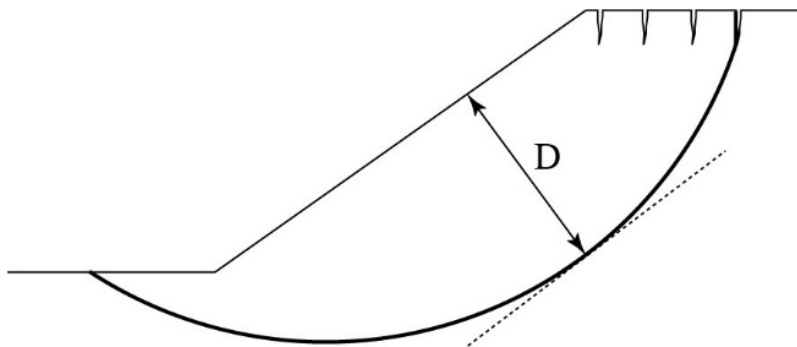


Figure 7. Drainage path length D in case of cutting.

The length of drainage path is taken as the distance between the closest drainage boundary to the point of study. The point with longest drainage path is considered as the critical point; see Figure 7 for direction on how to estimate D in case of cutting.

Figure 8 reports the time needed to reach t_{90} as a function of the length of drainage path D in case of Liminka clay. The figure dictates that reducing the drainage path to 1.0-2.0m would reduce t_{90} to the project time scale of 0.5-1.5 months. That could be achieved, if feasible, by installing drains that are spaced in a form satisfies the previous condition for drainage path length.

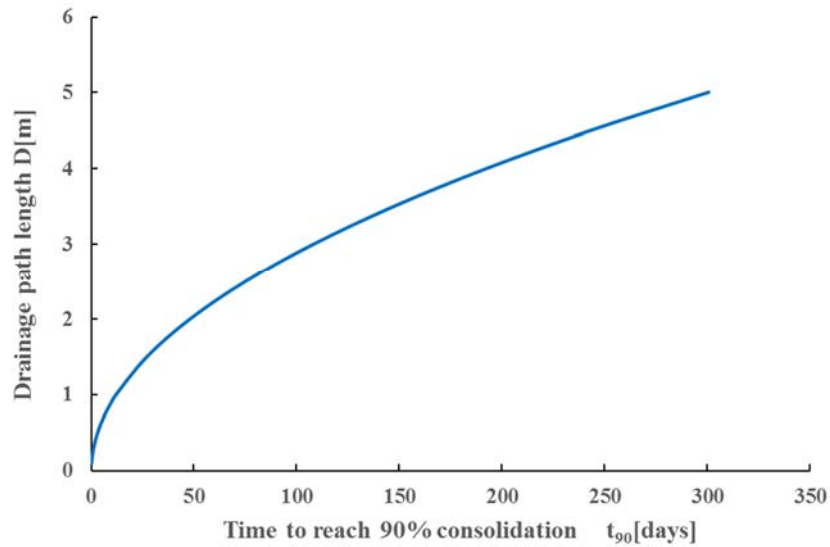


Figure 8. Required time to reach t_{90} as a function of available drainage path length.

4 Estimation of soil shear strength parameters

Triaxial compression test is mostly used in geotechnical practice to determine the soil shear strength parameters. It is also common to conduct the direct shear test but basically for sand testing. These tests are usually performed in combination with in-situ tests to derive suitable parameters for soil shear strength and stiffness. Considering the isotropically consolidated undrained triaxial test (CICU), Figure 9 and Formulas (6) show how to interpret the CICU results to determine shear strength parameters: c_{uc} , φ' and c' being the undrained shear strength in compression, effective friction angle and effective cohesion, respectively. They can be estimated using the triaxial testing data by employing the following formulas:

$$M = \frac{6 \sin \varphi'}{3 - \sin \varphi'} \xrightarrow{\text{yields}} \varphi' = \arcsin \left(\frac{3M}{6 + M} \right); \quad c' = \frac{q_o(3 - \sin \varphi')}{6 \cos \varphi'} \quad (6)$$

where M and q_o are measured directly from the graph after plotting the testing results in the $p' - q$ plane, see Figure 9.

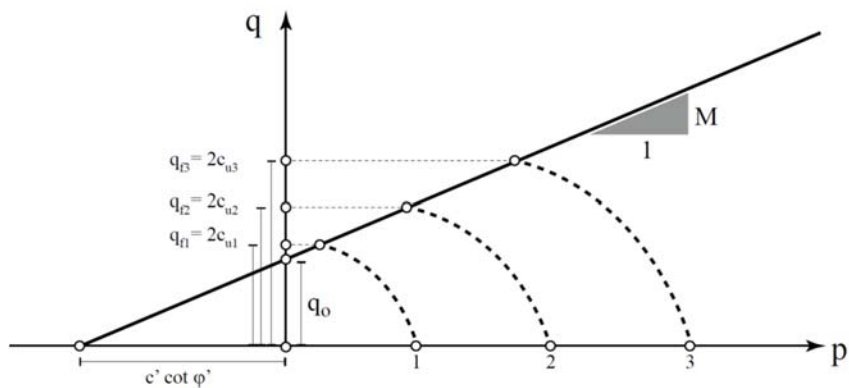


Figure 9. Graphical representation of the undrained compression triaxial tests.

4.1 Sources of uncertainties in estimating undrained shear strength in case of soft soil

In investigating the undrained shear strength of soft clay, researchers agree on some particular points that form the source of error upon estimating the undrained shear strength. These points can be summarized as follows (Ladd and Foott, 1974):

1. Sample disturbance

The sampler, sampling technics, transportation, storage, specimen preparation and the relief in confining stress are all sources of sample disturbance (Mataić, 2016). That causes a reduction in the value of the estimated undrained shear strength, which is estimated to be around 20%-50% if compared to that in the field (Ladd, 1971).

2. Strength and stress-strain anisotropy

Given the dominant stress states along the failure slip surface as introduced in Section (2.4), the experimental data shows that clay undrained shear strength is different for each followed stress path. The data in Table 1 show that the highest value for undrained shear comes from triaxial compression test making the adoption of values coming only from triaxial compression testing optimistic with a range of 1.5-2.5 of overestimation in comparison to the values obtained from other testing types.

Table 1. Undrained strength anisotropy of normally consolidated

(a) Boston blue clay after (Ladd and Foott, 1974)

Type of test	Ratio: c_u/c_{uTC}
Triaxial compression (TC)	1.0
Triaxial extension (TE)	0.47
Direct-simple shear test (DSS)	0.61

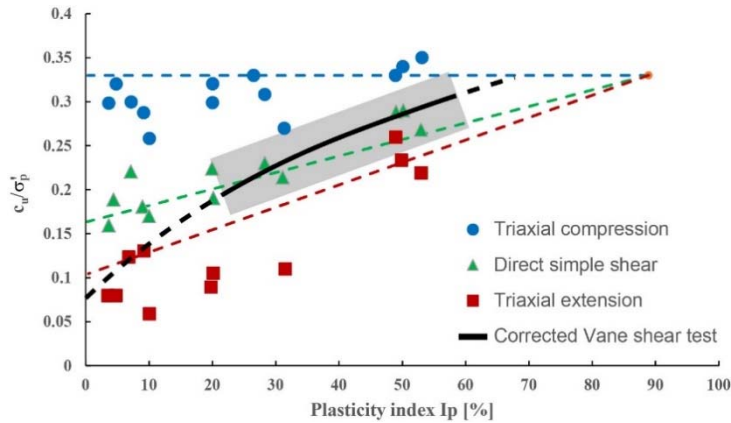
(b) Nordic soft soil after (BJERRUM, 1973)

Type of test	Ratio: c_u/c_{uTC}
Triaxial compression (TC)	1.0
Triaxial extension (TE)	0.45
Direct-simple shear test (DSS)	0.62

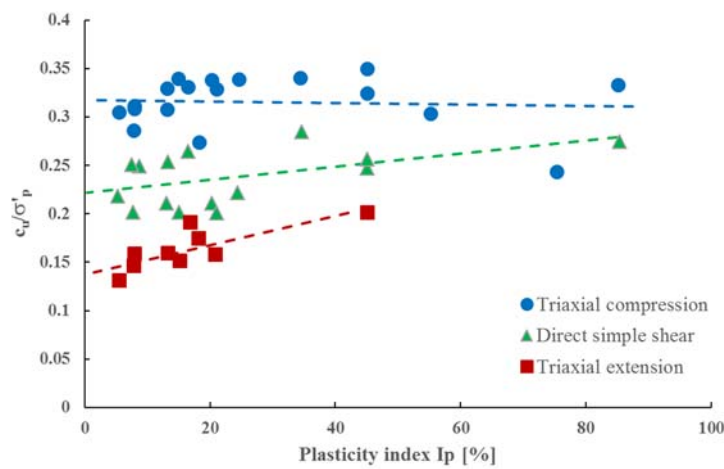
Table 2. Undrained strength anisotropy of different types of clays (BJERRUM, 1973)

Type of soil	Index properties [%]				Triaxial tests c_u/σ'_p		Simple shear	Vane shear tests c_u/σ'_p	
	w	w _L	w _p	I _p	Comp.	Exten.	c_u/σ'_p	Observed	Corrected
Bankok clay	140	150	65	85	0.70	0.40	0.41	0.59	0.47
Matagami clay, Canada	90	85	38	47	0.61	0.45	0.39	0.46	0.40
Drammen plastic clay	52	61	32	29	0.40	0.15	0.30	0.36	0.30
Vaterland clay, Oslo	35	42	26	16	0.32	0.09	0.26	0.22	0.20
Studentartunden, Oslo	31	43	25	18	0.31	0.10	0.19	0.18	0.16
Drammen lean clay	30	33	22	11	0.34	0.09	0.22	0.24	0.21

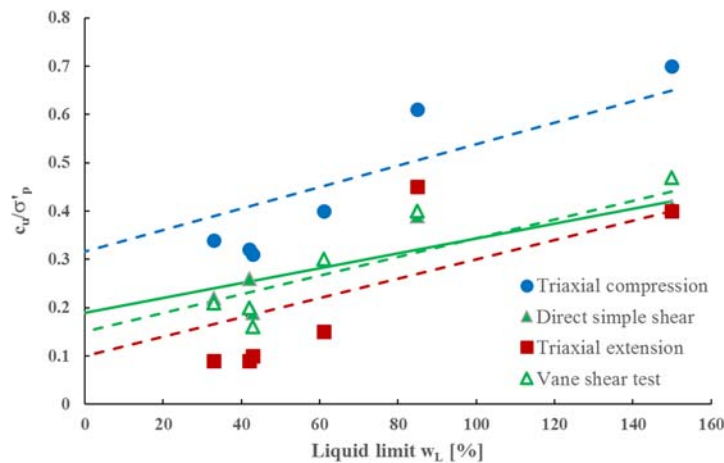
Similar observations are provided by (BJERRUM, 1973; JAMIOLKOWSKI, 1985; Larsson, 1980) who collected data of undrained shear test for several clays as shown in Table 2 and Figure 10. *Most interesting is that the anisotropy is more pronounced in low plasticity clay and silt.* The data in Figure 10(a) by Larsson (1980) demonstrates the good agreement between the vane shear test results and the direct simple shear measurements in the practical range of soil plasticity. That confirms the validity of adopting the undrained shear strength from vane test as an average value for cutting stability calculations.



(a) Undrained strength anisotropy in Scandinavian inorganic clays (Larsson, 1980)



(b) Undrained strength anisotropy for normally consolidated clays from different locations in the world (JAMIOLKOWSKI, 1985)



(c) Undrained strength anisotropy in normally consolidated soft clay including some Nordic soils (BJERRUM, 1973), corresponding to data in Table 2.

Figure 10. Undrained strength anisotropy for different normally consolidated soils.

For Finnish clays (D’Ignazio et al., 2016; D’Ignazio and Länsivaara, 2016) provide useful correlations for estimating undrained shear strength which designer can rely on in absence of experimental data.

Table 3. Reference parameters to be used with Equation (7) in case of data absence

Type of test	$\frac{c_{uNC}}{\sigma'_v}$	m
Plane strain compression	0.265	0.79
Plane strain extension	0.16	0.88
Direct-simple shear test (DSS)	0.25	0.77
Average	0.225	0.81

For overconsolidated clays, the undrained shear strength can be estimated depending on its normally consolidated value c_{uNC} by employing the following correlation:

$$\frac{c_u}{\sigma'_v} = \frac{c_{uNC}}{\sigma'_v} OCR^m; \quad (7)$$

where σ'_v is the vertical effective stress and m is a parameter depending on the testing type. If no experimental data is available about c_{uNC} the values provided in Table 3 by (Ladd and Foott, 1974) can be employed.

3. Strain-rate effects

Triaxial tests suggest that each strain rate decrease in log cycle is accompanied typically by decrease by $10 \pm 5\%$ in undrained shear strength (Ladd and Foott, 1974).

To account for the mentioned uncertainties in geotechnical practice when using the vane shear test, (BJERRUM, 1973) proposed a strength reduction factor which can be estimated using Figure 11 as a function of clay plasticity index. Instead, if one starts by liquid limit w_L as a reference value, one might get a slightly different correction factor based on Finnish practice, as given in Figure 12.

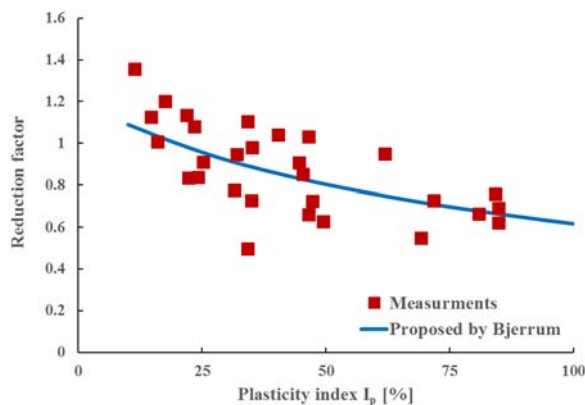


Figure 11. Bjerrum's factor for correcting vane shear test data after (Duncan et al., 2014).

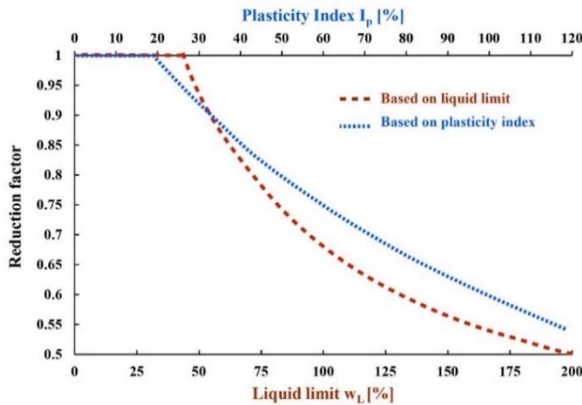
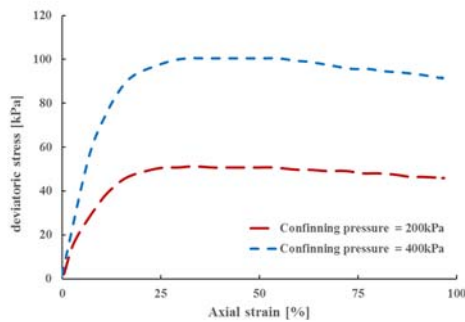


Figure 12. Finnish factor for correcting vane shear test results (SGY, 1999)

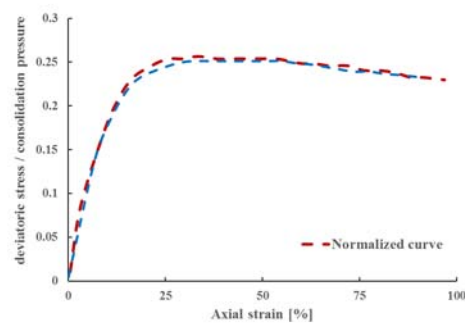
In principle, Figure 12 can also be used to migrate from liquid limit w_L to the corresponding estimated plasticity index I_p and vice versa. However, applying that in a real practical application, as will be discussed later, resulted in a difference of about 10% less in the reduction factor based on w_L value in comparison to that based on I_p value.

4. Normalized behaviour

It is well established that most of clays show the so-called normalized behaviour in the sense that plotting shear curve for different consolidation pressures but with the same OCR gives similar overlapped curves when plotted normalized with the consolidation confining pressure, see example in Figure 13, this feature allows to predict the behaviour of other samples under different confining pressure.



(a)



(b)

Figure 13. Example of normalized behaviour in triaxial compression: a) actual measured curves; b) normalized curves (Ladd and Foott, 1974)

4.2 SHANSEP method (Stress History and Normalized Soil Engineering Properties)

To account for all of the previous factors and reduce the number of required shear tests (Ladd and Foott, 1974) proposed the following procedure to estimate the value of undrained shear strength along the depth of soil profile, the procedure is summarized as follows:

1. A soil investigation is conducted, and a sufficient number of undisturbed samples are obtained at several depths of the soil.
2. Series of one-dimensional consolidation tests are ran on samples from various depths to define the over-consolidation ratio (OCR = maximum past consolidation pressure / the effective vertical stress at the required depth) versus depth in the soil profile.
3. Decide which shear test models best the situation in field. *In road cutting situation, the direct simple shear test DSS is a good choice.* Series of $\overline{CK_oU}$ (K_o consolidation followed by undrained shear) DSS test series are performed with OCR values of 1, 1.5, 2.5 and 4. Often, this testing program requires that the test specimens are consolidated to stresses well above those found in the field and then rebounded to lower levels of effective stress to obtain the desired OCRs.
4. Use tests results in step 3 to estimate the values of the ratio of c_u/σ'_v versus OCR and plotted them on a chart similar to that in Figure 14.
5. The OCR profile as estimated in step 2 is then used to obtain the undrained strength ratio from the chart constructed in step 4. Finally, the undrained shear strength is computed through multiplying the vertical effective stress by the strength ratio.

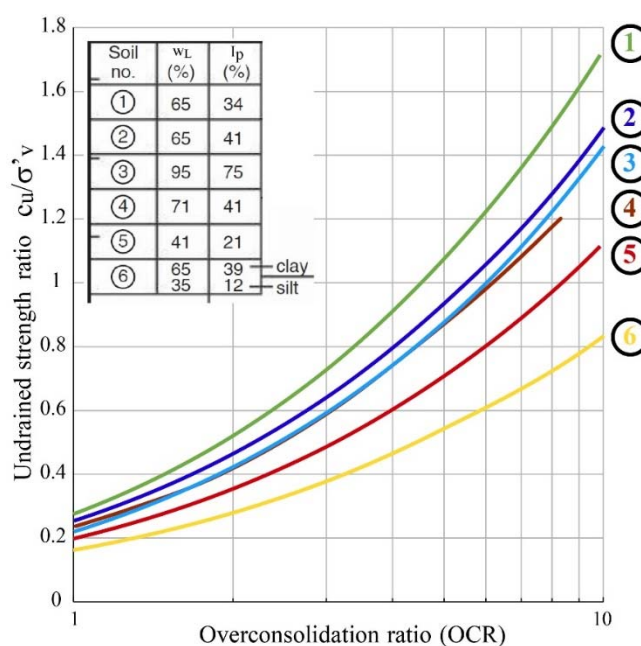


Figure 14. Variation of c_u/σ'_v with OCR for different clays measured in undrained DSS test after (Ladd and Foott, 1974)

5 The Limit Equilibrium Method (LEM) for slope stability

5.1 Definition of safety factor and LEM fundamentals

The Limit Equilibrium Method assumes that the soil is at the fringe of failure (just-stable) and the soil has reached its maximum shear resistance. The total factor of safety F is defined in terms of soil shear strength as:

$$F = \frac{\tau_f}{\tau_{mob}}, \quad (8)$$

where τ_{mob} is the mobilized shear strength and τ_f is the soil shear strength at failure (available, maximum or equilibrium shear strength). Accordingly, the mobilized shear force $T_m = \tau_{mob}L$ within length L , can be written in terms of factor of safety and available shear strength as:

$$T_m = \frac{\tau_f L}{F} \quad (9)$$

In most Limit Equilibrium Methods, the soil shear strength is assumed to be expressed by Mohr-Coulomb failure criterion, as introduced in Section 2.1, with:

$$\tau_f = c' + \sigma'_n \tan\phi' = c' + (\sigma_n - p_w) \tan\phi' \quad (10)$$

To calculate the safety factor, a slip surface (sliding surface) is assumed and static equilibrium equations are exploited to calculate the stresses along the slip surface. Eventually, the factor of safety is estimated using Equation (8). In LEM, the factor of safety is assumed to be *the same at every point along the slip surface*. The procedure is repeated for a number of different slip surfaces and the one, which produces the lowest safety factor, is termed as the *critical slip surface*, which should be unique for each problem. In what follows, only the method of slices is discussed among the other available LE methods (Logarithmic Spiral, Swedish Circle, etc.). The factor of safety can be calculated using *slices methods* by employing the static equilibrium equations:

1. equilibrium of vertical forces
2. equilibrium of horizontal forces
3. equilibrium of moments about a chosen reference point.

Figure 15 shows the used slices with the acting forces. The corresponding balance equations are:

Moment equilibrium:

$$\sum_{i=1}^n T_{mi}R - \sum_{i=1}^n W_i X_i + P_L Y_L - P_R Y_R = 0, \quad (11)$$

where T_{mi} is the mobilized shear force at the base of the i^{th} slice and n is the total number of slices. The total weight of the slice is denoted by W . The external water force

in the cracks and at the slope toe is P . The subscripts R and L are used to indicate right side and left side, respectively.

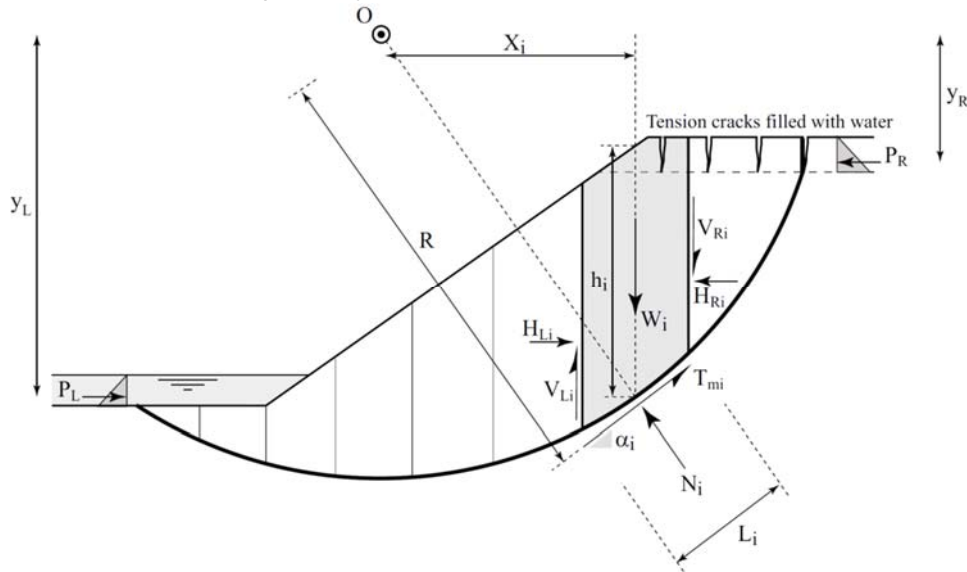


Figure 15. Forces acting on a slice of a slip surface in the limit equilibrium method.

The moment arms of the previously mentioned forces are shown in the Figure 15 and denoted as R , X_i and y , respectively. The inter-slices forces H and V do not appear explicitly in Equation (11) as their overall summation must vanish.

Horizontal forces equilibrium:

From Figure 15 it is possible to write the following balance equation for acting horizontal forces:

$$\sum_{i=1}^n T_{mi} \cos \alpha_i - \sum_{i=1}^n N_i \sin \alpha_i + P_L - P_R = 0, \quad (12)$$

where α_i is the angle between the tangent to the base of slice i at its centre and the horizon. The symbol N stands for the normal force on the base of the slice. Note that the inter-slice forces must cancel.

Vertical forces equilibrium:

The vertical equilibrium is exploited to derive a formula to calculate N_i

$$N_i = \frac{W_i + (V_{Ri} - V_{Li}) - \frac{L_i c'}{F} + \frac{L_i p_w \tan \phi' \sin \alpha_i}{F}}{\cos \alpha_i + \frac{\tan \phi' \sin \alpha_i}{F}} \quad (13)$$

The inter-slice forces V_{Ri} and V_{Li} appear explicitly for the first time and here lie most of the differences among the used slices methods in practice. Some assumptions are required concerning the distribution of these forces, which yields different method with different assumptions. For example Morgentern-Price method (Fredlund et al., 1981; Fredlund and Krahn, 1977) assumes that inter-slice forces are related to the horizontal forces at the slice sides through a function $f(x)$ whose value changes according to the position x . The so-called Half-Sine function is mostly used in this case with a maximum value of 1.0 and minimum of 0.0.

$$V = \lambda f(x)H \quad (14)$$

where λ is a constant representing the percentage of the used function in decimal form. The normal forces H are solved using an integration procedure that starts at a chosen end of the slope.

$$H_{Li} = H_{Ri} - \frac{L_i \cos \alpha_i}{F} (c' - p_w \tan \varphi') + N_i \left(\sin \alpha_i - \frac{\tan \varphi' \cos \alpha_i}{F} \right) \quad (15)$$

By noticing that the first slice at the right hand side of the slope has $H_{Ri} = 0.0$, a recursive procedure can be used to find the value of normal forces at any slice in the slope. As can be noticed for example in Equations (13) and (15), the problem is non-linear as the targeted value of the safety factor F appears as part of the solution and iterative procedure is needed in this case.

Table 4 (Krahn, 2003) summarizes the commonly used slices methods and the equilibrium equations that are satisfied during the solution. It shows that both Spencer and Morgenstern-Price methods meet all equilibrium requirements and as such they are *the most recommended to be used in practice* with more advantage to the latter which allows for more flexibility in defining the inter-slices forces. However, all of these methods use some assumptions to render the problem statically determinate.

Table 4. Summary of the most used LE methods and the corresponding assumptions.

Slice method	Moment equilibrium	Horizontal equilibrium	Inter-slice normal	Inter-slice shear	Inclination of V/H
Ordinary (Swedish)	✓	✗	✗	✗	No force
Bishop	✓	✗	✓	✗	Horizontal
Janbu	✗	✓	✓	✗	Horizontal
Spencer	✓	✓	✓	✓	Constant
Morgenstern-Price	✓	✓	✓	✓	Variable

5.2 About slip surface assumption

A circular slip surface is commonly used in practice, which is an acceptable assumption if the whole slip surface would lie in one homogeneous cohesive soil layer. However, this assumption should be treated carefully as soil-layering might tremendously affects the slip surface shape and therefore yields very different factor of safety.

5.3 Shear strength in the unsaturated zone

In the unsaturated zone the negative pore water pressure increases the soil strength (a soil in dry conditions has higher shear strength than in the fully saturated conditions). Usually this additional shear resistance is neglected as a conservative action. However, if the designer decides, based on enough engineering evidences, to include the effect of suction in stability calculations the following procedure can be adopted.

In the unsaturated zone, the normal Terzaghi's effective stress measure does not hold anymore and the measure modified by (Bishop, 1959) can be adopted. Accordingly, the working effective stresses in the unsaturated region is estimated as:

$$\sigma' = \sigma - p_a + \chi(p_a - p_w) \quad (16)$$

where χ is a factor depending on the soil degree of saturation S_r . The symbol p_a denotes pore air pressure. By definition, soil suction s equals the difference between pore air pressure and pore water pressure ($s = p_a - p_w$). For practical applications concerning normal isothermal slope stability calculations, the pore air pressure can be considered to remain atmospheric with $p_a = 0$. The parameters χ in Equation (16) can be replaced by the degree of saturation S_r yielding:

$$\sigma' = \sigma - 0.0 + S_r s = \sigma + S_r s \quad (17)$$

Considering Mohr-Coulomb failure criterion and replacing the normal effective stress by the one in Equation (17) the extended version for unsaturated state reads:

$$\tau_f = c' + (\sigma_n + S_r s) \tan\phi' = c' + S_r s \tan\phi' + \sigma_n \tan\phi' \quad (18)$$

As it is clear, negative pore pressure in the unsaturated zone adds a new cohesion component to the shear strength usually known as *apparent cohesion* or *capillary cohesion* $c^s = S_r s \tan\phi'$. As an example, for a water table at a depth of about 1.5m with an average negative pore water pressure of -10kPa in the unsaturated region, the corresponding suction $s = p_a - p_w = 0.0 - (-10.0) = 10.0 \text{ kPa}$. Given an average degree of saturation of about $S_r = 0.8$, the estimated additional capillary cohesion would be $c^s = 0.8 \times 10.0 \times \tan 25^\circ = 3.7 \text{ kPa}$. Here, the soil is assumed to have an effective internal friction angle of 25° . More about handling the shear strength in unsaturated zone can be found in (Abed, 2008; Abed and Sołowski, 2017; Fredlund and Rahardjo, 1993).

5.4 Strength and weaknesses of LEM analysis

The Limit Equilibrium method is widely used in practice. Some of the strong and weak points about the method are listed below:

- **Strength**
 - The method is well-established in practice with very good experience in employing it in practical applications.
 - The method is easy to understand and the mathematical background is not heavy.
 - The number of parameters to be used is reasonable.
- **Weakness**
 - Potential failure surface should be assumed beforehand.
 - Stress field is not realistic.
 - No information about the soil before failure is considered.
 - Consideration of excess pore pressure is tricky in undrained conditions.

6 The Finite Element Method (FEM) in slope stability calculations

To overcome the shortcomings of the Limit Equilibrium Method in slope stability analysis, one might employ the finite element method. As the application of such advanced method is not the focus of this report, only a short introduction about the possible use of this method for stability calculations is given.

6.1 About FEM

The Finite Element Method is employed in this report to solve the mechanical equilibrium and water mass balance equations. In this method, the subsoil is divided into many sub-regions called “finite elements”. They are connected at a discrete number of points being known as “nodes”. Such elements, which generally take simple shapes (e.g. triangular or rectangular) are then assembled to represent a solution domain of arbitrary geometry. The unknown variables to be solved are calculated at the nodes. Using special mathematical methods, a matrix expression is developed to relate the nodal variables of each element. The resulting matrix is commonly referred to as “element matrix”. The element matrices are combined or assembled to form a set of algebraic equations that describes the entire global system. The coefficient matrix of this final set of equations is called the “global matrix”. Finally the set of algebraic equations is solved to get the nodal values of the unknowns. The above procedure is very general and can be applied for a wide variety of problems, more details about the application of finite elements to solve geotechnical problems can be found in (Abed, 2008; Potts et al., 2001). For slope stability analysis, many commercial softwares offer the possibility to perform the so-called *Shear Strength Reduction* calculation, which eventually allows the global safety factor to be estimated.

6.2 Strength reduction method

During the strength reduction calculations, the computer code performs the following iterative steps:

1. The shear strength parameters of the soil are reduced by a certain factor (*Strength Reduction Factor SRF*) where:

$$SRF = \frac{c'}{c'_{reduced}} = \frac{\tan\phi'}{\tan\phi'_{reduced}}$$

2. The finite element stress calculations are performed using the reduced shear strength parameters.
3. If the calculations converge, the shear strength parameters are reduced further and step 2 is repeated.
4. This iterative procedure continues with further reduction in strength parameters until the slope fails (the computations does not converge).
5. The slope safety factor is estimated as the Strength Reduction Factor (SRF) at failure.

The FEM with strength reduction method allows for automatic capturing of the failure surface without any presumptions. The Finite element method itself allows for generating reasonable initial stress field and deformation history before reaching failure. In principle, any type of mechanical or hydraulic boundary conditions can be employed using this method. The full discussion about the capabilities and limitations of this method is out of the scope of this report; however, the following subsection gives some recommendations that should be kept in mind when using this method.

6.3 Recommendations for the use of FEM in slope stability analysis

- If possible, do fast LEM calculations to establish a primitive understanding of the problem and safety ranges.
- Always start with a simple model to understand the general response of the soil under the considered boundary conditions, before adding details that are more complicated.
- For sloping surfaces, the simple calculation of the initial stress field depending on the coefficient of soil lateral pressure at rest K_0 should be avoided. Instead, the full history of loading and unloading should be regenerated or the current situation of the slope should be analysed under the actual gravity loading. That should be done to capture the rotation in the principal stress directions and more realistic stress field.
- A mesh convergence study should be always performed to be sure that the number of the used finite elements is sufficient for results that are accurate enough.
- For stability calculations in drained conditions, Mohr-Coulomb failure criterion can be used.
- The simple linear elastic-perfectly plastic Mohr-Coulomb model should be avoided in undrained stability calculations based on effective stresses, as it overestimates the undrained shear strength of the soil.
- For undrained stability analysis using the effective stress concept, more advanced constitutive models that correctly accounts for the development of excess pore water pressure should be adopted (for example Hardening Soil model or S-Clay1 family of models (Karstunen et al., 2005)).

7 Pore water pressure estimation

The variation in pore water pressure reflects directly on the shear strength of the soil by varying the effective stresses. The water pressure is usually estimated by solving the mass balance equation of water in soil (Freeze and Cherry, 1979). In LEM calculations, the groundwater flow calculations and the slope stability are solved in a decoupled manner in the sense that seepage calculations are done first then the resulted pore water pressure is imported to conduct the slope stability calculations. No simultaneous interaction between the mechanical deformation and the flow field is possible. For undrained calculations, the water flow is not relevant in conjunction with LEM. However, for drained analysis it is of major importance in transient and in the final steady state. One of the most important parameters in this calculation is the saturated permeability of the soil. It is recommended that the permeability is estimated in the field by employing suitable test (in-situ falling head test or CPTU dissipation test (Robertson, 2010), for example). The permeability can be estimated in the laboratory to a lesser degree of accuracy using special tests like falling head test for soft clay or from consolidation test. In the absence of any experimental data, the following formulas and experimental correlations can be employed to estimate the permeability.

7.1 Estimation of soil permeability

The so-called Kozeny-Carman equation gained good reputation for being able to predict reasonable permeability values (Chapuis and Aubertin, 2003). The equation is given as follows:

$$k = C \frac{g}{\mu_w \rho_w} \frac{e^3}{S^2 G_s^2 (1 + e)} \quad (19)$$

or

$$\log(k) = A + \log\left(\frac{e^3}{S^2 G_s^2 (1 + e)}\right) \quad (20)$$

where g , ρ_w , μ_w and G_s are the gravitational constant, the density of water, the dynamic viscosity of water and the specific weight of solids, respectively. The symbols S , C , A stand for specific surface (m^2/kg) and constants that takes into account the shape and tortuosity of water channels with $A = 0.29 \sim 0.51$ and $C = 0.2 \sim 0.5$ (suggested value is $C = 0.2$ or $A = 0.5$). For fine-grained soil, the specific surface S can be estimated as:

$$\frac{1}{S} = 1.3513 \left(\frac{1}{w_L}\right) - 0.0089 \quad (21)$$

where the liquid limit w_L is estimated as percent [%]. Another option is to use the chart in Figure 16 to estimate the specific surface based on the percentage of fines in the sample and the plasticity index I_P .

In practical applications, part of the soil is usually not fully saturated with certain degree of saturation S_r . In such case, the actual permeability $k(S_r)$ is lower than the fully saturated $k(sat)$ and it can be linked using the formula:

$$k(S_r) = k(sat) \left[\frac{(S_r - S_o)}{(1 - S_o)} \right]^3 \quad (22)$$

where S_o is the residual degree of saturation when the soil is very dry. In absence of any data S_o can be taken as zero.

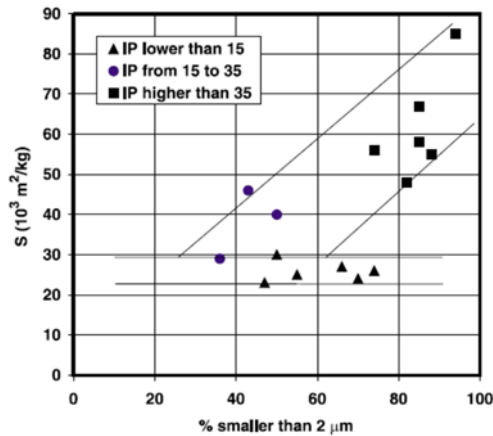


Figure 16. Estimation of specific surface based on fines in the sample and plasticity index I_P (Chapuis and Aubertin, 2003).

For fast preliminary estimation, Table 5 can be used (Terzaghi et al., 1996). In case more soil physical properties are available, the chart in Figure 17 can be exploited to derive a better estimation of the permeability.

Table 5. Ranges for coefficient of permeability

Soil	Coefficient of permeability, k [m/s]	Relative permeability
gravel	$> 10^{-3}$	high
sandy gravel, clean sand, fine sand	10^{-3} to 10^{-5}	medium
sand, dirt sand, silty sand	10^{-5} to 10^{-7}	low
silt, silty clay	10^{-7} to 10^{-9}	very low
clay	$< 10^{-9}$	practically impermeable

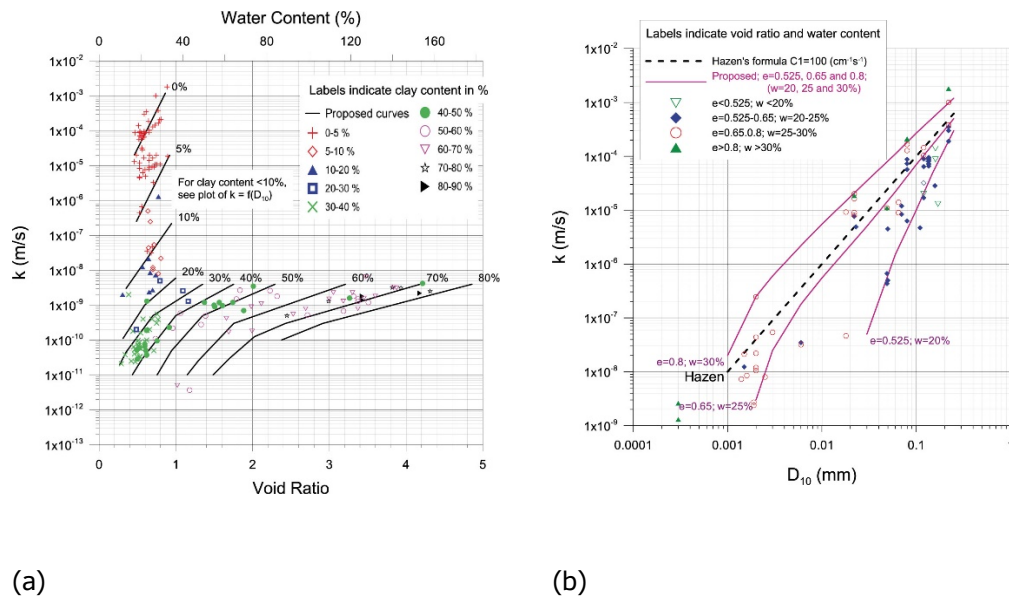


Figure 17. Permeability as a function of D_{10} , void ratio, water content and clay content: a) fine-grained soils; b) coarse-grained soils (Andersen and Schjetne, 2012)

7.2 In-situ pore water pressure measurements

The Charts in Figure 18 show actual total water head measurements (used to calculate the pore pressure) at selected depths together with rain precipitation in three weather stations near to Kimola canal (distances about 20kms). The measurements clearly show the variation in pore water pressure with time. The peak values reflect the high impact of environmental conditions (thawing of snow and rainfall).

What is important in this case is that the measured values turned to be considerably lower than the values that the designer would get by assuming a simple hydrostatic distribution based on phreatic level measurements or even by doing a proper steady state groundwater flow calculations. This has serious consequences on the estimated safety level and the related needed earthwork assessments. As such, it is recommended to equip important projects with an in-situ pore water pressure measuring system. These measurements are exploited by building a realistic pore water pressure profile and employ it directly in the related stability analysis.

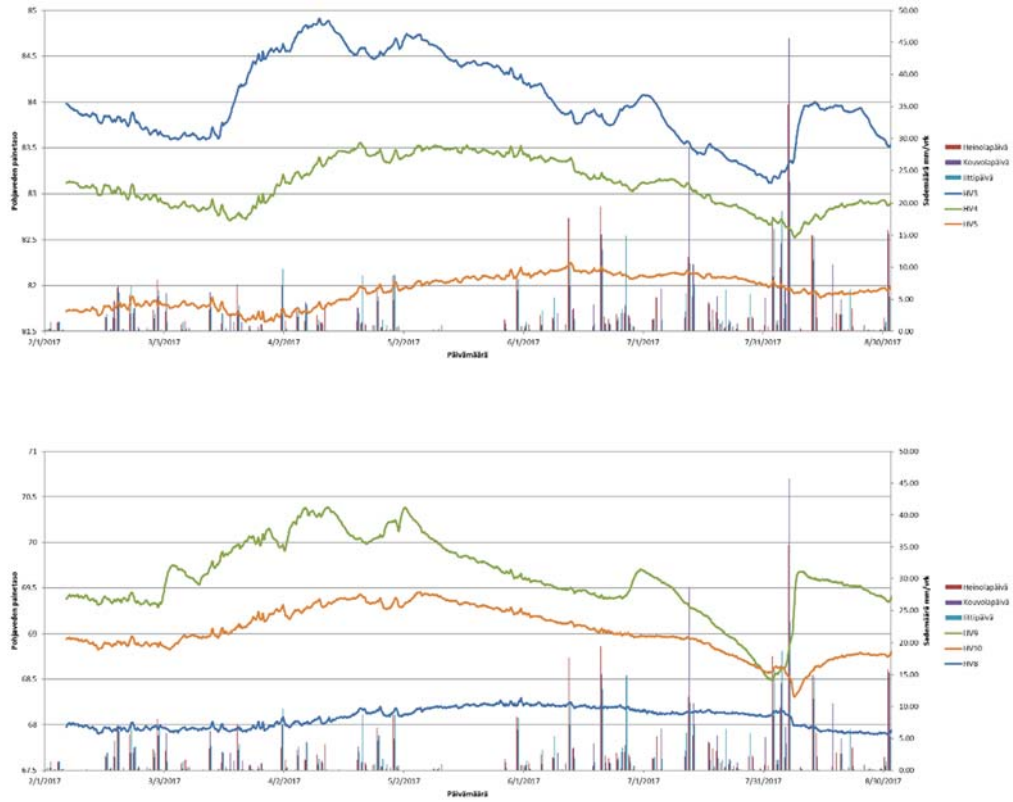


Figure 18. Example of in-situ measurements of total water head and rain precipitation with time at two different locations along Kimola canal.

8 Practical applications

8.1 Tuuliharju location as a master case

8.1.1 Soil profile and soil cutting geometry

Aalto University conducted series of laboratory tests on soils extracted from Liminka. The full details of the testing program, results and result analysis can be found in (Goncharko, 2018). In what follows only summary of the testing findings are listed and employed in the analysis.

The Aalto University testing program concentrated on the upper 7.0 meters of the soil at the site. The deeper soil layers are extracted from data provided by Liikennevirasto. At least for stability calculation, it is believed that the deep layers will not affect dramatically the analysis of the problem. The geometry of the analysed section at Tuuliharju is provided by Liikennevirasto (Liminka-Oulu, Tuuliharjun aks km 734+294 Alikulkuleikkaus, Y1 pl 140). It is worth mentioning that this geometry is the original configuration which has later suffered stability failures. The recent geometry of the section after handling the failure is different with flatter slopes. The soil layering with the main physical properties are showing in Figure 19, Figure 20 and Figure 21.

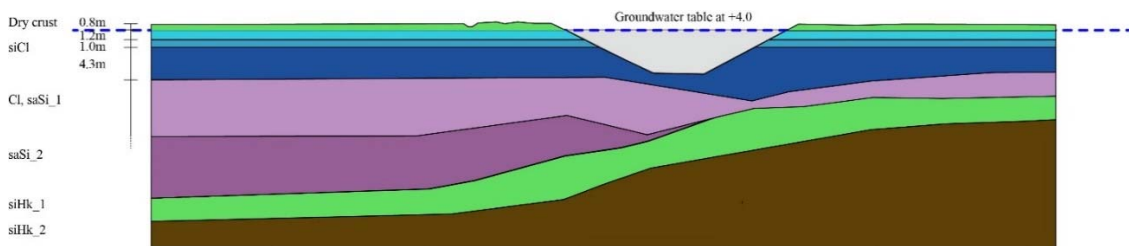


Figure 19. Soil profile and cutting geometry at Tuuliharju site (734+294)

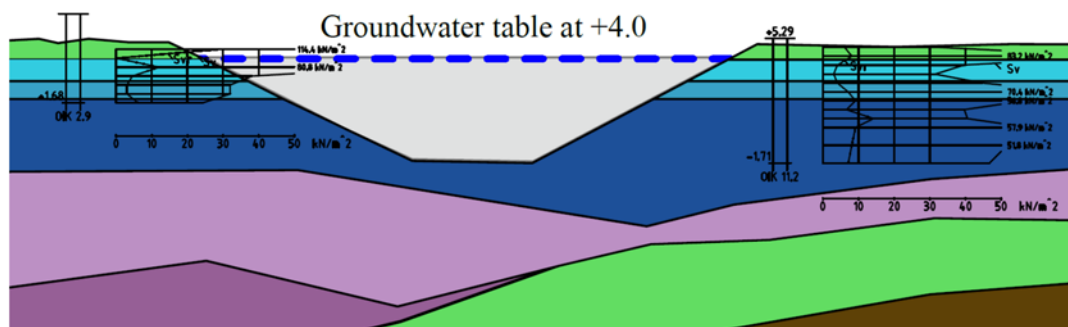


Figure 20. Available vane shear test results at Tuuliharju site (734+294)

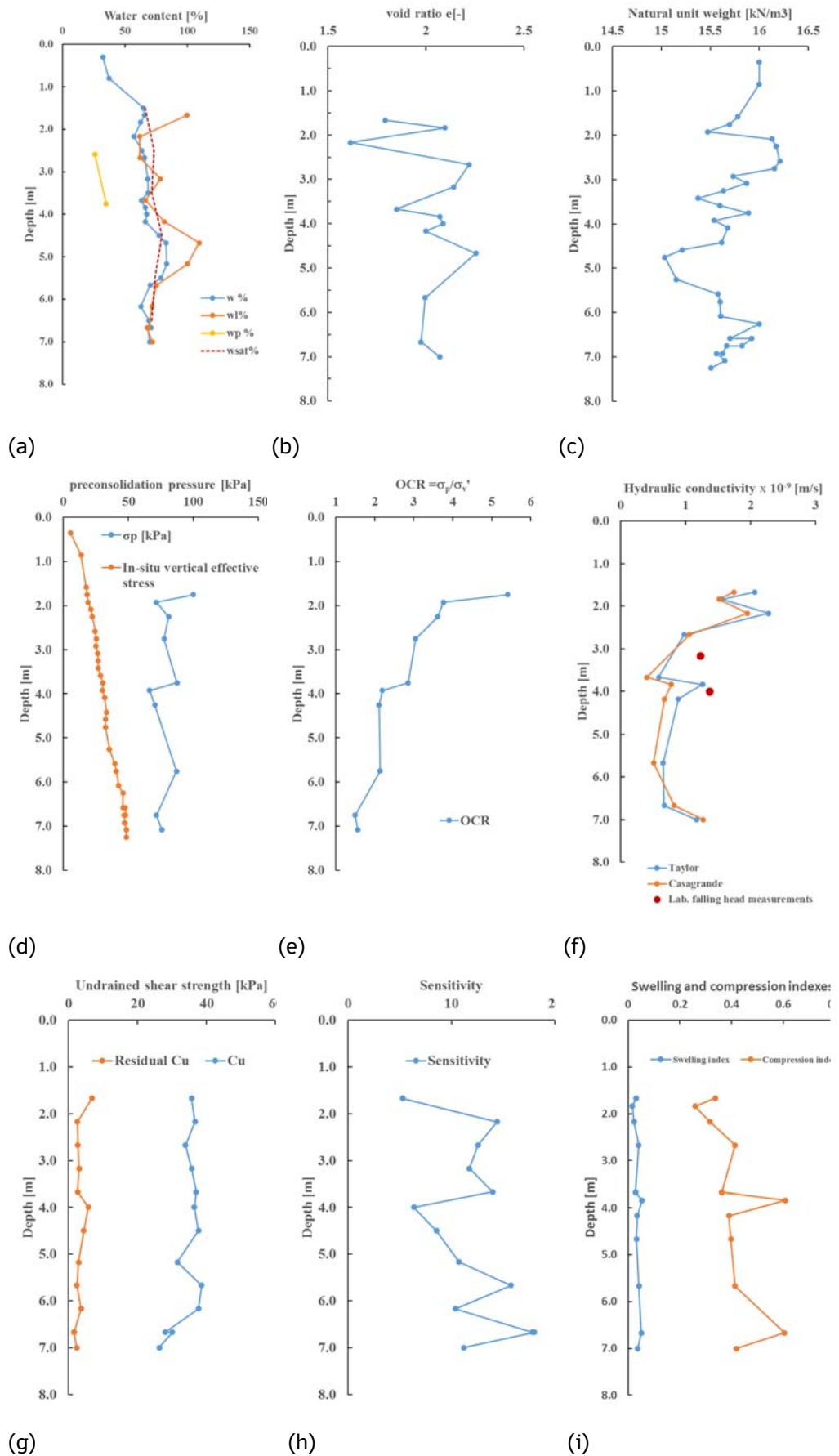


Figure 21. Soil properties at Tuuliharju site (Aalto testing program (Goncharko, 2018))

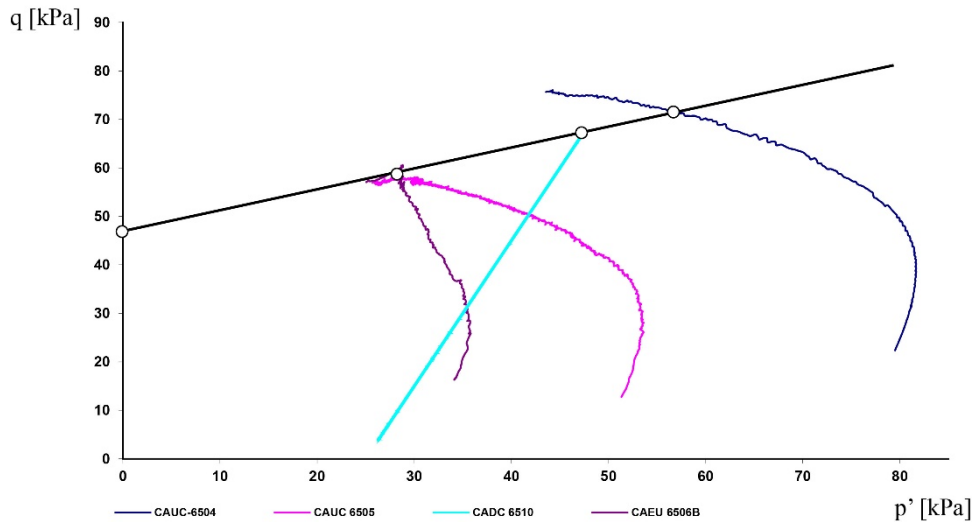


Figure 22. Consolidated undrained (CAUC) and drained standard triaxial compression (CADC) tests results on samples from an average depth of 2.5 m at Tuuliharju site.

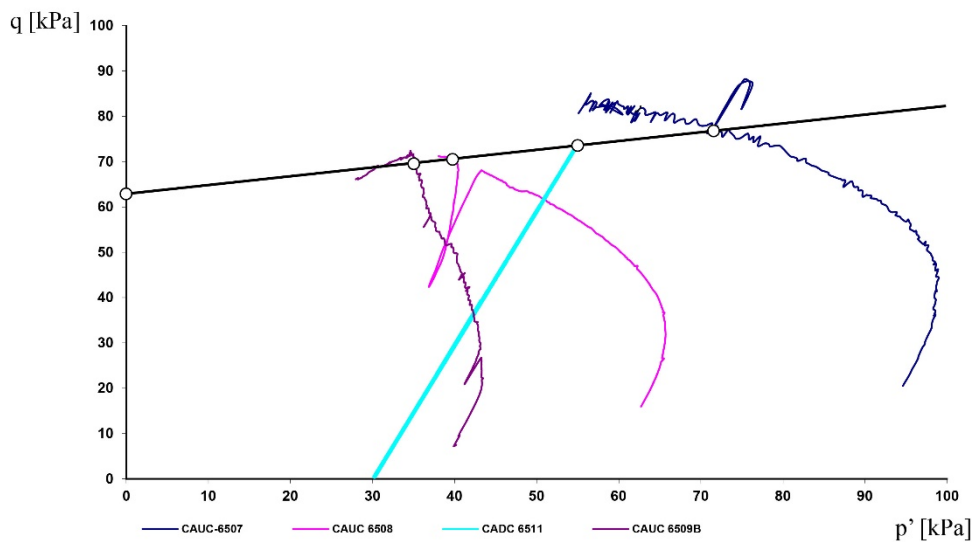


Figure 23. Consolidated undrained (CAUC) and drained standard triaxial compression (CADC) tests results on samples from an average depth of 4.0 m at Tuuliharju site.

8.1.2 Relevance of undrained behaviour

To check on the relevance of undrained behaviour, the time factor is calculated using the data from Liminka with $E_{oed} = 8000$ kPa, $D = 5$ m, $k = 10^{-9}$ m/s and estimated cutting time of 1.0 month which yields:

$$T = \frac{k E_{oed} t}{\gamma_w D^2} = \frac{10^{-9} \times 8000 \times 1 \times 30 \times 24 \times 60 \times 60}{10 \times 5^2} = 0,083$$

The value is higher than 0,01 and much less than 0,848 suggesting that both undrained and drained calculation are important in this case. The undrained conditions dominates the short-term behaviour whilst the drained condition controls the long-term stability of the cutting.

8.1.3 Drained and Undrained strength parameters

Series of undrained and drained triaxial tests were conducted at Aalto University geotechnical laboratory. The results of undisturbed samples that are extracted from depths 2,5m and 4,0m are depicted in Figure 22 and Figure 23, respectively. The undrained shear strength in triaxial compression and the effective shear strength parameters are estimated in accordance with the explanation in Section (4) and are listed in Table 6 and Table 7.

Table 6. Undrained shear strength from triaxial compression test.

Depth [m]	$\sigma'_3 = 25.0$ [kPa]	$\sigma'_3 = 50.0$ [kPa]	$\sigma'_3 = 75.0$ [kPa]
2.5	$c_{uTC} = 30.0$	$c_{uTC} = 30.0$	$c_{uTC} = 35.0$
4.0	$\sigma'_3 = 30.0$ [kPa]	$\sigma'_3 = 60.0$ [kPa]	$\sigma'_3 = 90.0$ [kPa]
	$c_{uTC} = 35.0$	$c_{uTC} = 35.5$	$c_{uTC} = 39.0$

Table 7. Effective shear strength parameters from triaxial compression test.

Depth [m]	c' [kPa]	φ' [o]
2.5	22.0	11.4
4.0	30.6	5.4

8.1.4 Design undrained shear strength

As discussed in Section (2.3), the dominant stress path in the field controls the strength parameters to be used in the stability analysis. In case of cutting, the unloading stress path is dominant with the soil strength parameters in extension being the most relevant. As such, the direct use of the triaxial compression test shear strength parameters is non-conservative. In what follows, the methods discussed previously will be applied on Tuuliharju case to evaluate the safety.

1. Undrained shear strength from vane shear test.

The results of one vane shear test from a point near to the site is used as given in Figure 20. The undrained strength values are reduced using Bjerrum's factor as given in Figure 11 to account for inaccuracy in direct field measurements. As an alternative, the reduction factor as proposed by the Finnish system (see Figure 12) is estimated as well. The results are as shown in Table 8.

Table 8. Original and corrected undrained shear strength from field vane shear test.

Depth [m]	Undrained shear strength from vane shear test [kPa]	Reduced values with ($I_p = 35\%$) and Bjerrum factor = 0.9	Reduced values with ($w_L = 70\%$) and Finnish factor =0.8
1.87	38	34.2	30.4
2.37	33	29.7	26.4
2.87	33	29.7	26.4
3.37	24	21.6	19.2

2. Prediction of undrained shear strength based on Jamiolkowski's chart

Based on the Chart presented in Figure 10 (JAMIOLKOWSKI, 1985) and by employing an average value of plasticity index $I_p = 35\%$ for the soil in Liminka, the values of undrained shear strength in normal consolidation conditions in compression, direct simple shear, extension and average values can be estimated at several depths of the soil. After that, the corresponding values to the in-situ overconsolidation ratio OCR can be estimated using the formula (7) with the suitable values of m and c_{uNC}/σ'_v from Table 3. The final estimated values in this case are listed in Table 9.

Table 9. Undrained shear strength as estimated using Jamiolkowski's chart.

Depth [m]	σ'_v [kPa]	OCR $= \sigma'_p/\sigma'_v$	c_{uTC} [kPa]	c_{uDS} [kPa]	c_{uTE} [kPa]	c_{uAv} [kPa]
1.87	19	5	21.0	16.4	14.9	17.5
2.37	23	3.5	19.2	15.1	13.2	15.9
2.87	26	2.9	18.7	14.8	12.6	15.4
3.37	26.9	2.5	17.2	13.6	11.4	14.1

3. Estimation of undrained shear strength based on SHANSEP

By employing the estimated undrained shear strength by Aalto laboratory and the estimated OCR in field, a relationship between OCR and c_u/σ'_v is built and plotted on the chart provided by (Ladd and Foott, 1974). The values yielded parameters $c_{uNC}/\sigma'_v = 0.43$ and $m = 0.9$ for the SHANSEP method as shown in Figure 24 and listed in Table 10. These values cannot be used directly as they refer to triaxial compression while the cutting is dominated by simple shear stress conditions. Due to the absence of data for simple direct shear tests, the previous triaxial values are converted to an average simple shear value based on the factor 0,61 given by (Ladd and Foott, 1974) and listed in Table 1. When converted and plotted in Figure 24, the new SHANSEP parameters become $c_{uNC}/\sigma'_v = 0.26$ and $m = 0.9$. The generated curve is in good agreement with the one given by (Ladd and Foott, 1974) for similar clay with $w_l = 65\%$ and $I_p = 35\%$. These curve is then used to derive the design c_u profile for stability analysis.

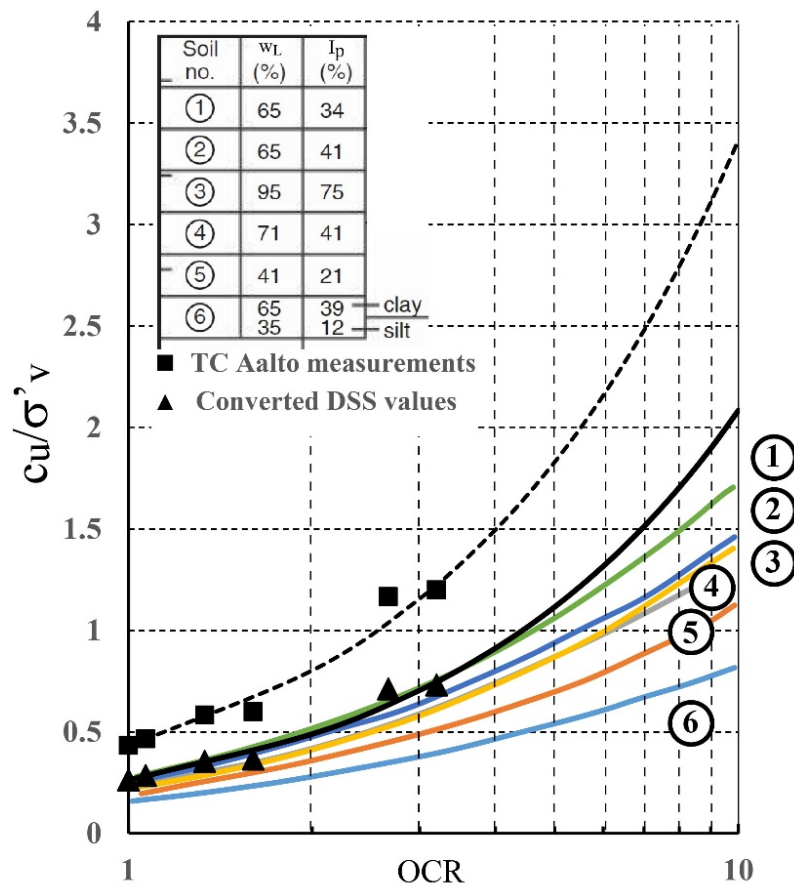


Figure 24. Estimated relationship for determining the undrained shear strength in Tuuliharju site in accordance with SHANSEP method.

Table 10. Undrained shear strength and OCR as derived from Aalto University triaxial compression and Oedometer tests.

σ'_v [kPa]	σ'_p [kPa]	c_{uTC} [kPa]	c_{uTC}/σ'_v	$OCR = \sigma'_p/\sigma'_v$
25.0	80.0	30.0	1.2	3.2
50.0	80.0	30.0	0.6	1.6
75.0	80.0	35.0	0.5	1.1
30.0	80.0	35.0	1.2	2.7
60.0	80.0	35.0	0.6	1.3
90.0	80.0	39.0	0.4	1.0

Table 11. Design undrained shear strength for Tuuliharju analysis.

Layer boundaries [m]	c_u value by Finnish recommendations [kPa]	c_u value by SHANSEP method [kPa]
0.8-2.0	30.0	21.0
2.0-3.0	26.0	18.0
3.0-8.0	20.0	16.0

For comparison, the estimated values of the undrained shear strength, as predicted by these different approaches, are plotted in Figure 25. Out of these values, the one resulted from the Finnish reduction factor and the one estimated by SHANSEP with direct simple shear (DSS) are used for the undrained calculations of the cutting stability in Tuuliharju site. For that purpose, the clay layer is subdivided into three sublayers with uniform c_u values averaged from the plot in Figure 25, yielding the values listed in Table 11.

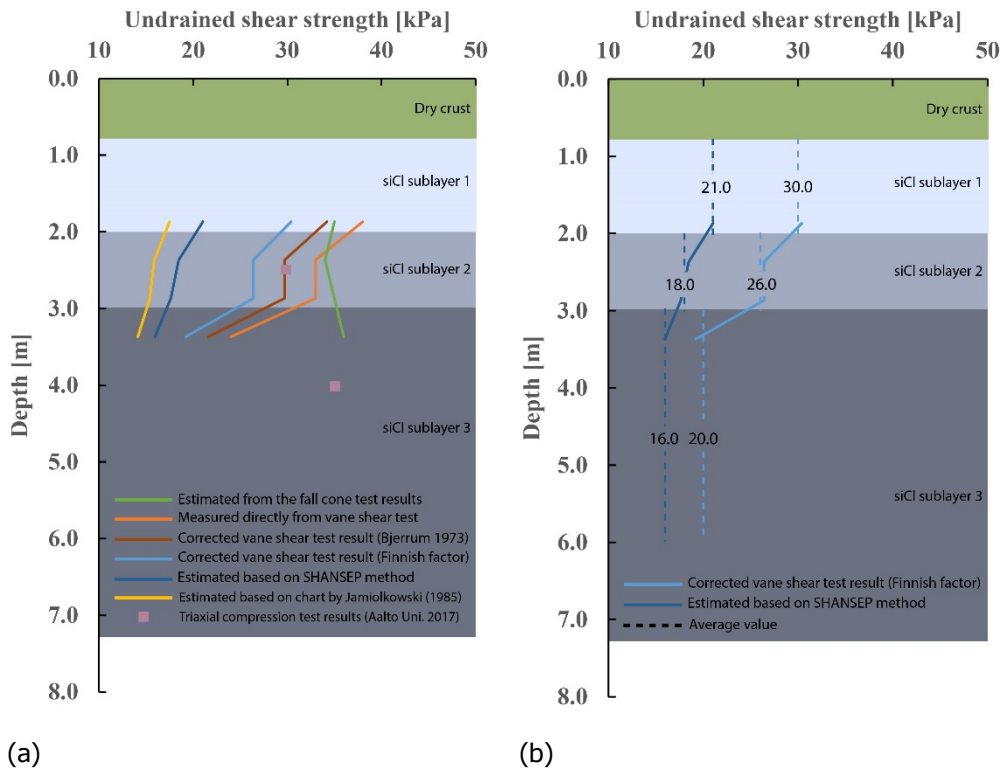


Figure 25. Undrained shear strength profile: a) estimated by several approaches; b) design values averaged based on SHANSEP and corrected vane shear test results.

8.1.5 Design drained strength parameters

For drained analysis, the triaxial effective strength parameters are employed directly in the analyses. In this case, the clay layer is subdivided into two layers only with the effective shear strength parameters as listed in Table 12. Similar logic to that followed in deriving the parameters for undrained shear strength should have been followed here, where the effective cohesion and effective friction angle should have been estimated using the simple shear device. However, due to limitation of data, the effective parameters coming only from triaxial compression are adopted here.

Table 12. Design drained shear strength for Tuuliharju analysis.

Layer boundaries [m]	c' [kPa]	φ' [°]
0.8-3.0	22.0	11.4
3.0-8.0	30.6	5.4

8.1.6 Undrained analysis results

The undrained analysis is conducted using Geostudio 2016 software. Morgenstern-Price's method is employed with the undrained shear strength and total unit weight are the only material input. The results as shown in Figure 26 suggest that the cutting is not stable in the short term with safety factor less than 1.3 in general. As this cutting suffered a real physical failure in field, the SHANSEP parameters are more realistic for this case as they predicts lower safety factors.

8.1.7 Drained analysis results

The drained analysis is performed using Mohr-Coulomb failure criterion with the effective strength parameters as listed in Table 12. The results (see Figure 27) show that the cutting would have been stable in long term, if measures would have been taken to insure stability during the short-term undrained phase.

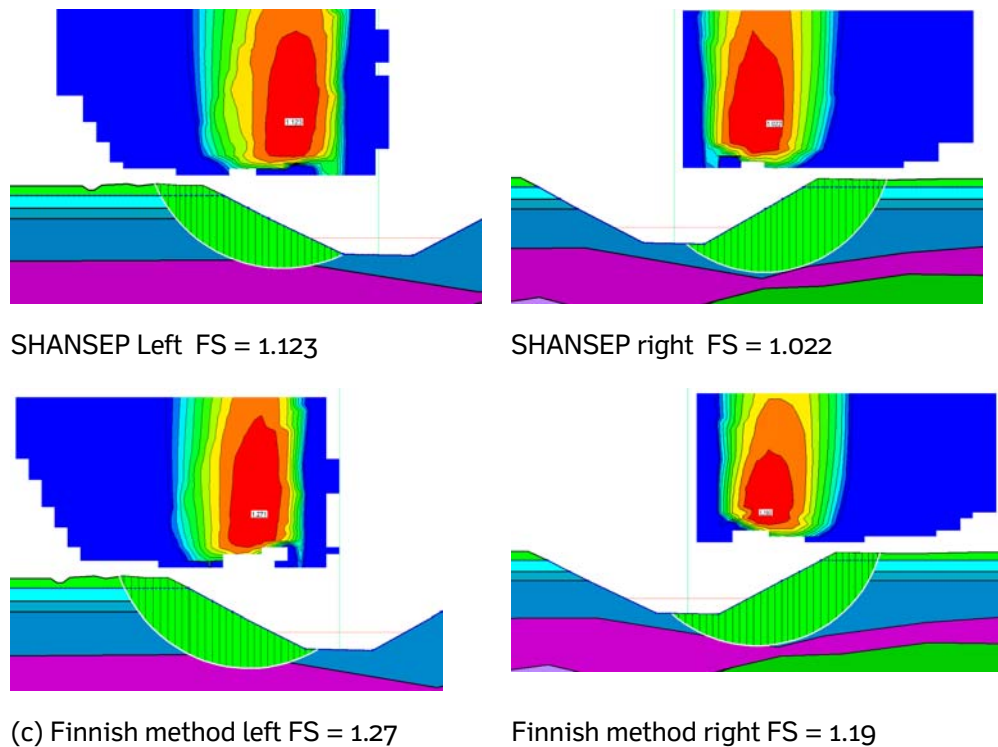


Figure 26. Undrained LE analyses results for Tuuliharju site.

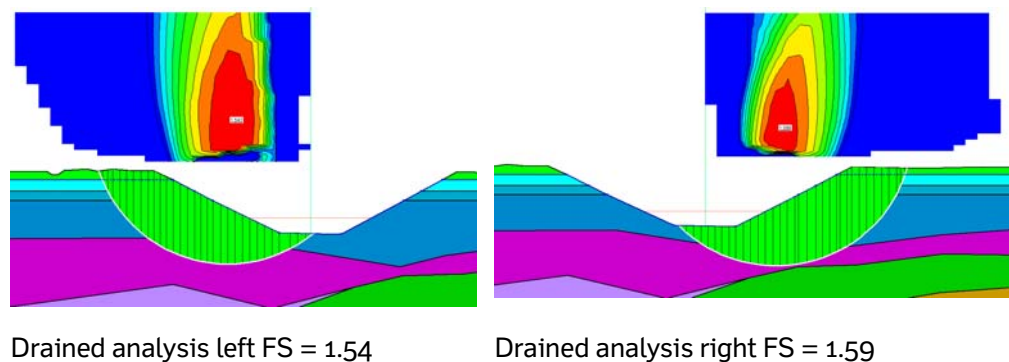


Figure 27. Drained LE analyses results for Tuuliharju site.

8.2 Safety evaluation at Zatelliitti site

This calculations concentrate on “Section 320-PL320” at “Zatelliitin AKS” in the area of Liminka, Oulu. According to the data provider, this site suffers slope failure after construction. Detailed information about the location, geometry, construction sequence, soil investigations and slope analyses are made available for the current study. Only the most relevant data is shown here for the sake of brevity. Figure 28 shows the general location of the site. The studied section is highlighted in red.

Even though similar logic to the calculations performed for Tuuliharju case can be followed here, the drained behaviour is given more weight here to further explore the problems that might occur during such calculations.

8.2.1 Soil profile

Based on the provided soil testing report “MPR/ 498/2013”, CPTU test results and the information given in “Tieleikkauksen laskentaportti_30.4.2015.docx” the soil profile is reconstructed to be as shown in Figure 29 with ground surface level at +7.0m. The dashed red lines in the figure represents the trace of soil layering used by the designer calculations. Report “Tieleikkauksen laskentaportti_30.4.2015.docx” mentioned that the deeper thin sand layer was neglected in the updated analyses because of its marginal effects. The used soil properties in the reported analyses are given in Table 13. However, it is not clear how the designer finally settled on the provided values. On the other hand, report “MPR/ 498/2013” provides the summarized soil properties listed in Table 14. The report mentions that the bottom layer is a hard silty soil which is justified by interpreting the provided static-dynamic penetration test in Figure 29. No information could be found on how the properties of the fill material was derived. Soil layering and properties listed in Table 15 are suggested for any possible new analysis. In fact, the updated soil layering is used in the following analyses but with similar soil properties to that used by the designer.

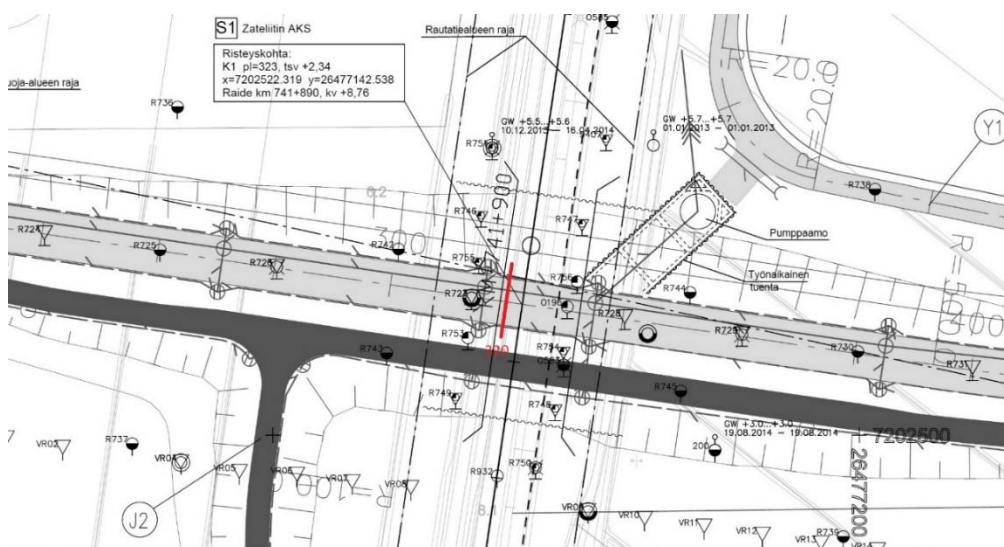


Figure 28. Location and coordinates of the studied cutting section.

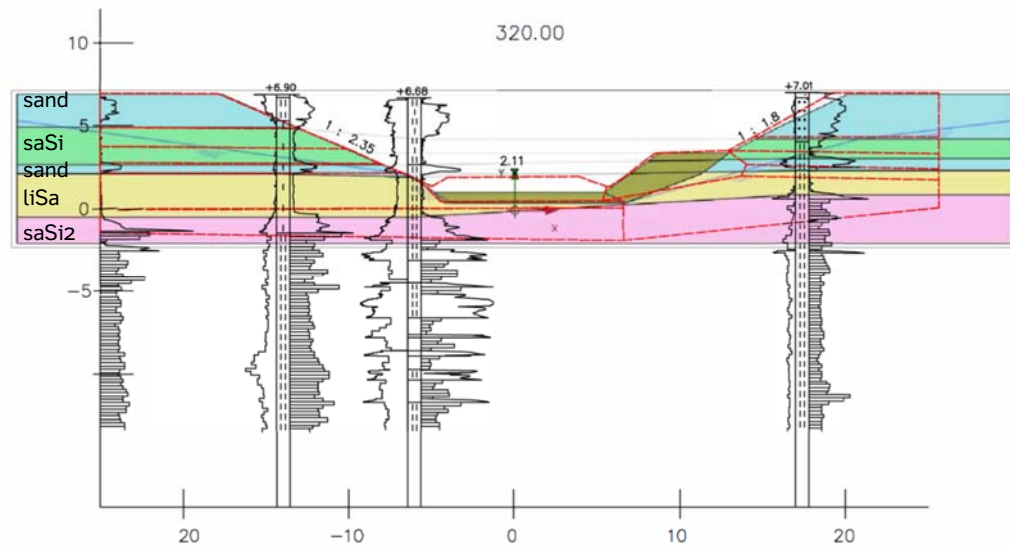


Figure 29. Static-dynamic penetration test results and the predicted soil layering at PL-320.

Soil properties are kept unchanged for comparison purposes. CPTU tests and data shown in Figure 28 indicate that the initial water table is at a depth of about 1.3m-2.0m from ground surface level.

Table 13. Soil properties provided by the designer.

Layer	Unit weight γ_b [kN/m ³]	Effective friction angle ϕ' [°]	Effective cohesion c' [kPa]	Undrained shear strength c_u [kPa]
Sand	19.0	35.0	0.2	
saSi	16.0	28.0	5.0	30.0
liSa	16.0	32.1	2.8	20.0
saSi2	16.0	27.8	3.8	
Fill	20.0	34	0.2	

Table 14. Soil properties as given by report MPR/498/201.

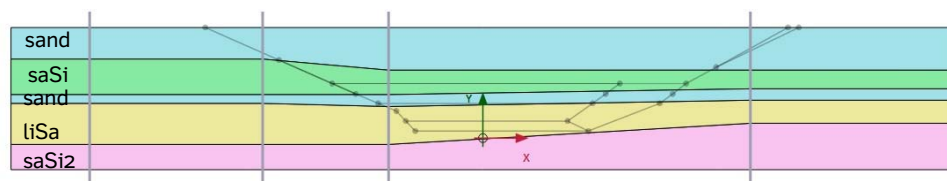
Layer	Depth [m]	Unit weight γ_b [kN/m ³]	Effective friction angle ϕ' [°]	Effective cohesion c' [kPa]
saSi	3.0 – 3.5	18.1 – 19.0	34.4, 28, 20.3	4.9, 16.0, 20.4
liSa	5.5	16.1 – 17.1	29.8	7.1
Bottom	6.0 – 6.5	16.1 – 17.5	31.5	4.6
Bottom	6.5-7.0	17.5-19.0	33.7	2.8
Bottom	0.0 – deeper	18.8-19.0		

Table 15. Soil layering and properties to be used in any possible new analysis.

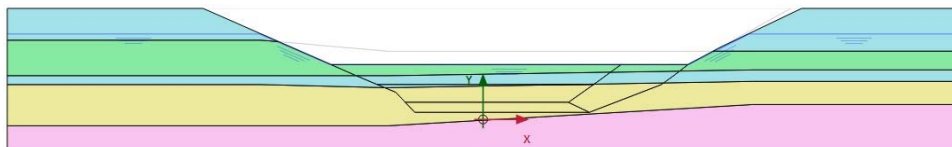
Layer	Depth [m]	Unit weight γ_b [kN/m ³]	Effective friction angle ϕ' [o]	Effective cohesion c' [kPa]
Sand	0.0-2.5	19.0	35.0	0.0
saSi	(2.0-2.7)-(1.8-3.9)	18.0	28.0	4.9
Sand	(4.2-4.9)- (4.7-4.65)	19.0	35.0	0.0
liSa	(4.7-4.65)- (6.2-7.0)	16.5	29.8	7.1
Hard silt	6.2-model bottom boundary	17.5	31.5	2.8

8.2.2 First approximation analysis

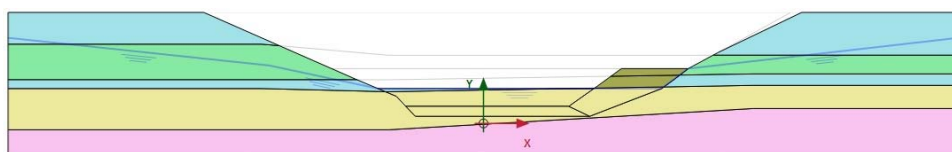
To gain deeper understanding of the problem, a preliminary analysis is performed using soil properties as provided by the designer. The soil layers thicknesses are slightly modified to better fit the provided penetration test data, see Figure 28. The soil excavation is performed in three stages as in Figure 30. The initial groundwater table locates at an average depth of 1.6m.



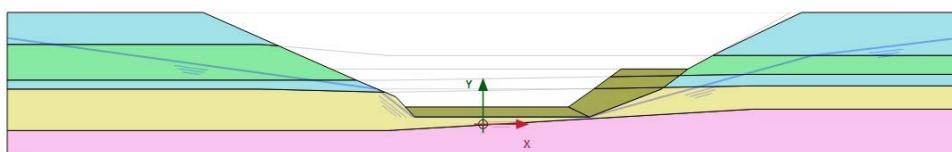
Soil layering with the position of boreholes



Excavation- Stage 1



Excavation- Stage 2



Excavation- Stage 3

Figure 30. Simulated soil cutting stages.

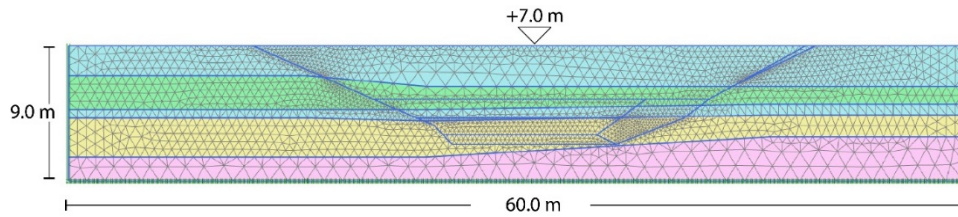


Figure 31. Used Finite Element model

During the development of the excavation, similar water table configuration to that used by the designer is adopted. However, it is believed that pore-water pressure distribution plays a very important role that directly affects the stability of the cutting and should be given a further detailed study.

Both Finite Element and Limit Equilibrium methods are employed in this analysis. For finite element analyses, Plaxis 2D is used while Geostudio 2016 is used for LEM calculations. The adopted finite element mesh is shown in Figure 31. It consists of 5733 15-noded triangular elements with 12 stress integration points per element. The average element size is 0.3m which is an acceptable approximation of physical reality. A separated convergence study shows that the results are insensitive for any further refinement of the mesh.

8.2.3 Analysis of excavation stage 1

To follow as close as possible the designer method of analysis, the calculation is performed using Mohr-Coulomb (MC) model with drained conditions and effective soil strength parameters. The calculation type is plastic and water pressure is to be derived from the hydrostatic water table. The deeper thin sand layer is replaced by clayey silt material in one analysis, and kept as a separated layer in another. Again, to follow the designer suggestions, the shallow sand layer at the ground surface is considered dry and not affected by water table. To check on that, the analysis is repeated with full consideration of groundwater table effect.

- **Analysis results after ignoring the intermediate thin sand layer and assuming a dry shallow sand layer**

LEM result in Figure 32(a) shows that the total factor of safety is $FS=1.369$ which is acceptable from design provisions point of view (FS should be > 1.3). The Finite Element results in Figure 32(b) yields $FS=1.26 < 1.3$ suggesting an unacceptable design.

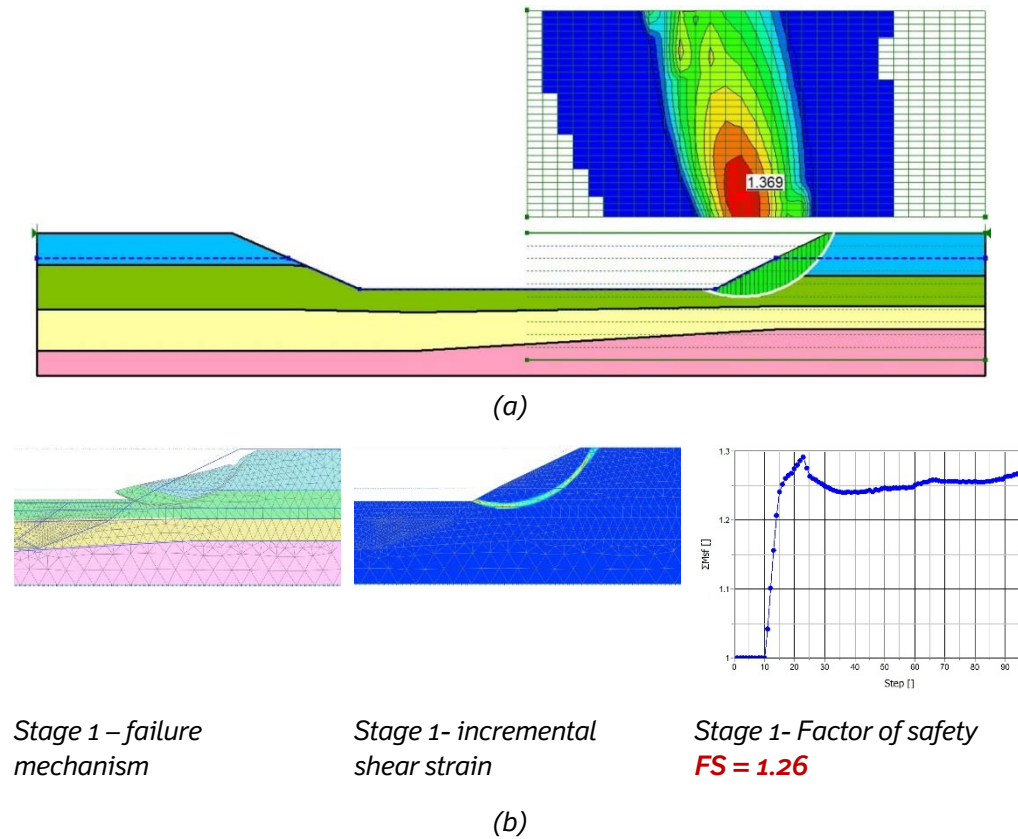


Figure 32 Stability analysis of the first excavation stage with ignoring the deeper thin sand layer a) LEM results with dry sand; b) FEM results with dry sand

- Analysis results including the intermediate thin sand layer and assuming a dry shallow sand layer

On repeating the analysis but keeping the thin sand layer, both LEM result in Figure 33(a) and the Finite Element results in Figure 33(b) yield an unacceptable design-wise factor of safety values. This result show that neglecting the deeper sand layer is not on the safe side.

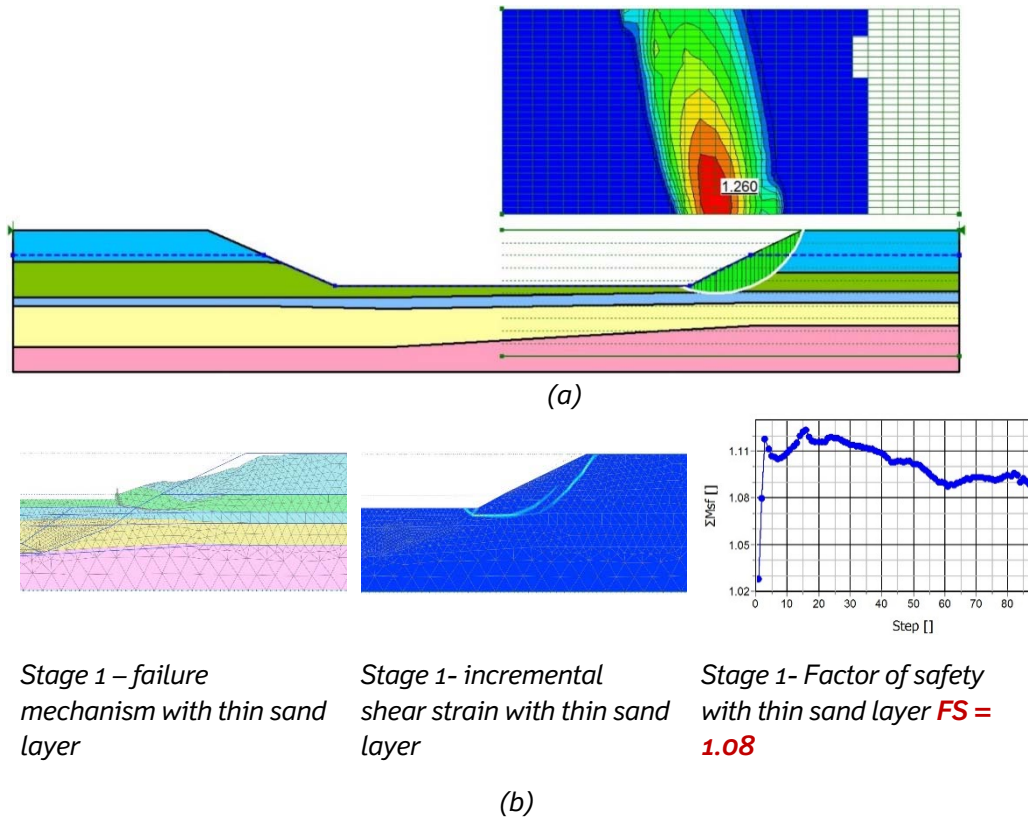


Figure 33 Stability analysis of the first excavation stage considering the deeper thin sand layer a) LEM results with dry sand; b) FEM results with dry sand

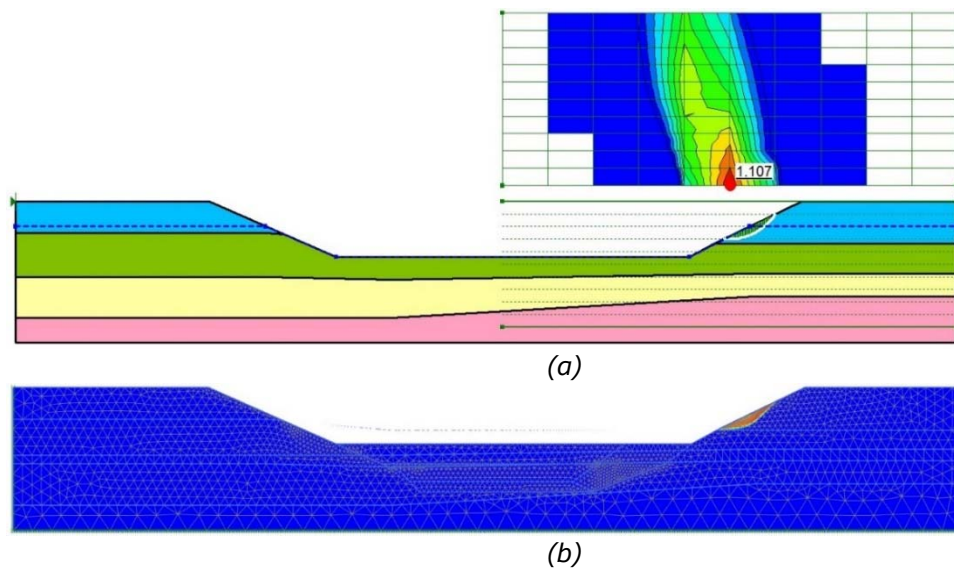


Figure 34 Stability analysis of the first excavation stage considering the shallow sand layer to be affected by water table a) LEM results; b) FEM results

- Analysis results assuming that the shallow sand layer is affected by groundwater table

If the shallow sand layer is considered to be affected by pore water pressure (which is the logical assumption), LEM and FEM analyses shows local failure concentrated in the sand layer, as indicated in Figure 34(a) and (b). In fact, FEM analysis predicted a physical soil failure during the excavation phase ($FS < 1.0$). This shows that one should be very careful when dealing with the hydraulic boundary conditions.

8.2.4 Analysis of excavation stage 2

- **Analysis results assuming that the fill geometry and properties are as used by the designer**

The fill material in this analysis is modelled as MC material with the properties listed in Table 13. Both LEM and FEM results show that the fill material body is not safe enough. The inclination of the slope should be changed or the material strength should improve. LEM result in Figure 35(a) shows that $FS = 1.245 < 1.3$ whereas FEM result in Figure 35(b) predicts that FS is swinging around 1.08 (non-convergence) with a high risk of physical failure.

- **Analysis results assuming a linear elastic fill material**

To check on other possible failure mechanism at this stage, the fill material is assumed to be linear elastic with no possibility for failure. In this case LEM and FEM predicted an acceptable safety factor of $FS = 1.56$ and $FS = 1.45$ respectively.

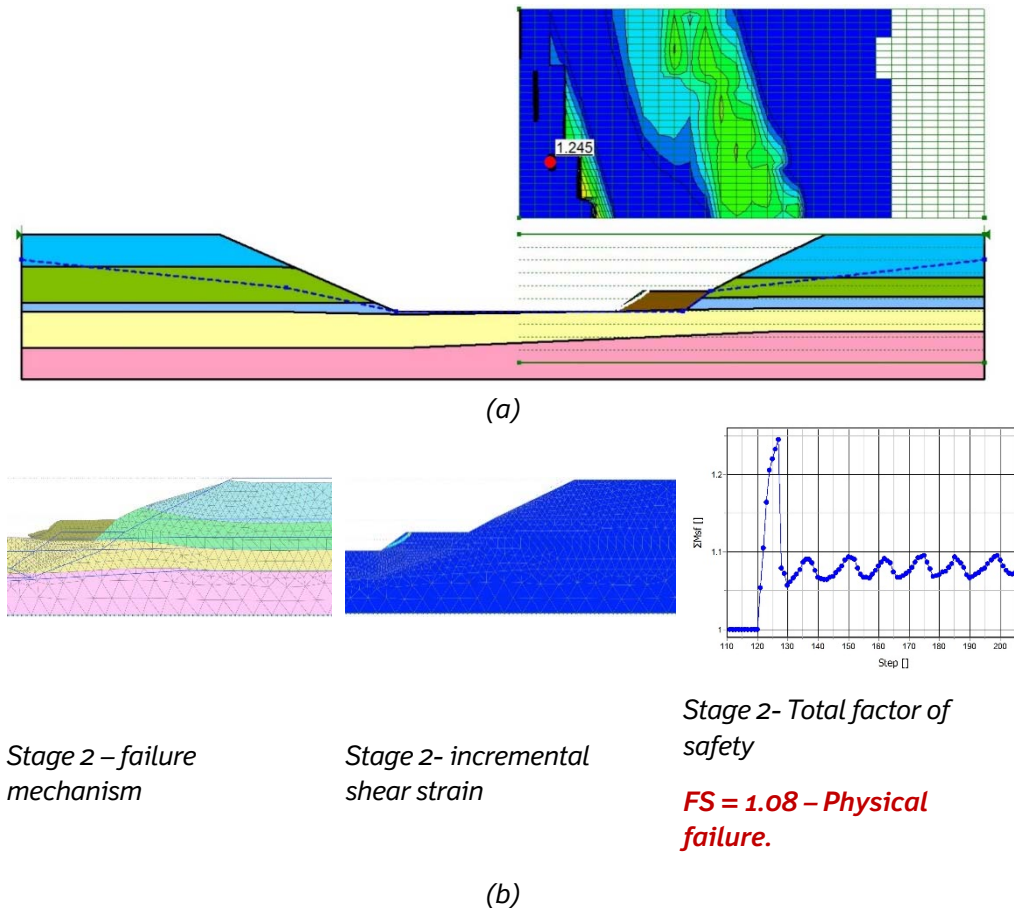


Figure 35 Stability analysis of the second excavation stage with granular fill material a) LEM results; b) FEM results

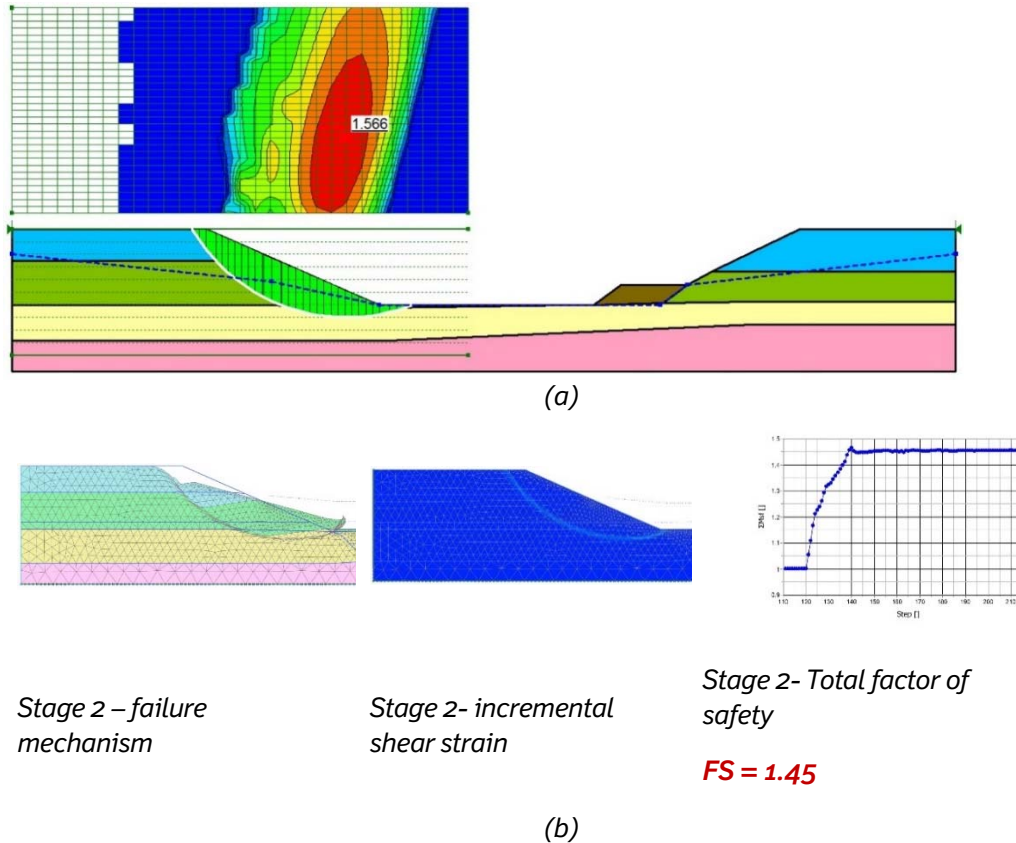


Figure 36 Stability analysis of the second excavation stage with linear elastic fill material a) LEM results; b) FEM results.

8.2.5 Analysis of excavation stage 3

- **Analysis results assuming that the fill geometry and properties are as used by the designer**

Similarly to Stage 2, both LEM and FEM results show that the fill material body is not safe enough. The slope should be changed or the material strength should be improved. LEM result in Figure 36(a) shows that $FS=1.1 < 1.3$ whereas FEM result in Figure 36(b) predicts a physical failure with $FS < 1.0$.

- **Analysis results assuming a linear elastic fill material**

To check on other possible failure mechanism during stage 3, the fill material is assumed to be linear elastic with no possibility for failure. LEM and FEM predicted an acceptable safety factor of $FS=1.496$ and $FS=1.34$ respectively.

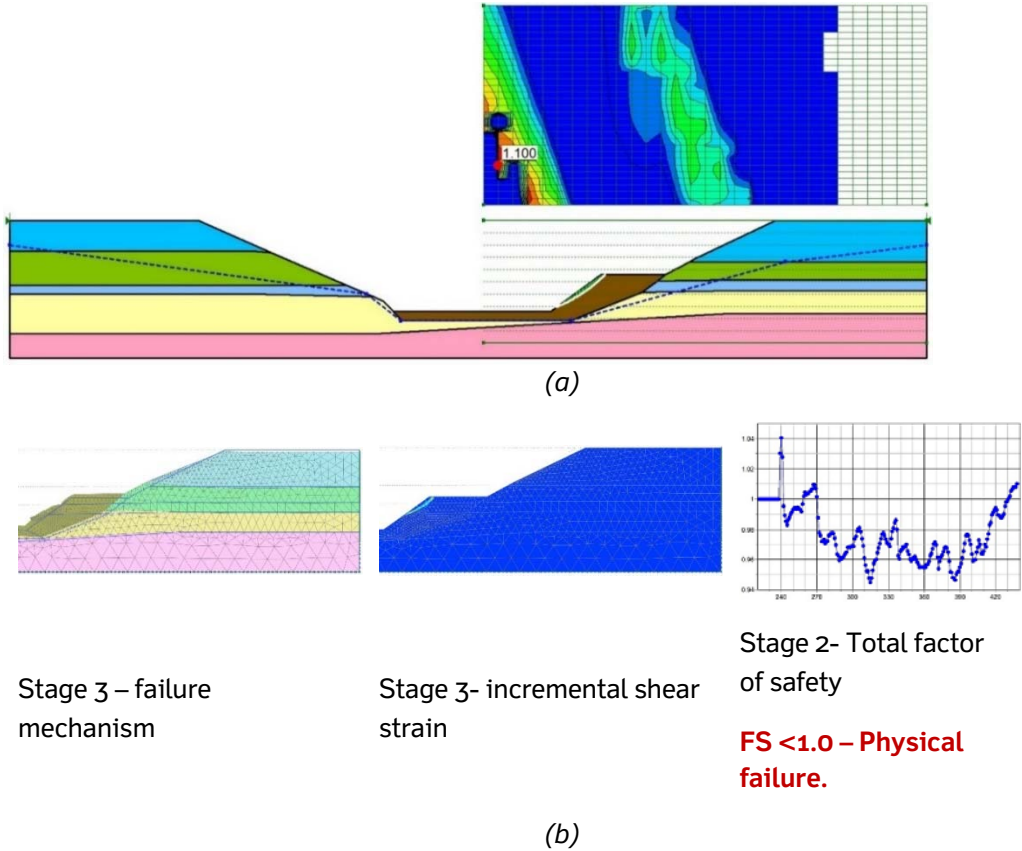


Figure 37 Stability analysis of the third excavation stage with granular fill material a) LEM results; b) FEM results.

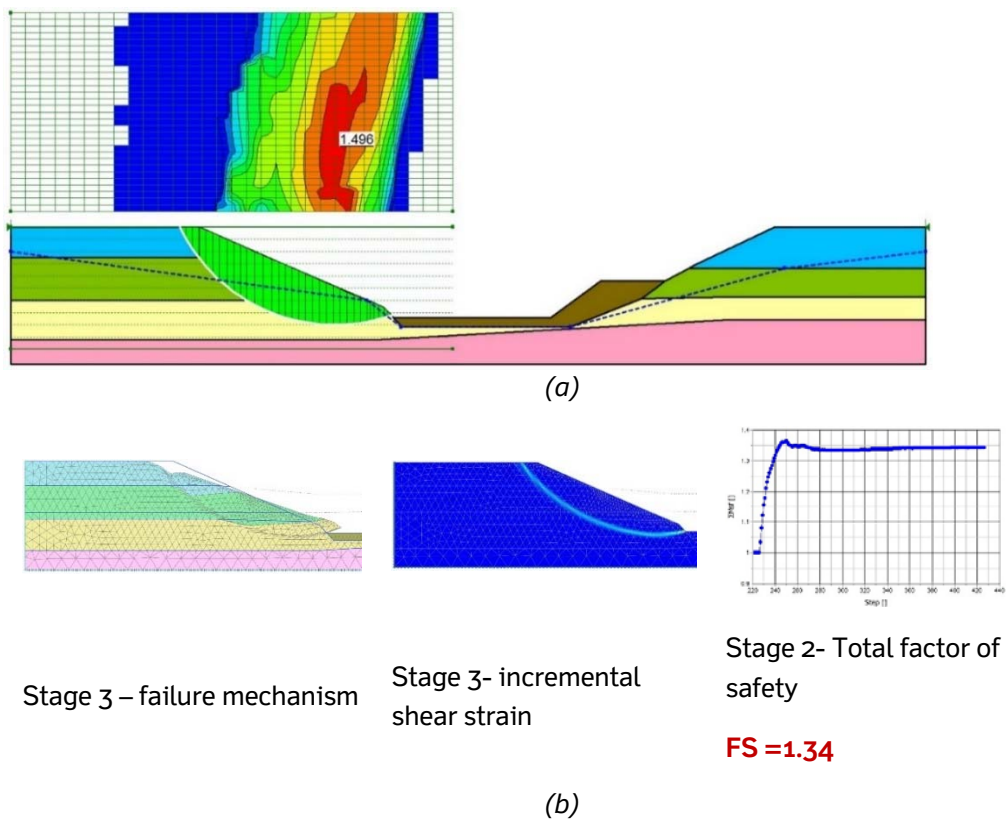


Figure 38 Stability analysis of the third excavation stage with linear elastic fill material a) LEM results; b) FEM results.

8.2.6 Sensitivity to the groundwater table position.

In the course of the previous analyses, it was noticed that the results are sensitive to the position of the groundwater table. In light of that, a quick variation in the position of the groundwater table is performed to investigate its effect on the predicted factor of safety. This calculation concentrates only on the left side of the final excavation using LEM. Results in Figure 39 show that the factor of safety is very sensitive to the position of the groundwater table with varying factor of safety in the range 1.087-1.531.

8.2.7 Notes on Zatelliiti site calculations

- 1- By taking the effect of groundwater table on the shallow sand layer into account, the calculation shows local failure during the early stage of the excavation.
- 2- Ignoring the thin sand layer is not on the safe, at least during the early stages of the excavation.
- 3- The Finite Element calculations indicate unsafe inclination of the filling body with a possible physical failure in stage 2 and stage 3 of the excavation. The limit equilibrium analyses give similar predictions.
- 4- By assuming that the failure will not happen in the fill body (linear elastic material is assigned to the body), both Finite element calculations and LEM show that the factor of safety is higher than 1.3.
- 5- During the calculations it was noticed that the stability is very sensitive to the location of the groundwater table and as a consequence to the pore-water pressure value. A quick sensitivity analysis shows a dramatic reduction in the value of the safety factor at a relatively small variation in the groundwater table position.
- 6- In all calculations, FEM predicts lower values for the safety factor in comparison to that predicted by LEM. For problems that show low margin of safety (predicted factor of safety by LEM was only slightly higher than 1.3 in the designer calculations) it would be highly recommended to re-check stability with a more advanced numerical methods (FEM for example).

This analysis suggests that an accurate groundwater flow calculation is a crucial factor for a safe prediction of stability. Good quality of soil testing and evaluation of soil properties and soil layering is also very important issue. Furthermore, a combined design procedure that employs FEM and LEM would give a better overview on the possible failure location (local and global).

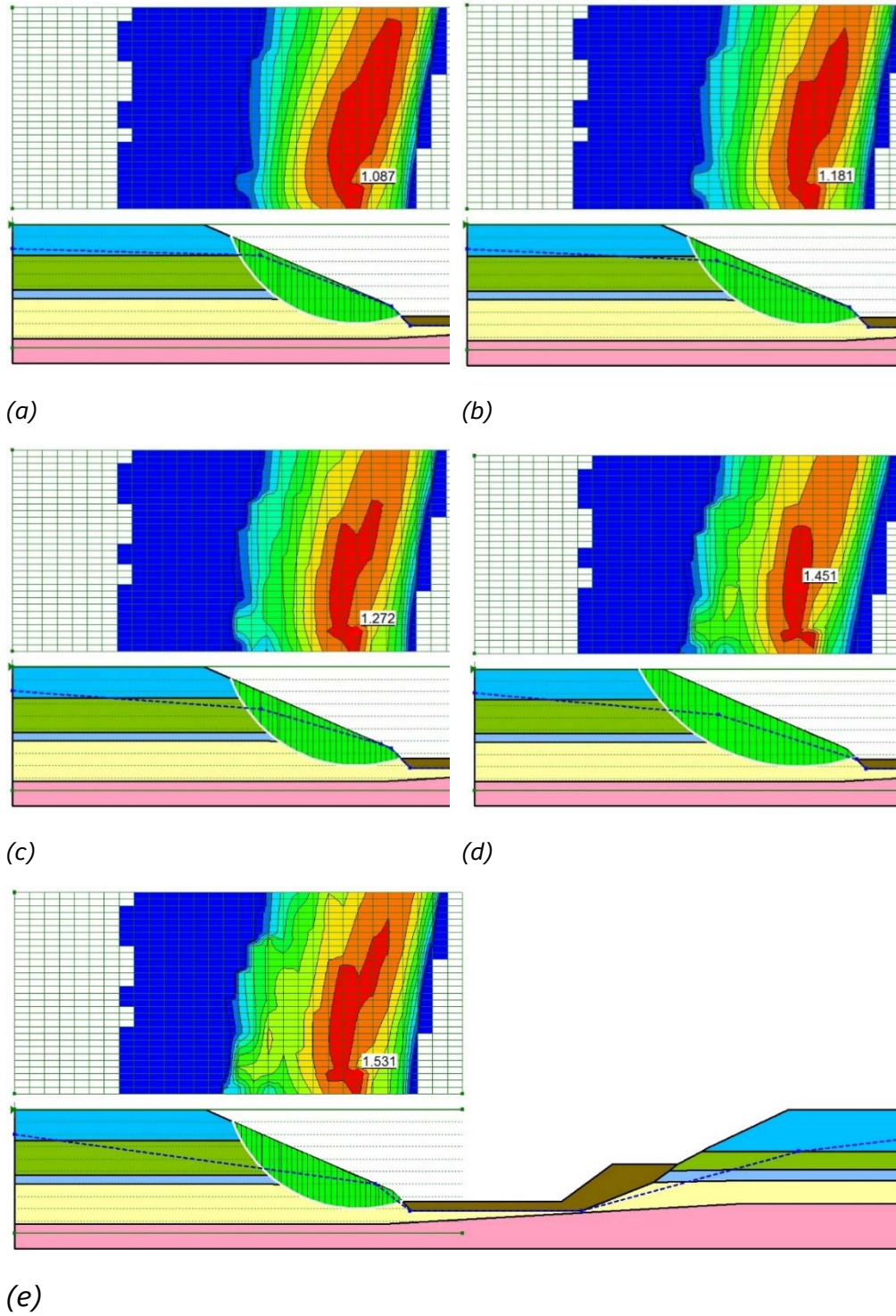


Figure 39 Effect of varying groundwater table on slope stability.

9 Design guidance

9.1 Recommendations for LEM calculations

(including: parameters identification, water flow conditions, layering, permeability, drained/undrained calculations)

1. The interpretation of soil layering and soil profile should be carefully conducted. No a-prior assumptions are recommended regarding the layering (removing thin layers with good strength parameters and replacing it with weaker material will not necessarily produce lower safety factor). Strong layers could form preferable sliding surfaces with lower safety factor.
2. Among the available slices methods, Morgenstern-Price's method and Spencer's method are recommended as they fully satisfy the balance equations.
3. Because unloading path is dominant in road cutting projects, it is recommended to estimate the shear strength parameters using the direct simple shear test (DSS).
4. If triaxial testing is adopted, then an average value for shear strength parameters in compression and in extension should be used.
5. Among in-situ tests, the vane shear test represents the best option to derive the undrained shear strength for cutting stability analysis. However, to avoid the overestimated strength due to high strain rate of the test and to consider soil anisotropy and disturbance, the test measurements must be corrected preferably using the Finnish factor (SGY, 1999). The field data should be supported by shear strength estimation at the laboratory following the recommendations in items (2) and (3).
6. To judge on the problem type (drained or undrained) one of the criteria discussed in Section (3) can be applied. However, t_{90} as given in Equation (5) is recommended to be used as a maximum time that is dominated by undrained behaviour.
7. In low to moderate plasticity clay and silt ($w_L < 80\%$, $I_p < 50\%$) the strength anisotropy is pronounced and the strength parameters estimated by direct simple shear test are highly recommended in this case.

8. To account for soil disturbance, anisotropy and strain rate the SHANSEP procedure for determining the design undrained shear strength parameters can be applied. For cutting projects the undrained shear strength should be strictly determined using the direct simple shear test (DSS) or converted from the triaxial counterpart using a suitable formula (using Table 1 or Charts in Figure 10, for example).
9. Some methods for LE undrained calculations that basis on effective stress are available (see for example (Lehtonen, 2015)). The problem associated with these methods is the uncertainties related to the correct estimation of excess pore water pressure at failure. If available in the used software, these methods can be used for comparison purposes and for gaining more confidence about the design.
10. In LEM, once the undrained shear strength value is employed, the analysis must be performed using the total stress concept.
11. In drained analysis, the groundwater flow plays a major role in determining stability. It is recommended to use a special routine to calculate the pore water pressure under the imposed hydraulic boundary conditions. The employed permeability values should be estimated as accurate as possible (from in-situ falling head test for example).
12. The safety factor is very sensitive to the location of the hydrostatic phreatic level and pore water pressure distribution. It is highly recommend that the location to be estimated based on field measurements and observations.
13. The field experience with soft clays showed that in some cases the actual measured pore water pressure values are considerably lower than that predicted by simple hydrostatic or steady flow calculations. If feasible, it is highly recommended to measure and observe the pore water pressure in field and employ them directly in LEM calculations.
14. In absence of reliable permeability measurements, the empirical formula and charts as provided in Section (7.1) can be employed.
15. For low permeability clay ($k < 10^{-9} \text{m/s}$), on top of the decided calculations, a check on stability in drained conditions is recommended assuming full saturation (by locating the groundwater table directly under the crust layer).
16. In case of problems with high risk of failure (safety factor is just satisfied), a check with more advanced numerical methods such as the finite element method is recommended.

17. Some stress paths are not automatically captured by LEM analysis as in the case of sequential unloading in staged construction of undrained cutting. The variation in excess pore pressure and the mechanical uplift should be investigated further with more advanced methods (finite element method, for example).

9.2 Recommendations for site investigation

18. In the case of cutting, it is recommended to determine shear strength parameters using the direct simple shear (DSS) test.
19. If the shear test apparatus is not available, then at least triaxial compression and extension test should be conducted to determine an average value for the shear parameters.
20. The undrained shear strength can be estimated based on the in-situ vane shear test after applying a suitable correction factor as discussed in Section (4.1).
21. The in-situ permeability is a key issue in determining the hydraulic system and as such, it is very important to be estimated as accurate as possible. In-situ falling head test and CPTU dissipation test are recommended for this purpose.

9.3 Recommendations for construction

(feasibility of lowering water table and staged construction)

22. Site measurements and investigations showed that the drainage system was not effective in lowering the groundwater table on the long run. That is attributed to the low permeability of the prevailing soft soil.
23. Parametric study on the effect of site permeability and the drainage system capacity (see Appendix A) shows that the drainage system used to lower the water table would be effective only for workability during the construction stages. However, for calculation and design purposes, the soil should be taken as saturated underneath the normal level of the groundwater at the studied area (at a depth of about 1.5-1.6m).

9.4 Recommendations for erosion protection of superficial slope failure

24. The erosion protection of the slope should be done according to the guidelines of chapter 8 in "Tiepenkereiden ja -leikkausten suunnittelu" (Liikennevirasto, 2010)

10 Notation

Roman

c	Cohesion	t_{90}	Time needed for 90% of consolidation to take place
c'	Effective cohesion	T	Consolidation time factor
c_u	Undrained cohesion	T_m	Mobilized shear force
c_{uDS}	Undrained cohesion from Direct Simple Shear test	w	Water content
c_{uNC}	Undrained cohesion for normally consolidate clay	w_L	Liquid limit
c_{uTC}	Undrained cohesion from Triaxial Compression test	w_P	Plastic limit
c_{uTE}	Undrained cohesion from Triaxial Extension test	w_{sat}	Water content at full saturation
c_v	Coefficient of consolidation	z	Depth
D	Drainage path length		
e	Void ratio	<i>Greek</i>	
E_{oed}	Constrained elasticity modulus	γ	Unit weight
f	Failure function	γ_b	Bulk unit weight
F, FS	Factor of Safety	γ_w	Unit weight of water
G_s	Specific gravity	ρ_w	Density of water
I_p	Plasticity index	μ_w	Water dynamic viscosity
K_0	Coefficient of earth pressure at rest	θ	Lode angle
k	Permeability	τ	Shear stress
L	Length	τ_D	Shear stress at failure due to Direct Simple Shear path
m	Soil parameter	τ_f	Shear stress at failure
M	Slope of the critical state line	τ_L	Shear stress at failure due to Loading path
p'	Effective isotropic pressure	τ_{mob}	Mobilized shear stress
p_a	Pore air pressure	τ_U	Shear stress at failure due to Unloading path
p_w	Pore water pressure	$\sigma'_1, \sigma'_2, \sigma'_3$	Principal stress
q	Deviatoric stress	σ_n	Normal stress
q_o	Assistant variable for triaxial test calculations	σ'_n	Effective normal stress
S	Specific surface	σ'_p	Consolidation pressure
S_o	Degree of saturation at residual state	σ'_v	Effective vertical stress
S_r	Degree of saturation	χ	Bishop's factor for effective stress in unsaturated soil
t	Time		

Abbreviations

CADC	Consolidated drained triaxial compression test
CAUC	Consolidated undrained triaxial compression test
DSS	Direct simple shear test
FEM	Finite element method
LE	Limit equilibrium
LEM	Limit equilibrium method
OCR	Over consolidation ratio
SHANSEP	Soil history and normalized soil engineering properties
SRF	Strength reduction factor

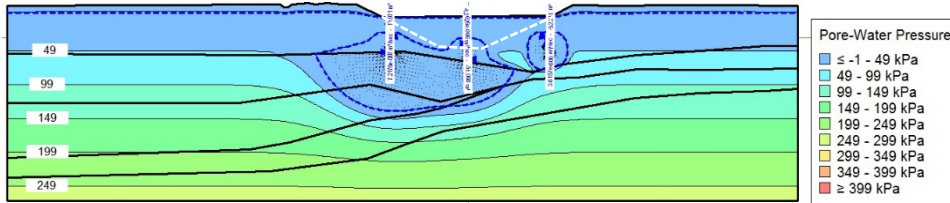
References

- Abed, A.A., 2008. Numerical modeling of expansive soil behavior. Instituts für Geotechnik (IGS).
- Abed, A.A., Sołowski, W.T., 2017. A study on how to couple thermo-hydro-mechanical behaviour of unsaturated soils: Physical equations, numerical implementation and examples. *Comput. Geotech.* 92, 132–155.
- Andersen, K.H., Schjetne, K., 2012. Database of friction angles of sand and consolidation characteristics of sand, silt, and clay. *J. Geotech. Geoenvironmental Eng.* 139, 1140–1155.
- Bishop, A.W., 1959. The principle of effective stress. *Tek. Ukebl.* 39, 859–863.
- BJERRUM, L., 1973. Problems of soil mechanics and construction of soft clays and structurally unstable soils. *Proc 8th Intl Conf SMFE Mosc. 1973* 3, 111–159.
- Chapuis, R.P., Aubertin, M., 2003. On the use of the Kozeny Carman equation to predict the hydraulic conductivity of soils. *Can. Geotech. J.* 40, 616–628.
- D'Ignazio, M., Lämsivaara, T., n.d. Strength increase below an old test embankment in Finland.
- D'Ignazio, M., Phoon, K.-K., Tan, S.A., Lämsivaara, T.T., 2016. Correlations for undrained shear strength of Finnish soft clays. *Can. Geotech. J.* 53, 1628–1645.
- Duncan, J.M., Wright, S.G., Brandon, T.L., 2014. *Soil strength and slope stability*. John Wiley & Sons.
- Fredlund, D.G., Krahn, J., 1977. Comparison of slope stability methods of analysis. *Can. Geotech. J.* 14, 429–439.
- Fredlund, D.G., Krahn, J., Pufahl, D.E., 1981. The relationship between limit equilibrium slope stability methods. pp. 409–416.
- Fredlund, D.G., Rahardjo, H., 1993. *Soil mechanics for unsaturated soils*. John Wiley & Sons.
- Freeze, R.A., Cherry, J.A., 1979. *Groundwater*, 604 pp. Prentice-Hall, Englewood Cliffs, NJ.
- GeoStudio 2016, 2016. . Geo-Slope.
- Goncharko, O., 2018. Master thesis. Aalto University.
- Jamiolkowski, M., 1985. New development in field and laboratory testing of soils. pp. 57–153.
- Kankare, E., 1969. Failures at Kimola floating canal in Southern Finland. pp. 609–616.
- Karstunen, M., Krenn, H., Wheeler, S.J., Koskinen, M., Zentar, R., 2005. Effect of anisotropy and destructuration on the behavior of Murro test embankment. *Int. J. Geomech.* 5, 87–97.
- Krahn, J., 2003. The 2001 RM Hardy Lecture: The limits of limit equilibrium analyses. *Can. Geotech. J.* 40, 643–660.
- Ladd, C.C., 1971. Strength parameters and stress-strain behavior of saturated clays. Res. Rep. R71-23, Soils publication 278 280.
- Ladd, C.C., Foott, R., 1974. New design procedure for stability of soft clays: 10F, 3T, 39R. *J. Geotech. Engng. Div. V100, N. GT7, July, 1974, P763-786*. Pergamon, pp. A220–A220.
- Lambe, T.W., 1997. The Selection of soil strength for a stability analysis. Fifth Spencer JBuchanan Lect. Tex. M Univ.
- Larsson, R., 1980. Undrained shear strength in stability calculation of embankments and foundations on soft clays. *Can. Geotech. J.* 17, 591–602. <https://doi.org/10.1139/t80-066>

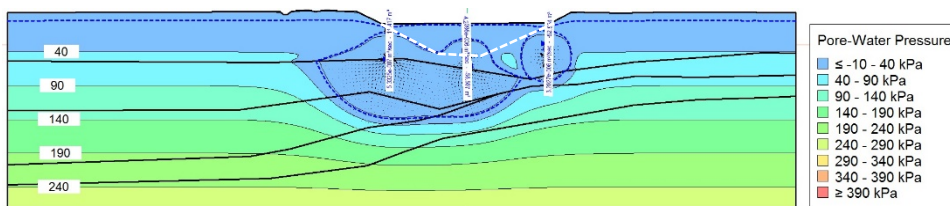
- Lehtonen, V., 2015. Modelling undrained shear strength and pore pressure based on an effective stress soil model in Limit Equilibrium Method. Tampereen Tek. Yliop. Julk.-Tamp. Univ. Technol. Publ. 1337.
- Mataić, I., 2016. On structure and rate dependence of Perniö clay.
- Potts, D.M., Zdravkovic, L., Zdravković, L., 2001. Finite element analysis in geotechnical engineering: application. Thomas Telford.
- Robertson, P.K., 2010. Estimating in-situ soil permeability from CPT & CPTu, in: Memorias Del 2nd International Symposium on Cone Penetration Testing, California State Polytechnic University Pomona, CA. [Http://www. Cpt10. Com/PDF_Files/2-51Robehc. Pdf](http://www.cpt10.com/PDF_Files/2-51Robehc.Pdf).
- SGY, 1999. Kairausopas II.
- Tavenas, F., Leroueil, S., 1980. The behaviour of embankments on clay foundations. *Can. Geotech. J.* 17, 236–260.
- Terzaghi, K., Peck, R.B., Mesri, G., 1996. Soil mechanics in engineering practice. John Wiley & Sons.
- Liikennevirasto, 2010. Tiepenkereiden ja -leikkausten suunnittelu (Design of road embankments and cuttings) in Finnish, Guidelines of Finnish Transport Agency. Liikennevirasto.
- Vermeer, P.A., Meier, C.P., 1998. Stability and deformations in deep excavations in cohesive soils.

Results of numerical study about the effect of permeability and discharge rate on lowering the groundwater table at Tuuliharju site

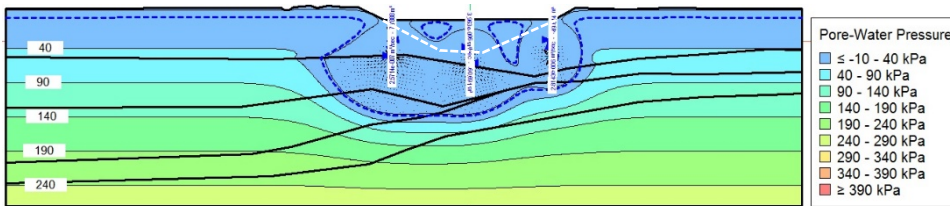
Results after 6 months with discharge rate of 0.5 m³/day



$k = 0.5 \times 10^{-9} \text{ m/s}$

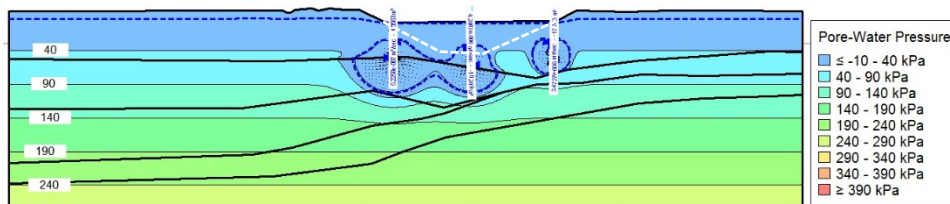


$k = 1.0 \times 10^{-9} \text{ m/s}$

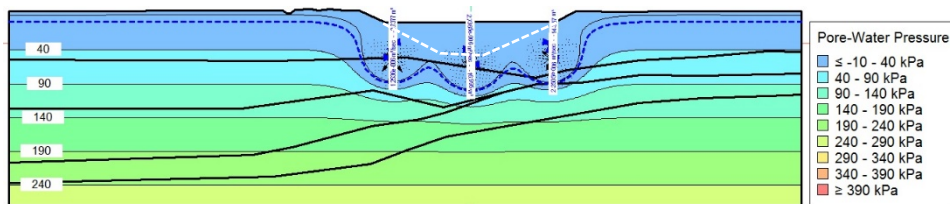


$k = 2.0 \times 10^{-9} \text{ m/s}$

Results after 2 months with discharge rate of 0.5 m³/day



$k = 2.0 \times 10^{-9} \text{ m/s}$



$k = 3.0 \times 10^{-8} \text{ m/s}$

This appendix illustrates how to implement the provided recommendations in Chapter 9 into practical applications. Accordingly, the safety is evaluated for three different typical road-cutting cases. The adopted soil profiles and properties are assumed based on practical experience with Finnish soils in the areas of the cuttings.

Example 1

This example tackles the case of a road cutting in homogeneous clayey silt. The clay has low hydraulic conductivity yielding relatively long undrained behaviour controlled stage after final cutting takes place.

E1.1 Geometry and soil properties

Figure 40 illustrates the cutting geometry and soil profile. The hydraulic conductivity of each layer is shown on the graph. The soil consists of one homogeneous clayey silt layer. The initial groundwater table is at a depth of 2.0m from the ground level, coinciding with the bottom boundary of the dry crust. The adopted physical and mechanical properties are given in Table 16. The results of in situ vane shear test is depicted in Figure 41 and will be the main tool to estimate the undrained shear strength for short-term stability evaluation. Given the liquid limit $w_L = 70\%$ and by exploiting Figure 12, a reduction factor of 0.8 is applied on the measured values of the vane shear test values at Tuuliharju. Following (Tavenas and Leroueil, 1980) method in defining the dry crust undrained shear strength; a maximum 50.0kPa cut-off value is applied to the design undrained shear strength. As a result, the crust layer is assigned a design undrained shear strength of 50.0kPa. The deeper soil has an average design undrained shear strength of 25.0kPa as presented by the dashed black line in Figure 41. The soil has an average constrained modulus of $E_{oed} = 8.0\text{MPa}$, which yields a consolidation coefficient:

$$C_v = \frac{k E_{oed}}{\gamma_w} = \frac{1.0 \times 10^{-9} \times 8.0 \times 10^3}{10.0} = 8.0 \times 10^{-7} \text{ m}^2/\text{s}$$

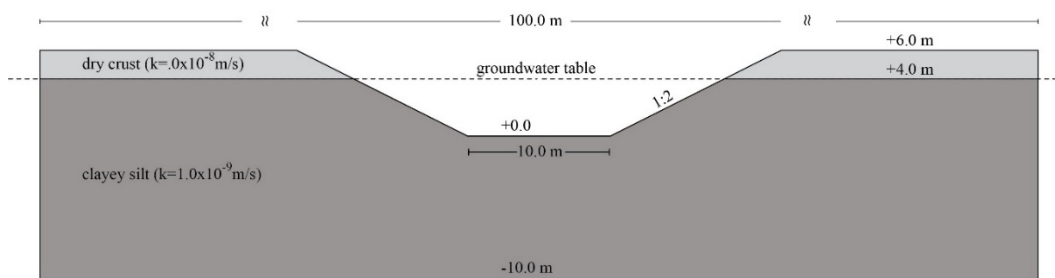


Figure 40. Example1: geometry and soil profile.

Table 16. Example1: physical and mechanical properties of soil.

Layer	Liquid limit w_L [%]	Total unit weight γ_b [kN/m ³]	Effective friction angle ϕ' [°]	Effective cohesion c' [kPa]
Dry crust	70.0	19.0	35.0	5.0
Clayey silt	70.0	17.0	28.0	10.0

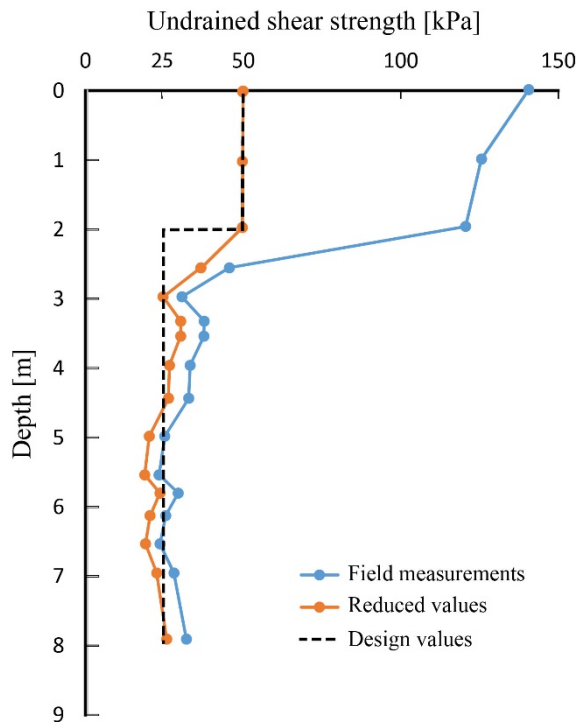


Figure 41. Example 1: measured at Tuuliharju, reduced and design undrained shear strength profile (vane shear test).

E1.2 Estimation of t_{90}

Based on the proposed procedure in Chapter 3 to estimate the length D of the longest drainage path, an approximate value of $D=4.0\text{m}$ is adopted in this calculations.

$$t_{90} = 0.848 \frac{D^2}{C_v} = 0.848 \times \frac{4.0^2}{8.0 \times 10^{-7}} = 1.696 \times 10^7 \text{ s} = 196.3 \text{ days} \approx 6.5 \text{ months}$$

It means that the first six months are controlled by undrained behavior and only undrained analysis is required during this period. After that including the transitional period between undrained and drained behavior, the drained behavior dominates and the effective shear strength parameters should be employed in the stability analysis.

E1.3 Hydraulic boundary conditions

As the pore water pressure plays a major role in long-term stability, the stability is checked after 3, 6, 12 months and at groundwater flow steady state after final cutting. That requires both limit equilibrium and transient groundwater flow analysis. The imposed hydraulic boundary conditions are clarified in Figure 42 and Figure 43.

In practice before start cutting the soil, the initial groundwater table has to be lowered to a level below the bottom of designed cutting section. Usually “suction wells” are used for this purpose, which pump water out through applying a suction in the range 30-50kPa. These values are quite high value and might be challenging to achieve in field. In these calculations suction value of 50kPa is used to show what kind of effect the pumping can in maximum achieve. The position of suction tips are chosen following the common practice and depicted Figure 42. The suction wells are simulated as hydraulic boundary condition lines that have constant water pressure head of -

5.0m that corresponds to an applied suction of 50.0kPa. The transient groundwater flow analysis is performed by SEEP/W (*GeoStudio 2016*, 2016) and has two main phases:

- a) suction wells are active during the first two months; see Figure 42 for geometry and boundary conditions.
- b) after two months, the suction wells are deactivated and the groundwater analysis continued up to steady state after final cutting (26 months in total); see Figure 43 for geometry and boundary conditions. The cutting surface is assigned a potential seepage face; a special option for possible water flow on the surface.

The pore water pressure profiles at certain points of time (2.0months, 2.0+3.0 months, 2.0+6.0months, 2.0+12.0 months, steady state) are then used during checking the stability of the cutting. The soil is modelled as saturated only without any consideration for unsaturated flow.

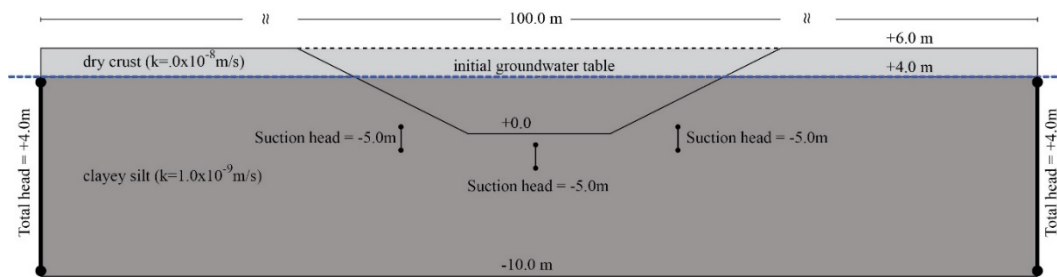


Figure 42. Example 1: Imposed hydraulic boundary conditions to model the dewatering during the first two months using suction wells (applied suction is 50kPa).

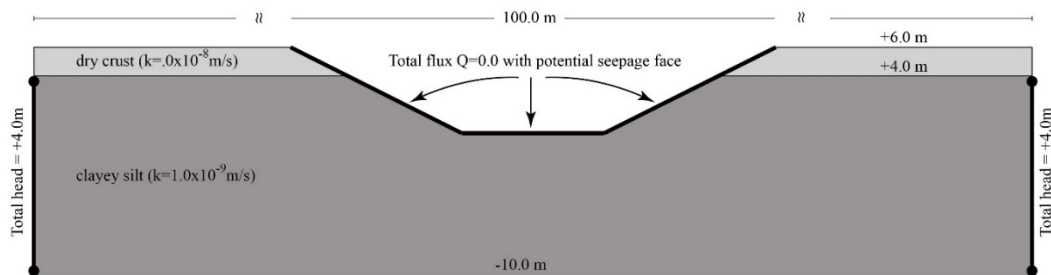


Figure 43. Example 1: Imposed hydraulic boundary conditions after final cutting and removal of dewatering system.

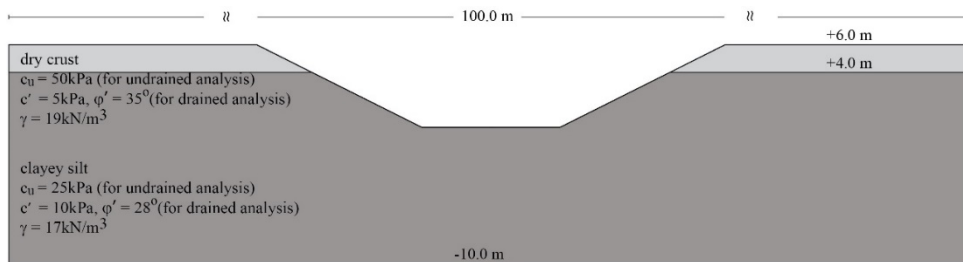


Figure 44. Example 1: shear strength parameters used for drained and undrained conditions.

It is worth mentioning that following the recommendations, Morgenstern-Price's method is employed in the current stability analyses.

E1.4 Material behavior for stability analysis

For undrained behavior ($t < t_{90}$ where t is the construction time), the option “Undrained (Phi=0)” with undrained cohesion, is assigned to the soil layers. Once t becomes greater than t_{90} (6.5 months after final cutting) the soil layers are modelled as “Mohr-Coulomb” material with effective shear strength parameters. In both cases, the *total* soil weight is used in the analysis. Figure 44 shows the employed shear strength parameters in short and long-term stability calculations.

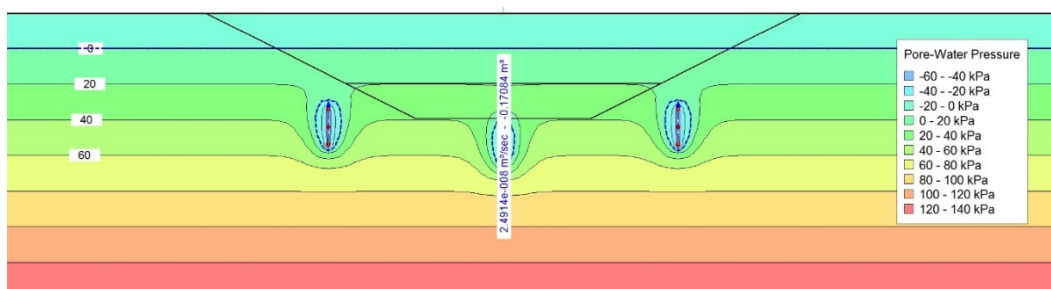
E1.5 Analyses sequence

The following list summarizes the steps followed in this analysis. The next section illustrates the calculation results that correspond to each step.

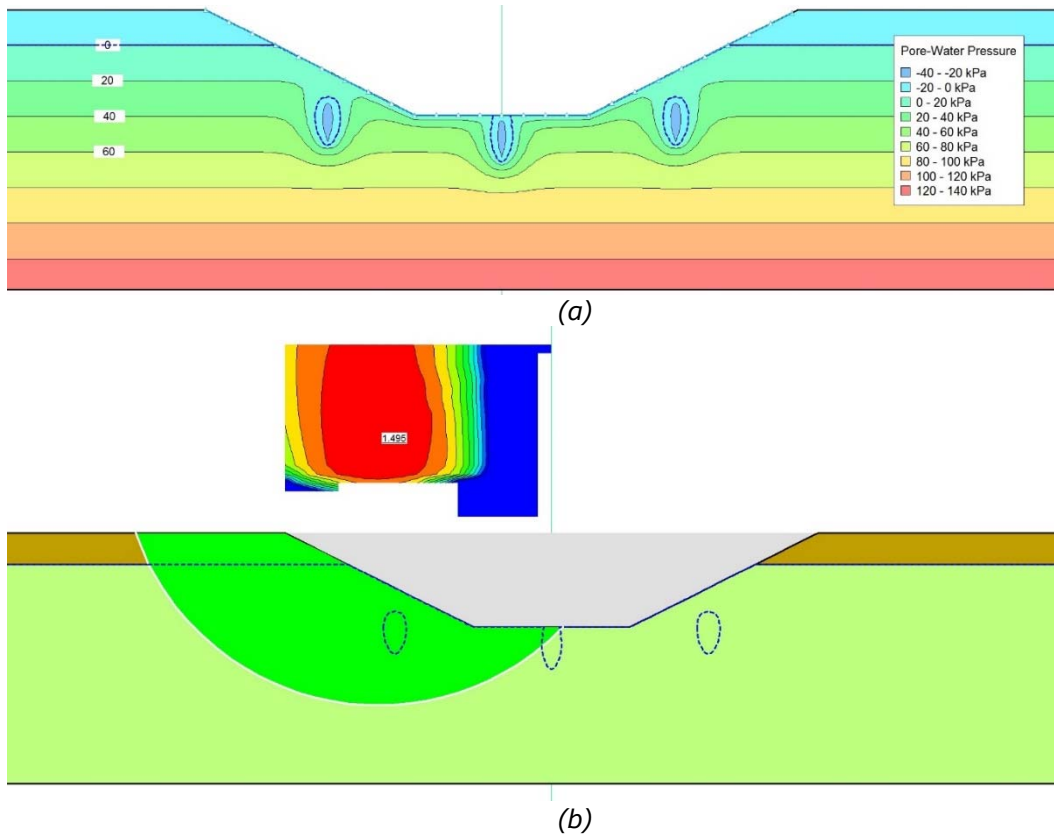
1. Transient groundwater flow for $t = 2$ months to simulate dewatering before cutting starts; hydraulic boundary conditions as in Figure 42.
2. Cutting the soil and performing undrained stability calculation ($t < t_{90}$).
3. Transient groundwater flow for 3 months after final cutting and removal of suction tips; hydraulic boundary conditions as in Figure 43 and $t = 2+3$ months.
4. Undrained stability calculation ($t < t_{90}$).
5. Transient groundwater flow for 6 months after final cutting and removal of suction tips ($t = 2+6$ months).
6. Undrained stability calculation ($t \approx t_{90}$).
7. Drained stability calculation ($t \approx t_{90}$).
8. Transient groundwater flow for 12 months after final cutting and removal of suction tips ($t = 2+12$ months).
9. Drained stability calculation ($t > t_{90}$).
10. Steady state groundwater flow ($t = 26$ months).
11. Drained stability calculation ($t > t_{90}$).

E1.6 Calculation results

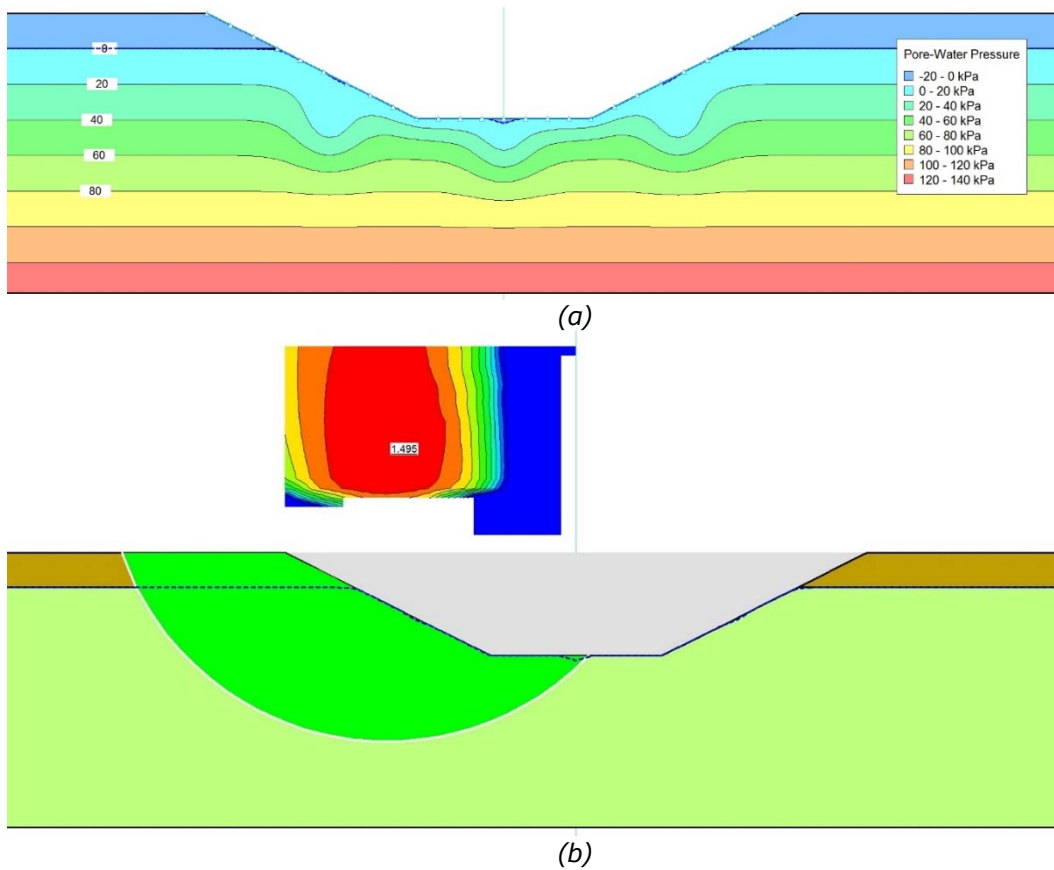
1. Water pressure profile at $t = 2$ months.



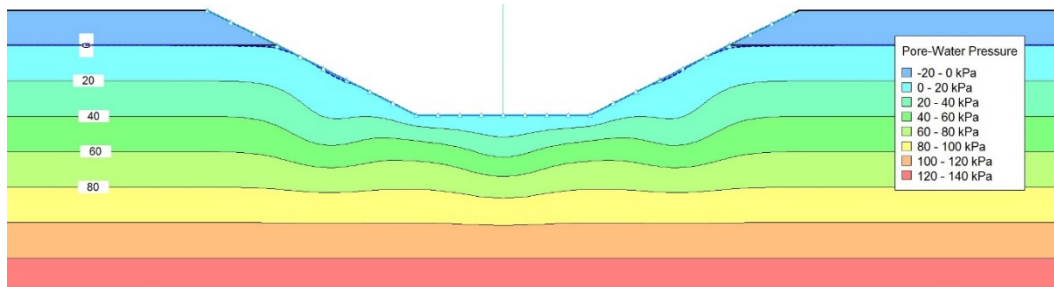
2. (a) water pressure profile and (b) undrained safety factor ($FS=1.495$) directly after cutting ($t = 2$ months).



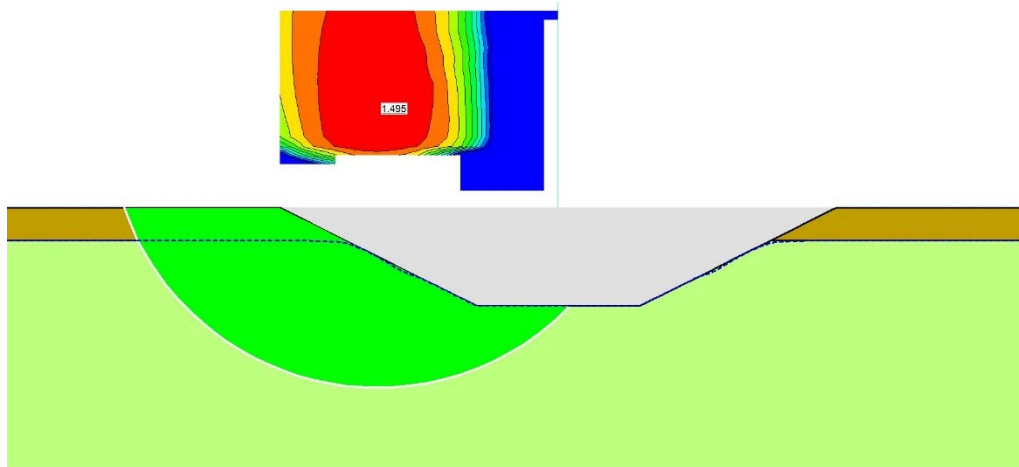
3+4. (a) water pressure profile and (b) undrained safety factor ($FS=1.495$) after 3 months of final cutting and deactivation of suction tips ($t = 2+3$ months).



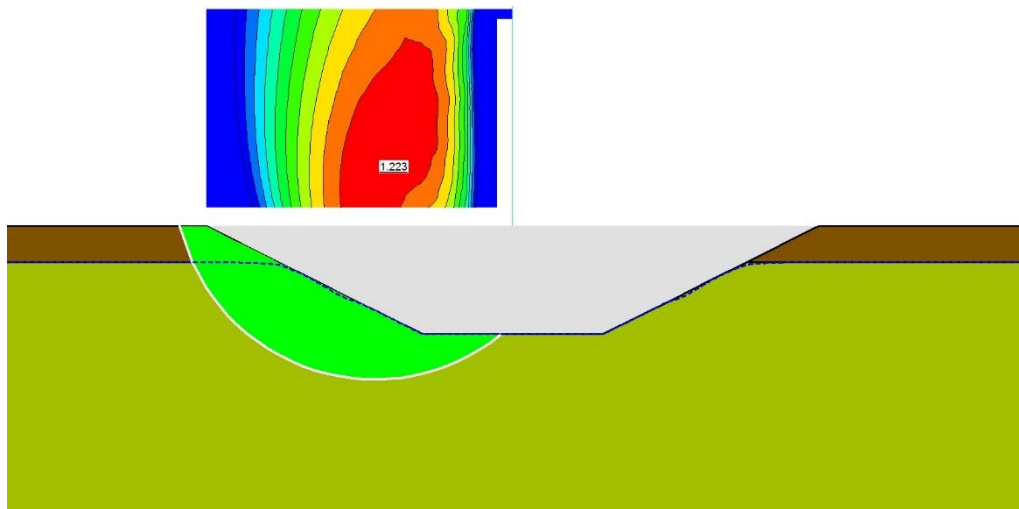
5+6+7. (a) water pressure profile, (b) undrained safety factor ($FS=1.495$) and (c) drained safety factor ($FS=1.223$) after 6 months of final cutting and deactivation of suction tips ($t = 2+6$ months).



(a)

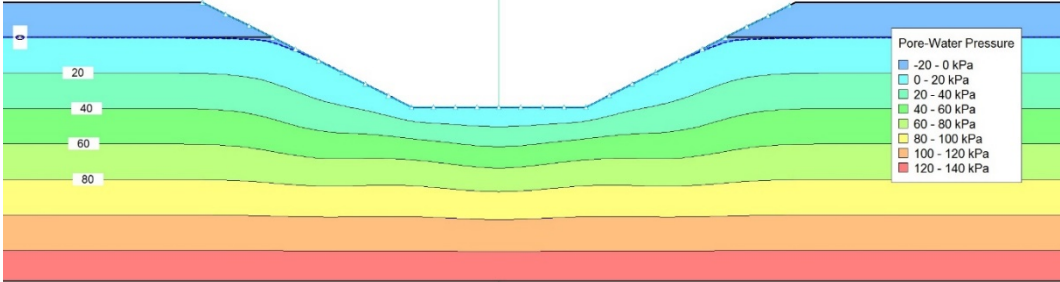


(b)

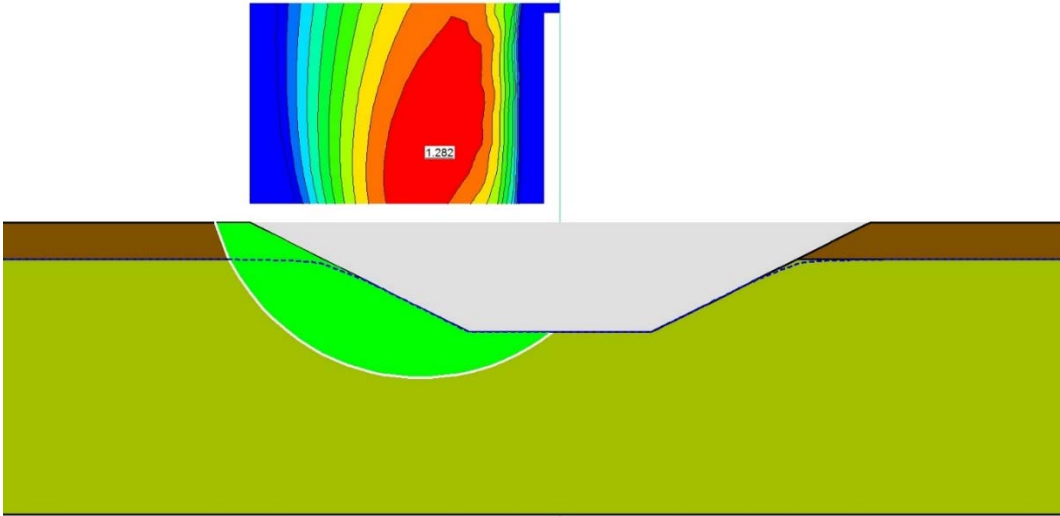


(c)

8+9. (a) water pressure profile and (b) drained safety factor (FS=1.282) after 12months of final cutting and deactivation of suction tips (t = 2+12months).

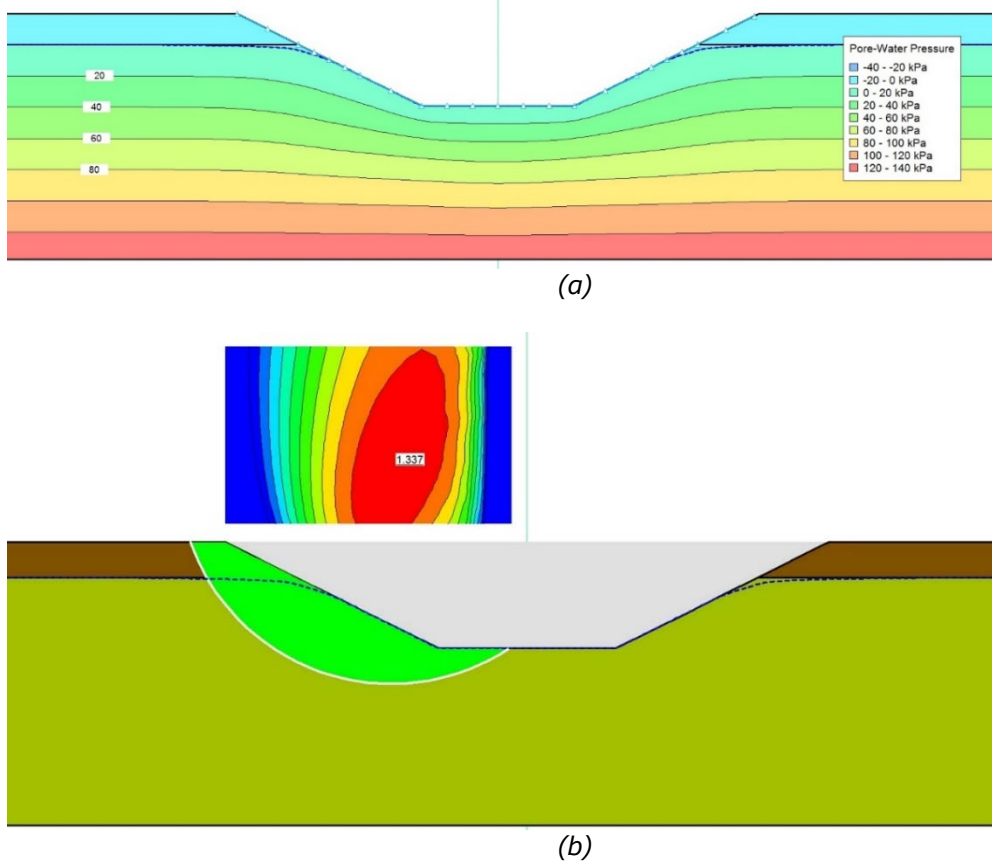


(a)



(b)

10+11. (a) water pressure profile and (b) drained safety factor (FS=1.337) at steady state after final cutting and deactivation of suction tips (t = 2+24months).



E1.7 Remarks on Example 1

Figure 45 summarizes the previous calculations, which shows that the cutting is safe with FS = 1.495 > 1.3 during the undrained period ($t < t_{90}$) and not affected much by the transient change in pore water pressure. On long-term, however, the cutting is not safe once drained behavior takes over. The transitional phase between undrained and drained behavior (t_{90} - t_{99}) is critical showing that the safety factor drops from FS=1.495 to around FS=1.23 rendering the cutting unsafe. The long-term safety factor improves overtime and the cutting satisfies safety criterion again at steady state with FS = 1.337. The dashed line represents the evolution of safety factor that is likely to happen in reality as discussed in Section (3).

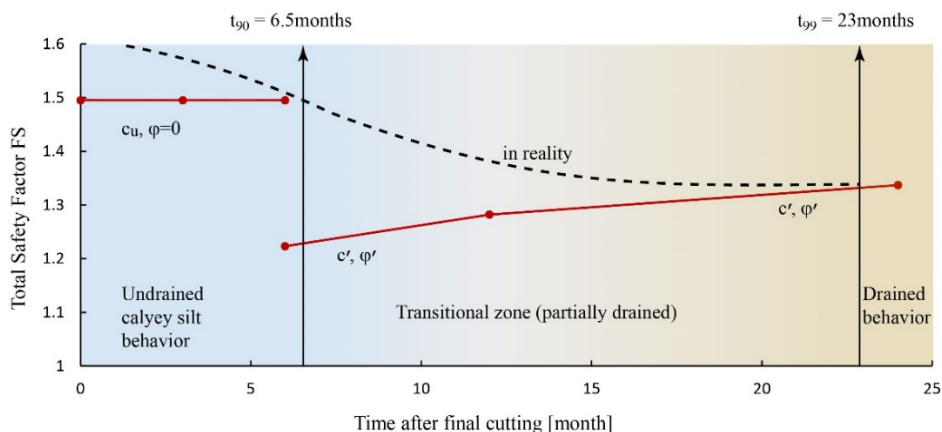


Figure 45. Example 1: safety factor evolution after final cutting.

Example 2

This example shows a special case of thin coarse sandy silt layer being sandwiched by homogeneous clayey silt. The sandy silt has much higher hydraulic conductivity if compared to the surrounding clayey silt, providing additional drainage boundary.

E2.1 Geometry and soil properties

Figure 46 illustrates the cutting geometry and soil profile. The hydraulic conductivity of each layer is shown on the graph. In addition to the dry crust layer, the soil profile consists of thin sandy silt layer being sandwiched in clayey silt layer. Similar to Example 1, the initial groundwater table is at a depth of 2.0m, coinciding with the bottom boundary of the dry crust. The adopted physical and mechanical properties are given in Table 17. The results of in situ vane shear test is depicted in Figure 47. The reduced undrained shear strength values are estimated as in Example 1 and as a result, the crust layer is assigned a design undrained shear strength of 50.0kPa. The clayey silt layer has an average design undrained shear strength of 25.0kPa whereas the thin sandy silt layer has a design undrained shear strength of 35.0kPa as presented by the dashed black line in Figure 47. The clayey silt has an average constrained modulus of $E_{oed} = 8.0\text{MPa}$ yielding a consolidation coefficient:

$$C_v = \frac{k E_{oed}}{\gamma_w} = \frac{1.0 \times 10^{-9} \times 8.0 \times 10^3}{10.0} = 8.0 \times 10^{-7} \text{ m}^2/\text{s}$$

The sandy silt has an average constrained modulus of $E_{oed} = 20.0\text{MPa}$, which yields a consolidation coefficient:

$$C_v = \frac{k E_{oed}}{\gamma_w} = \frac{1.0 \times 10^{-5} \times 20.0 \times 10^3}{10.0} = 2.0 \times 10^{-2} \text{ m}^2/\text{s}$$

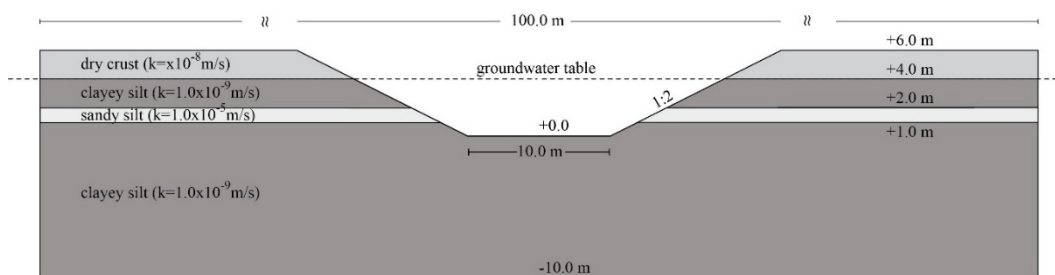


Figure 46. Example2: geometry and soil profile, the thickness of the permeable sandy silt layer is 1.0m.

Table 17. Physical and mechanical properties of soil

Layer	Liquid limit w_L [%]	Total unit weight γ_b [kN/m ³]	Effective friction angle ϕ' [°]	Effective cohesion c' [kPa]
Dry crust	70.0	19.0	35.0	5.0
Clayey silt	70.0	17.0	28.0	10.0
Sandy silt	-	18.0	32.0	3.0

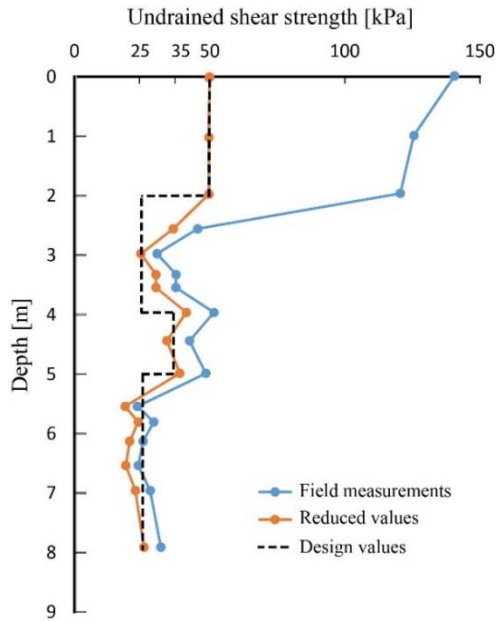


Figure 47. Example 2: measured, reduced and design undrained shear strength profile (vane shear test).

E2.2 Estimation of t_{90}

In this case the sandy silt layer works as a drainage for the clayey silt layer and the critical drainage paths would be different compared to Example 1. The estimation of the critical drainage path for both layers is demonstrated in Figure 48.

1. t_{90} for clayey silt:

$$t_{90} = 0.848 \frac{D_1^2}{C_v} = 0.848 \times \frac{3.0^2}{8.0 \times 10^{-7}} = 0.954 \times 10^7 s = 110.4 \text{ days} \approx 3.5 \text{ months}$$

2. t_{90} for sandy silt:

$$t_{90} = 0.848 \frac{D_2^2}{C_v} = 0.848 \times \frac{8.5^2}{2.0 \times 10^{-2}} = 3.063 \times 10^3 s \approx 0.85 \text{ hour}$$

It means that for the first three months the clayey silt layer is controlled by undrained behavior whereas the sand silt layer is almost immediately under drained conditions and effective strength parameters should be always used. Note that t_{90} for sandy silt is relatively very short, however t_{99} for this layer is much longer than that.

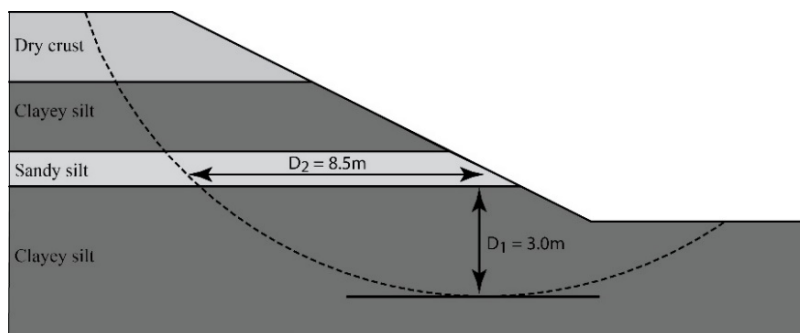


Figure 48. Example 2: estimation of drainage path length D for Clayey silt and Sandy silt layers.

E2.3 Hydraulic boundary conditions

The groundwater flow analysis is performing following similar steps to that in Example 1, where:

- a) suction wells are active during the first two months; see Figure 49 for geometry and boundary conditions.
- b) after two months, the suction wells are deactivated and the groundwater analysis continuous up to steady state after final cutting (26 months in total); see Figure 50 for geometry and boundary conditions. The cutting surface is assigned a potential seepage face; a special option for possible water flow on the surface.

The pore water pressure profiles at certain points of time (2.0months, 2.0+3.0 months, 2.0+6.0months, 2.0+12.0 months, steady state) are then used during checking the stability of the cutting.

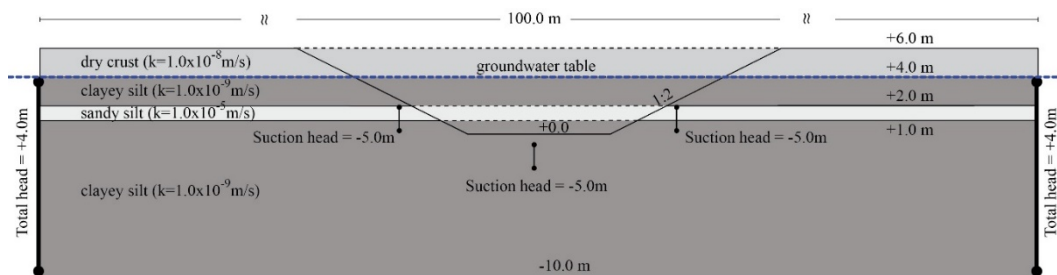


Figure 49. Example 2: Imposed hydraulic boundary conditions to model the dewatering during the first two months using suction wells (applied suction is 50kPa).

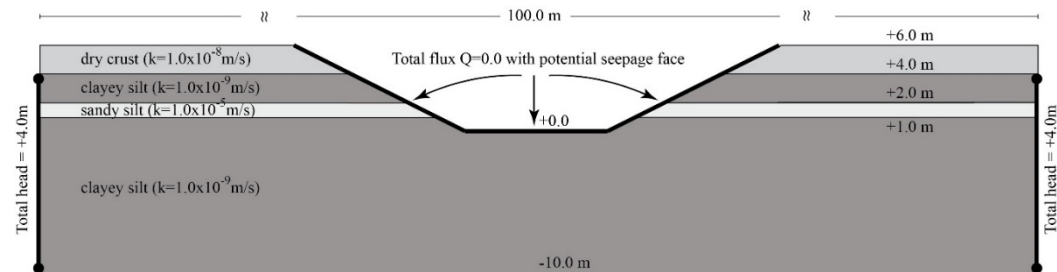


Figure 50. Example 2: Imposed hydraulic boundary conditions after final cutting and removal of dewatering system.

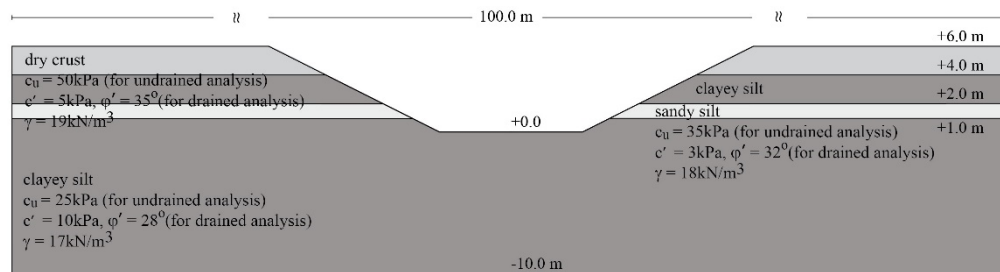


Figure 51. Example 2: shear strength parameters used for drained and undrained conditions.

E2.4 Material behavior for stability analysis

For undrained behavior ($t < t_{90}$ where t is the construction time), the option “Undrained ($\Phi=0$)” with undrained cohesion, is assigned to the clayey silt and dry crust layers. Once t becomes greater than t_{90} (3.5 months after final cutting) these soil layers are modelled as “Mohr-Coulomb” material with effective shear strength parameters. The sandy silt layer is always modelled with

effective shear strength parameters (t_{90} is negligible for this layer). Figure 51 shows the shear strength parameters in short and long-term stability calculations.

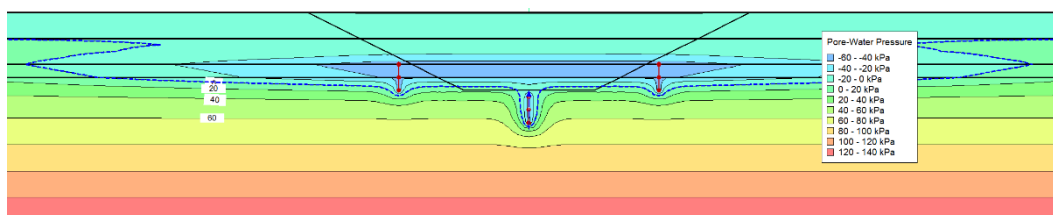
E2.5 Analyses sequence

The following list summarizes the steps followed during the calculations. The next section illustrates the calculation results that correspond to each step.

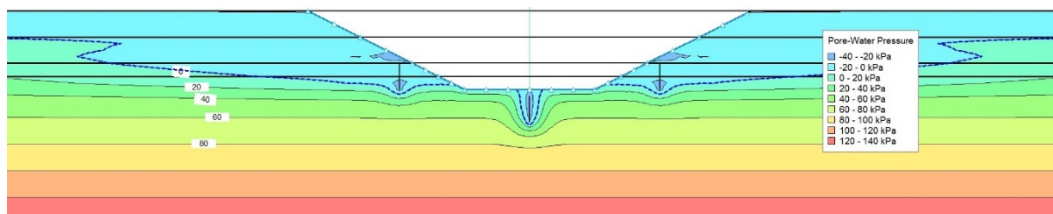
1. Transient groundwater flow for $t = 2$ months to simulate dewatering before cutting starts; hydraulic boundary conditions as in Figure 49.
2. Cutting the soil and performing stability calculation (clayey silt with undrained conditions, sandy silt with drained shear parameters).
3. Transient groundwater flow for 3 months after final cutting and removal of suction tips; hydraulic boundary conditions as in Figure 43 and $t = 2+3$ months.
4. Stability calculation (clayey silt with undrained conditions ($t \approx t_{90}$), sandy silt with drained shear parameters).
5. Stability calculation (clayey silt with drained conditions ($t \approx t_{90}$), sandy silt with drained shear parameters).
6. Transient groundwater flow for 6 months after final cutting and removal of suction tips ($t = 2+6$ months).
7. Drained stability calculation.
8. Transient groundwater flow for 12 months after final cutting and removal of suction tips ($t = 2+12$ months).
9. Drained stability calculation ($t > t_{90}$).
10. Steady state groundwater flow ($t = 26$ months).
11. Drained stability calculation ($t > t_{90}$).

E2.6 Calculation results

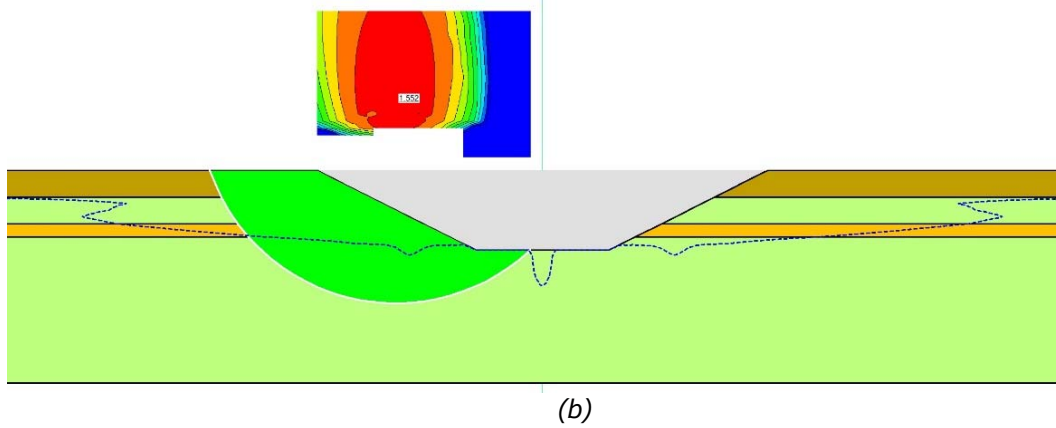
1. Water pressure profile at $t = 2$ months.



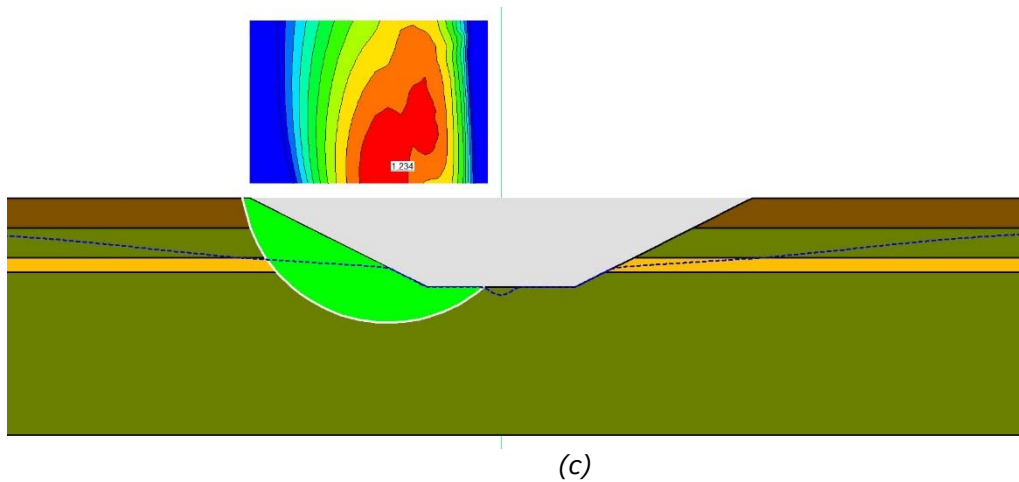
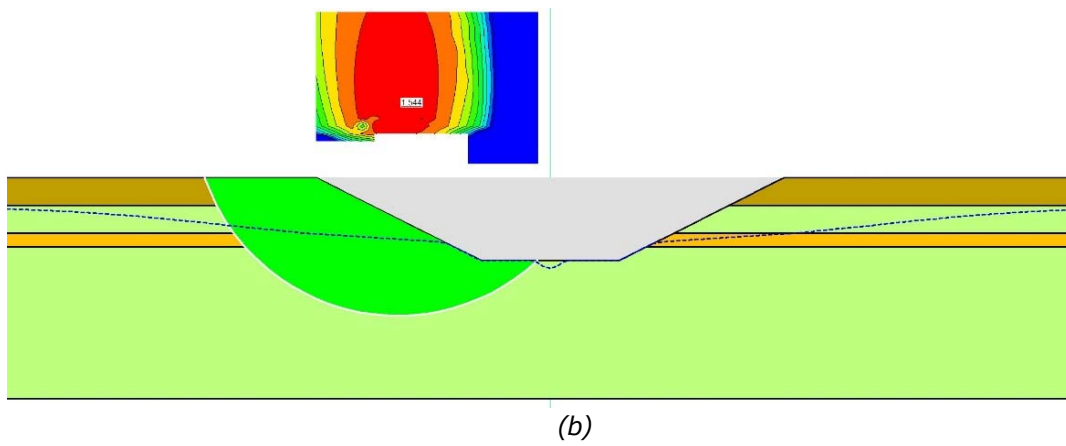
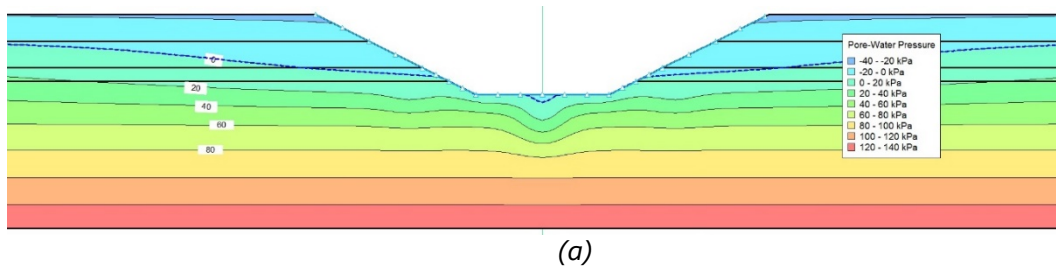
2. (a) water pressure profile and (b) safety factor ($FS=1.552$) directly after cutting ($t = 2$ months).



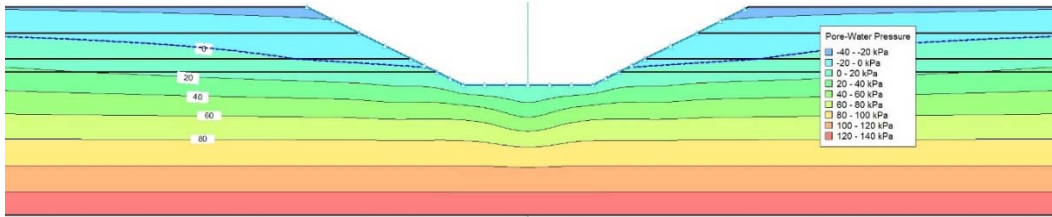
(a)



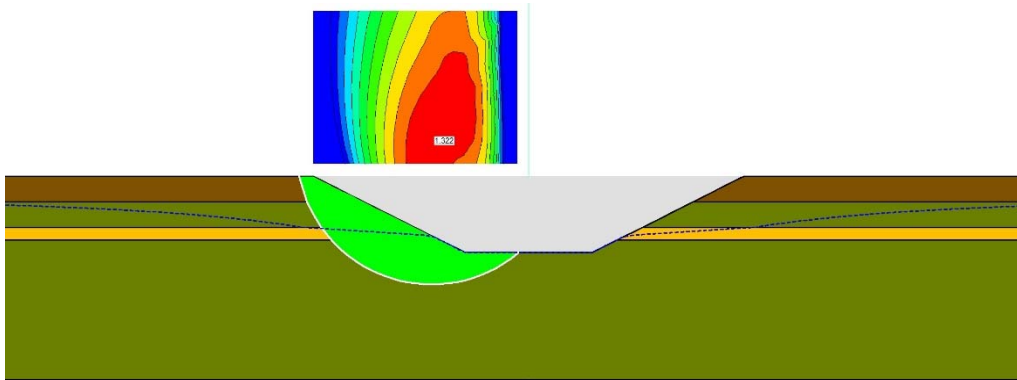
3+4+5. (a) water pressure profile, (b) safety factor ($FS=1.544$, undrained clayey silt) and (c) drained safety factor ($FS=1.234$) after 3 months of final cutting and deactivation of suction tips ($t = 2+3$ months).



6+7. (a) water pressure profile and (b) drained safety factor ($FS=1.322$) after 6 months of final cutting and deactivation of suction tips ($t = 2+6$ months).

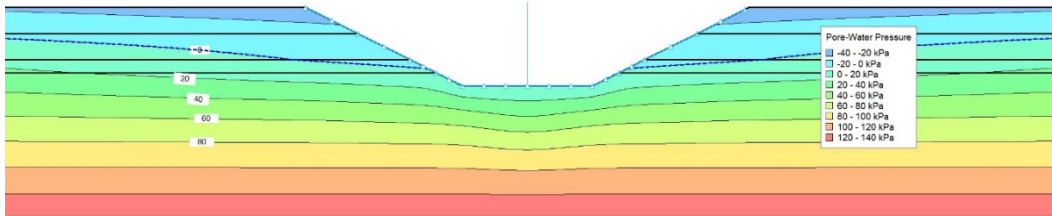


(a)

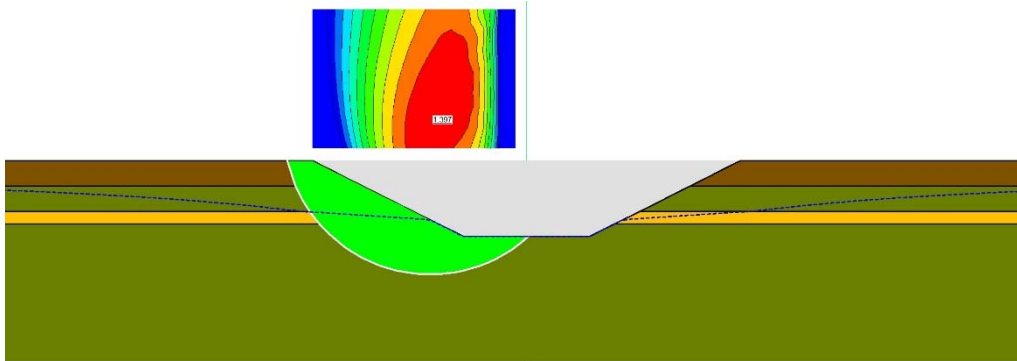


(b)

8+9. (a) water pressure profile and (b) drained safety factor ($FS=1.397$) after 12 months of final cutting and deactivation of suction tips ($t = 2+12$ months).

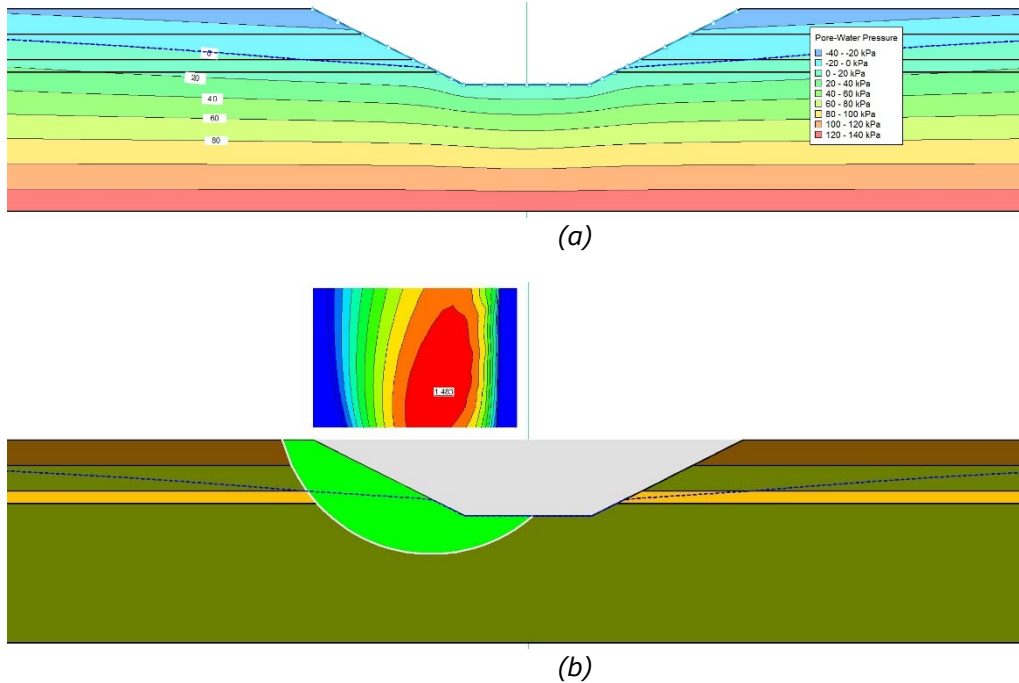


(a)



(b)

10+11. (a) water pressure profile and (b) drained safety factor ($FS=1.483$) at steady state after final cutting and deactivation of suction tips ($t = 2+24$ months).



E2.7 Remarks on Example 2

- During dewatering phase, the suction tips should be positioned within the sandy silt layer for best efficiency of the drainage system.
- The critical drainage length D changes if a permeable layer exists. Proposal for estimating D in this case is illustrated in Figure 48.

The evolution of safety factor is depicted in Figure 52. The results show that the existence of coarse sandy silt layer plays a role in reducing the undrained period from 6.5 months (see Example 1) to 3.5 months. Again, the calculations show that the transitional (intermediate) phase around t_{90} represents the most critical time where safety factor drops from $FS = 1.544$ to $FS = 1.234$. After that, the safety improves over time. The dashed curve represents the evolution of safety factor that is likely to happen in reality, see Section (3).

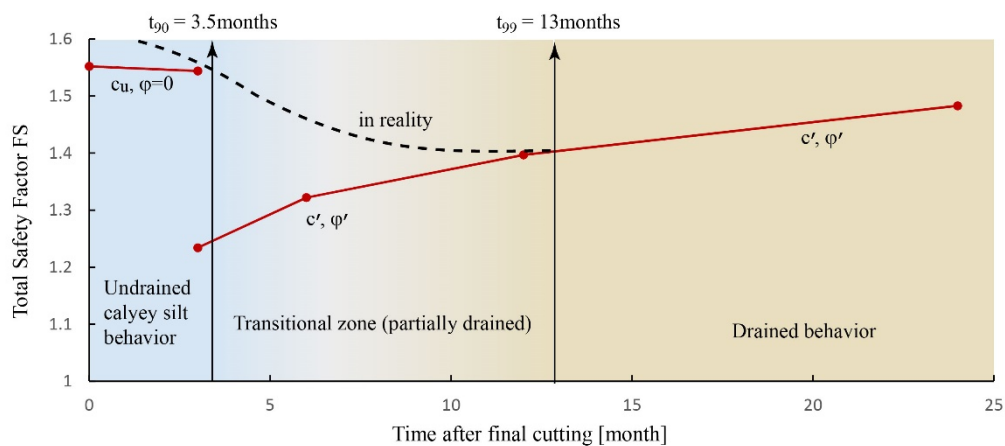


Figure 52. Example 2: safety factor evolution after final cutting.

Example 3

This example is similar to Example 1 but the clayey silt layer has limited depth and deposits over a harder Moraine layer.

E3.1 Geometry and soil properties

Figure 53 illustrates the cutting geometry, hydraulic properties and soil profile. The physical and mechanical properties are listed in Table 18. The profile of undrained shear strength is shown in Figure 54. This example follows similar methods to that in Example 1 and 2 for the estimation of soil the properties. The Moraine layer is assumed to be always controlled by drained conditions.

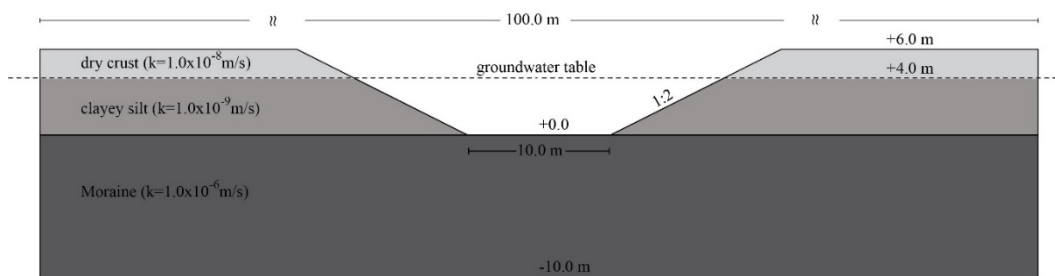


Figure 53. Example3: geometry and soil profile.

Table 18. Example 3: physical and mechanical properties of soil.

Layer	Liquid limit w_L [%]	Total unit weight γ_b [kN/m ³]	Effective friction angle ϕ' [°]	Effective cohesion c' [kPa]
Dry crust	70.0	19.0	35.0	5.0
Clayey silt	70.0	17.0	28.0	10.0
Moraine	-	20.0	38.0	10.0

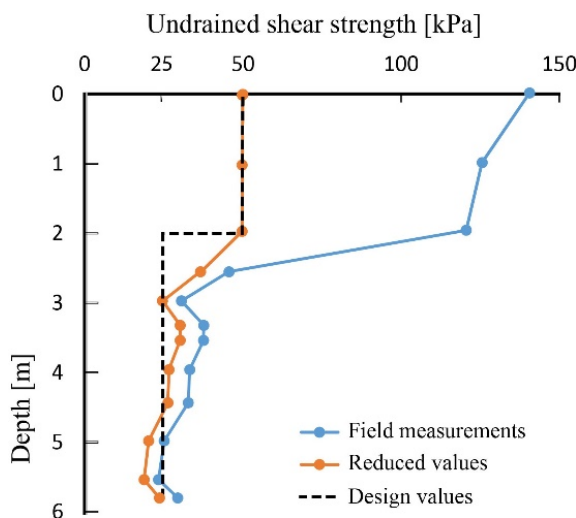


Figure 54. Example 3: measured, reduced and design undrained shear strength profile (vane shear test).

Similar to previous examples, the clayey silt has an average constrained modulus of $E_{oed} = 8.0\text{MPa}$ yielding a consolidation coefficient:

$$C_v = \frac{k E_{oed}}{\gamma_w} = \frac{1.0 \times 10^{-9} \times 8.0 \times 10^3}{10.0} = 8.0 \times 10^{-7} \text{ m}^2/\text{s}$$

E3.2 Estimation of t_{90}

The estimated drainage path length in this case is $D = 4.0\text{m}$ and consequently:

$$t_{90} = 0.848 \frac{D^2}{C_v} = 0.848 \times \frac{4.0^2}{8.0 \times 10^{-7}} = 1.696 \times 10^7 \text{ s} = 196.3 \text{ days} \approx 6.5 \text{ months}$$

It means that clayey silt layer will be subjected to only undrained analysis during the first six months.

E3.3 Hydraulic boundary conditions

The imposed hydraulic boundary conditions during dewatering period and after final cutting are given in Figure 55 and Figure 56, respectively.

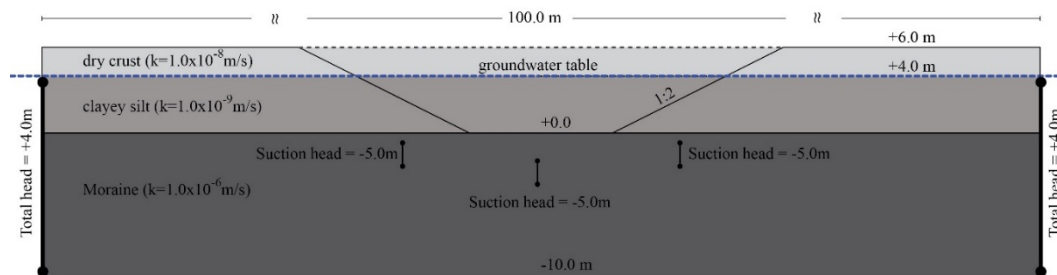


Figure 55. Example 3: Imposed hydraulic boundary conditions to model the dewatering during the first two months using suction wells (applied suction is 50kPa).

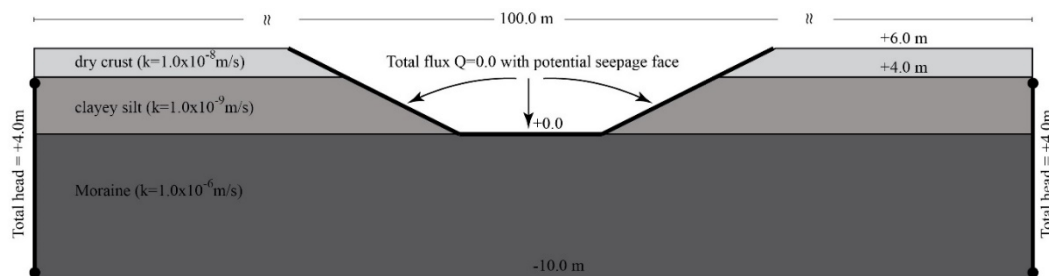


Figure 56. Example 3: Imposed hydraulic boundary conditions after final cutting and removal of dewatering system.

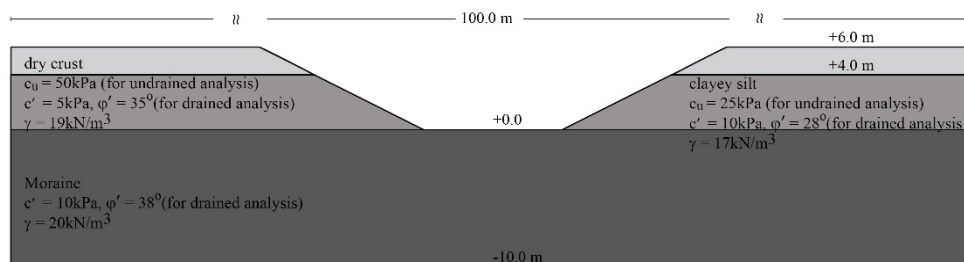


Figure 57. Example 3: shear strength parameters used for drained and undrained conditions.

E3.4 Material behavior for stability analysis

For undrained behavior of clayey silt, the option “Undrained (Phi=0)” with undrained cohesion, is adopted. Once t becomes greater than t_{90} (6.5 months after final cutting) the clayey silt is modelled as “Mohr-Coulomb” material with effective shear strength parameters. The Moraine is modelled as “Mohr-Coulomb” material throughout the whole analysis time. Figure 57 shows the employed shear strength parameters in short and long-term stability calculations.

E3.5 Analyses sequence

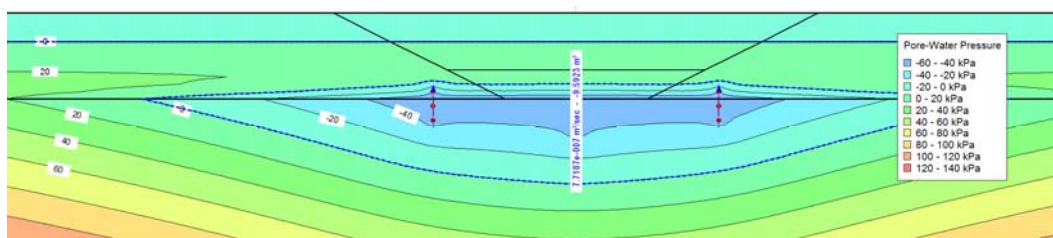
This and the next paragraphs clarifies the followed steps and corresponding results of the analysis.

Analysis steps:

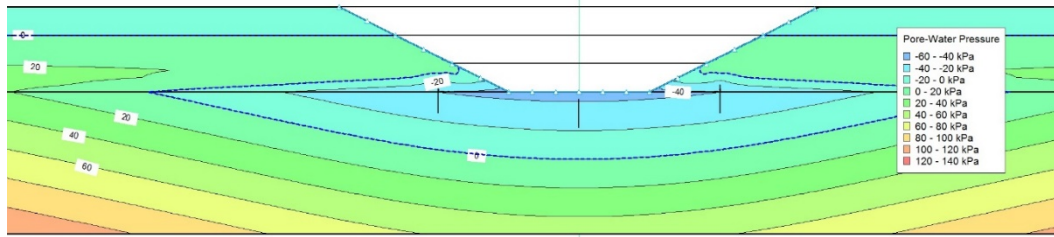
1. Transient groundwater flow for $t = 2$ months to simulate dewatering before cutting starts; hydraulic boundary conditions as in Figure 55.
2. Cutting the soil and performing stability calculation (clayey silt is undrained: $t < t_{90}$).
3. Transient groundwater flow for 3 months after final cutting and removal of suction tips; hydraulic boundary conditions as in Figure 56 and $t = 2+3$ months.
4. Stability calculation (clayey silt is undrained: $t < t_{90}$).
5. Transient groundwater flow for 6 months after final cutting and removal of suction tips ($t = 2+6$ months).
6. Stability calculation (clayey silt is undrained: $t \approx t_{90}$).
7. Stability calculation (clayey silt is drained: $t \approx t_{90}$).
8. Transient groundwater flow for 12 months after final cutting and removal of suction tips ($t = 2+12$ months).
9. Drained stability calculation ($t > t_{90}$).
10. Steady state groundwater flow ($t = 26$ months).
11. Drained stability calculation ($t > t_{90}$).

E3.6 Calculation results

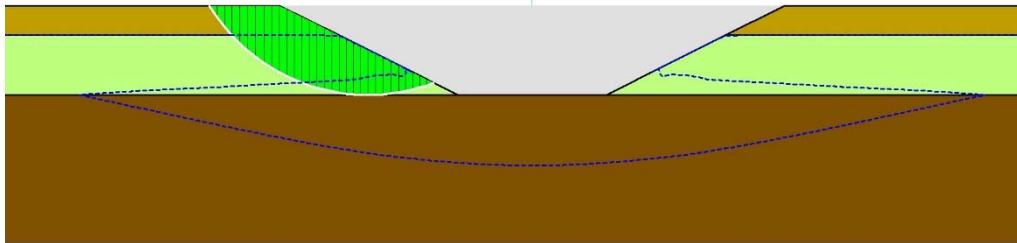
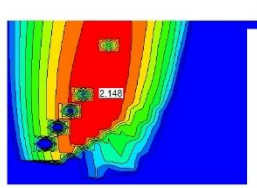
1. Water pressure profile at $t = 2$ months.



2. (a) water pressure profile and (b) undrained safety factor ($FS=2.148$) directly after cutting ($t = 2$ months).

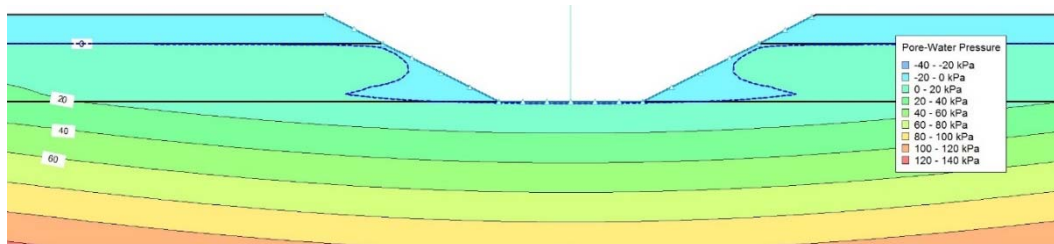


(a)

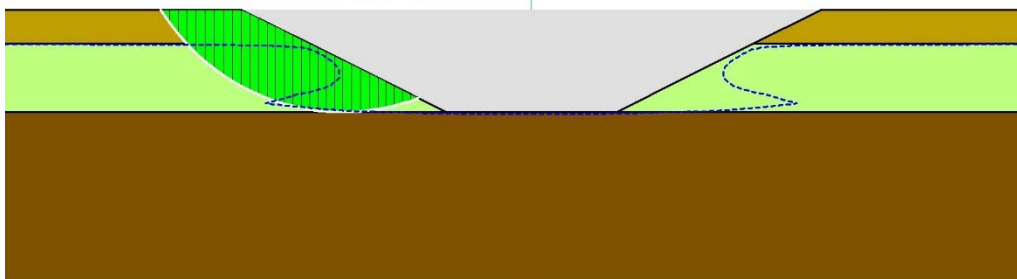
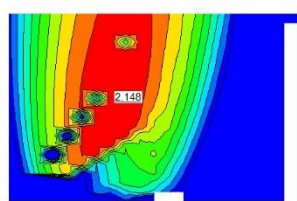


(b)

3+4. (a) water pressure profile and (b) safety factor ($FS=2.148$) after 3 months of final cutting and deactivation of suction tips ($t = 2+3$ months).

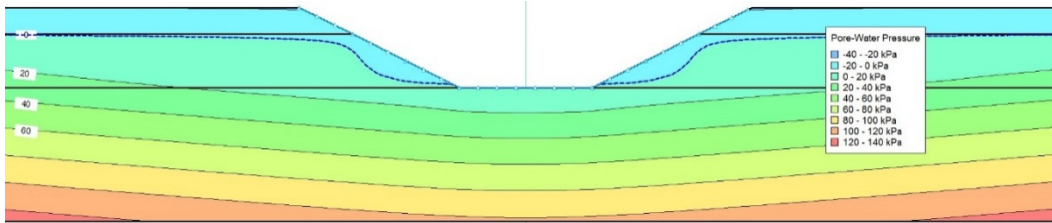


(a)

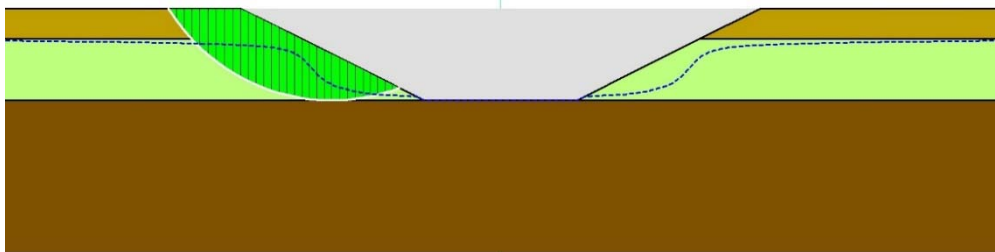
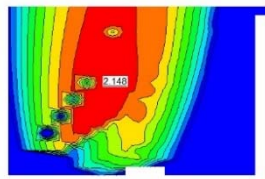


(b)

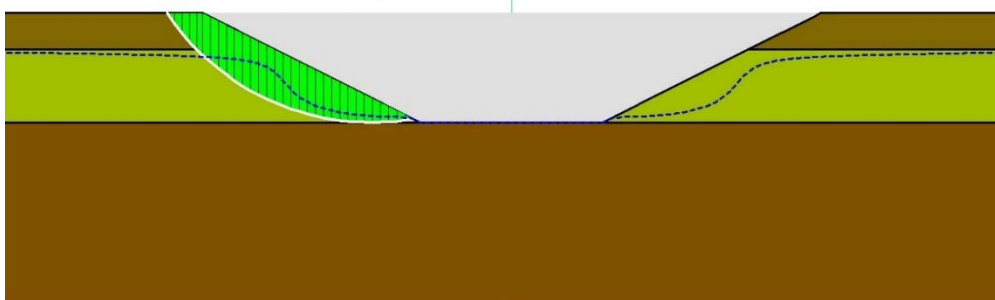
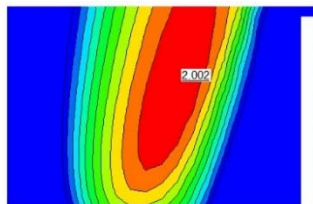
5+6+7. (a) water pressure profile, (b) safety factor ($FS=2.148$, undrained clayey silt) and (c) safety factor ($FS=2.002$, drained clayey silt) after 6 months of final cutting and deactivation of suction tips ($t = 2+6$ months).



(a)

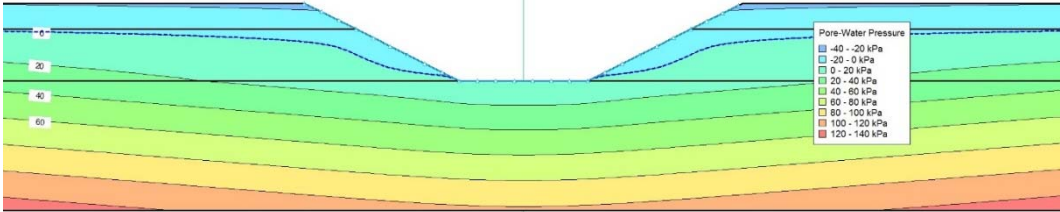


(b)

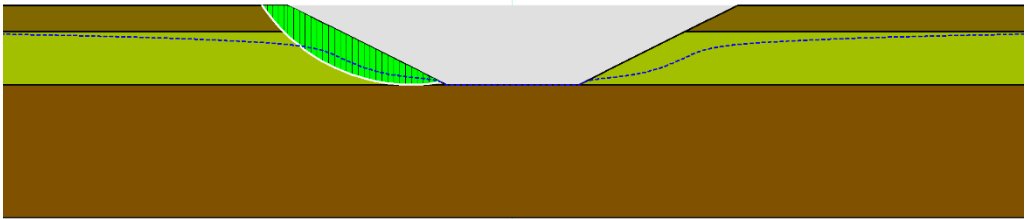
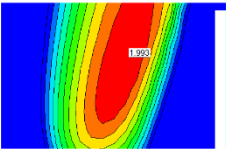


(c)

8+9. (a) water pressure profile and (b) drained safety factor (FS=1.993) after 12months of final cutting and deactivation of suction tips (t = 2+12months).

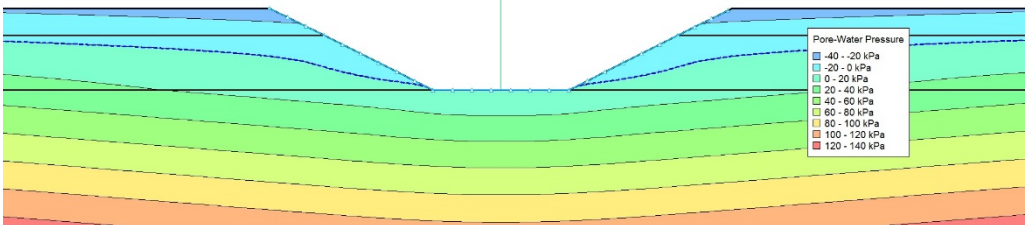


(a)

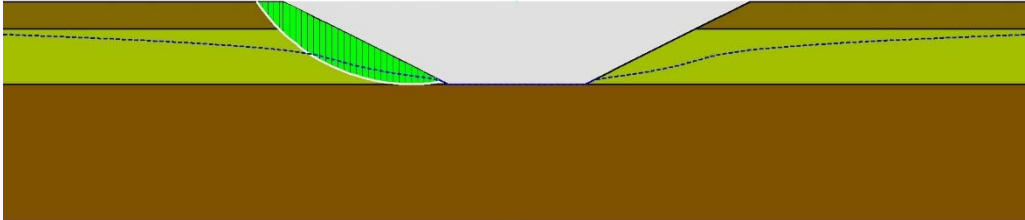
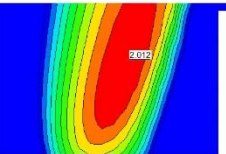


(b)

10+11. (a) water pressure profile and (b) drained safety factor (FS=2.012) at steady state after final cutting and deactivation of suction tips (t = 2+24months).



(a)



(b)

E3.7 Remarks on Example 3

Figure 58 shows the evolution of safety factor during the analysis time. Even though a jump in the safety factor takes place at the transitional time between undrained and drained behavior, its value kept well above the allowed threshold. With time advancement, the safety factor keeps improving in long-term until reaching the steady state. This example represents a clear case of a safe cutting design. Again, the dashed curve represents the evolution of safety factor that is likely to happen in reality as discussed in Section (3).

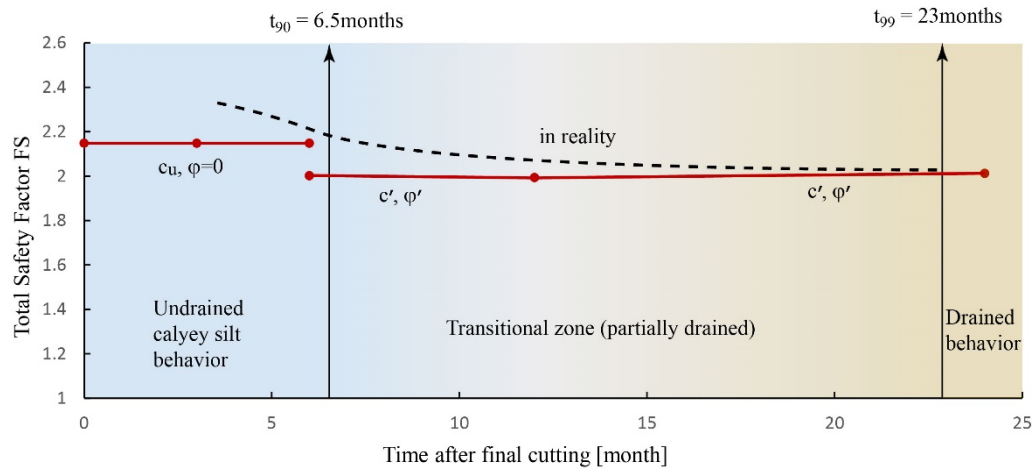


Figure 58. Example 3: safety factor evolution after final cutting.

ISSN-L 1798-6656
ISSN 1798-6664
ISBN 978-952-317-608-9
www.liikennevirasto.fi

Liik
enne
vira
sto

